Master Thesis

Wireless Navigation for Tumor Localization and Resection Margin Assessment during Laparoscopic Rectal Cancer Surgery

By

W.F. ten Bolscher

A thesis submitted in fulfillment of the requirements for the degree of Master of Science

in

Technical Medicine
Track: Medical Imaging and Interventions
Faculty of Science and Technology

15 June 2021

UNIVERSITY OF TWENTE.

NETHERLANDS CANCER INSTITUTE
ANTONI VAN LEEUWENHOEK

Graduation Committee

Chairman and technological supervisor:	Dr. ir. F. van der Heijden Faculty of Science and Technology Department of Robotics and Mechatronics University of Twente Enschede, The Netherlands
Clinical supervisor:	Dr. A. Aalbers Department of Surgery Netherlands Cancer Institute Amsterdam, The Netherlands
Process supervisor:	Drs. P. van Katwijk Faculty of Science and Technology University of Twente Enschede, The Netherlands
Additional supervisor:	Dr. ir. H. Groen Department of Surgery Netherlands Cancer Institute Amsterdam, The Netherlands
Additional supervisor:	Dr. W. Heerink Department of Surgery Netherlands Cancer Institute Amsterdam, The Netherlands
External member:	Dr. V. Retel Faculty of Behavioural, Management and Social sciences Department of Health Technology and Services Research University of Twente Enschede, The Netherlands

Table of Contents

List of Abbreviations

3D	Three-dimensional
5DOF	Five degrees of freedom
6DOF	Six degrees of freedom
APR	Abdominoperineal resection
CBCT	Cone-beam computed tomography
CT	Computed tomography
DFR	Distortion free reference
DV	Da Vinci
eFOV	Extended field of view
EM	Electromagnetic
EMI	Electromagnetic interference
EMTS	Electromagnetic tracking system
FG	Field generator
FOV	Field of view
IGS	Image guided surgery
IMU	Inertial measurement unit
LAR	Low anterior resection
MRI	Magnetic resonance imaging
NKI	Netherlands Cancer Institute
OR	Operating room
OTS	Optical tracking system
OTV	One transponder vector (sensor fusion method)
RM	Resection margin
RMSE	Root-mean-square error
SUS	System Usability Scale
TA	Tracking Array
TME	Total mesorectal excision
TRE	Target registration error
TTFG	Tabletop field generator
TTV	Two transponder vector (sensor fusion method)
ZDR	Z-axis direction reversal

Chapter 1: Introduction

Introduction

Clinical introduction

Rectal cancer is the eight most common cancer worldwide with an annual incidence of 704,000, constituting 3.9 percent of all diagnosed cancers [1]. In the Netherlands, rectum cancer amounts to more than 4.500 diagnosis in 2018, while incidence has more than doubled over the last three decades [2]. Survival rates of rectal cancer depend greatly on the stage at diagnosis with a 91% 5-year survival for stage I, dropping to 13% in stage IV [3]. Since 18% of new diagnosis are stage IV, rectal cancer contributes to more than 1000 deaths a year in the Netherlands [4]. However, 5-year survival rates have been increasing in the last decades due to advances in diagnostics and treatment of the disease.

Rectal cancer presents with symptoms, such as a change in bowel habits, tenesmus, anaemic symptoms and the addition of blood or mucus to the stool [5]. When a patient presents with these symptoms, a digital rectal examination is essential and a colonoscopy is indicated [5], [6]. During this colonoscopy, which is the gold standard diagnostic test, a biopsy can be taken for histological conformation of malignancy. After conformation of a rectal tumor, the tumor grade and stadium is determined based on the TNM staging system utilizing imaging techniques to examine local spread and lymphatic or distant metastases [5], [6].

Treatment of rectum carcinoma depends on several factors such as the stage of cancer, patient condition and patient preferences. Worldwide, surgery is the primary curative option in non-metastasized rectal cancer, which accounts for 75% of all diagnoses. Furthermore, in the Netherlands as much as 95% of patients with stadium I-III rectal cancer get surgical treatment [7] [8]. For stadium II and III rectal cancer, 76% of patients received additional neoadjuvant radiotherapy and in 43% of cases also chemotherapy was given [8].

The surgical procedure can be performed using an open or laparoscopic approach. A laparoscopic approach is widely used due to favorable short-term outcomes, such as less pain, reduced blood loss, and improved recovery time and accounts for 82% of colorectal surgery in the Netherlands in 2015 [9]–[11]. Rectal cancer surgery is commonly performed using the Low anterior resection (LAR) or Abdominoperineal Resection (APR). APR surgery, where both rectum and anus are resected, is performed when the distal border of the tumor is located close - order: cm - or inside of the anal sphincter. An LAR, where the rectum is resected after which the colon is attached to the anus, can be performed when a coloanal anastomosis is a surgical option and is usually preferred to APR since it will prevent a permanent colostomy [6]. However, this coloanal anastomosis is subject to anastomotic leakage in approximately 10% of patients, with increased risk for older patients or patients suffering from serious comorbidity. Furthermore, major bowel-, urinary-, and sexual dysfunctions, also known as LAR Syndrome (LARS), are experienced by 30%–80% patients after a LAR [12]. An important risk factor for both anastomotic leakage and LARS is a low level of anastomosis [12], [13]. The level of anastomosis is based on the tumor location and distal resection margin. Therefore, tumor localization and intraoperative assessment of this margin can have direct and severe consequences on functional outcome.

For oncological outcome, tumor localization and consequent margin assessment – i.e. distal, proximal and circumferential margin - is also essential, since positive resection margin rates of 10-15% are observed after laparoscopic rectal cancer surgery [10], [14], associated with local recurrence and overall poor survival [15]. During surgery, the surgeon must locate the tumor based on images of the laparoscopic camera in the narrow space of the pelvis without the possibility of intraoperative palpation. This is especially challenging when the target area is threatened and anatomical planes are disturbed due to the tumor ingrowth, previous surgery or fibrosis resulting from neoadjuvant radiotherapy [16].

Concluding, during laparoscopic rectal cancer surgery, tumor localization and consequent margin assessment are crucial for both oncological and functional outcome. To aid the surgeon in this challenging task, image guided surgery (IGS) is proposed.

Technical introduction

The use of IGS has evolved rapidly over the past decades. Basically, preoperative imaging, such as MRI- and CT-scans, is made available for intraoperative guidance, allowing for planning an optimal approach, anticipate on the presence of critical anatomical structures and potentially increase surgical accuracy. At the Netherlands Cancer Institute (NKI), an IGS navigation technique has been developed and is currently applied as standard care for open tumor surgery in the lower abdominal and pelvic area [17]. All surgical navigation applications rely on an accurate tracking system to continuously monitor the pose of a sensor in a specified field of view (FOV). A pose represents an object in a three-dimensional (3D) space, giving the 3 degree of freedom (DOF) position and 3DOF orientation. Two main tracking systems can be distinguished for tracking during surgery, namely optical tracking systems (OTS) and

electromagnetic tracking systems (EMTS). Since, a direct line of sight to the target area is needed for OTS, which is not feasible in lower abdominal surgery. Therefore, the current navigation technique relies on the use of an EMTS to register the preoperative imaging to the intraoperative setting.

At the NKI, contrast-enhanced CT-scans are acquired preoperatively and combined with other imaging data of the patient to create a 3D model of anatomical structure, such as bone, arteries, veins, ureters, nerves, lymph nodes and the tumor. Subsequently, wired patient sensors are placed intraoperatively on the skin of the patient and a subsequent cone beam CT (CBCT) is acquired. This CBCT is acquired to correlate the patient sensors to the patient's anatomy. In addition to the patient sensors, a surgical pointer or tools can be tracked by the EMTS, where the intraoperative navigation user interface shows the position of the pointer in three orthogonal slices of the CT and in the 3D model. The surgeon can use the pointer and user interface for spatial orientation in the 3D model and correlation to the intraoperative setting.

The surgical navigation setup, which is currently applied as standard care in the NKI, has two main limitations: 'Movement between patient sensors and target area' and 'Registration using CBCT'. Most anatomical structures - e.g. vessel or lymph nodes - in the pelvis lay relatively rigid due to a close relation to pelvic bones and fascia. However, during rectal cancer surgery dissection of the tumor and mesorectum causes them to mobilize. A recent study by Kok et al. tried to solve this, next to tracking of surrounding structures using patient sensor on the skin, by placement of an additional EM sensor on the tumor using a proctoscope, resulting in a feasible, safe and accurate workflow [18]. However, during the workflow as proposed by Kok et al., CBCT registration was still needed due to intraoperative placement of wired EM sensors. During acquisition, the patient receives additional radiation dose and surgical workflow is interrupted, since all surgical staff is required to leave the OR. Furthermore, a hybrid OR is needed hindering broader implementation of surgical navigation techniques.

In this study, we propose a novel wireless electromagnetic tracking setup for surgical navigation. This setup will allow for real-time tumor tracking and enable utilization of pre-operative imaging during surgery. The incorporated wireless EM tracking system, Calypso's GPS for the Body®, has shown sub millimeter accuracy in both laboratory, radiotherapy and operation room environments [19], [20]. Comparable to the approach of Kok et al. [18] EM sensors can be implanted near the tumor for tracking of a mobilized rectum. However, the wireless transponders can be implanted preoperatively, enabling preoperative registration and eliminating the need for intraoperative CBCT imaging. Therefore, overcoming important workflow related obstacles of the earlier wired EM tracking approach for accurate navigation in rectal surgery[18][18].

The main constraint of the wireless navigation setup is that the Calypso system is limited to tracking of three transponders. In a surgical setting, one transponder is needed for use in a tracked surgical tool, e.g. Pointer or Stapler, and two sensors are available for 6DOF tumor tracking. Therefore, the setup, in contrast to the wired approach, is not able to track any surrounding structures, limiting the spatial orientation in the 3D model and correlation to the intraoperative setting by the surgeon.

Furthermore, the transponders are designed for placement in prostate tissue before radiotherapy. It is unclear whether placement of the transponders in the rectal wall will yield the stability needed for intraoperative navigation. Furthermore, promising results have been published for use of this system in the operating room, outlining sub millimeter accuracy and acceptable distortion effects of metallic cylinders (< 3.2 mm) on tracking accuracy in this proposed environment [19], [20]. However, distortion effects of surgical instruments or surgical robotics remain unclear. Furthermore, while Electromagnetic interference (EMI) is a relatively common issue in the OR [21]–[23], no information is published on EMI of EMTS on surrounding equipment.

Research Aims

The aim of this study is: to investigate the safety, accuracy and usability of a wireless surgical navigation setup for real-time rectal tumor tracking in laparoscopic surgery.

First, a standardized accuracy and distortion assessment of the Calypso wireless electromagnetic transponder tracking system is performed. Second, the potential EM interference of the Calypso system on critical operation room equipment is functionally assessed. Third, software for the navigation setup is developed and subsequently tested on usability and accuracy following the proposed intraoperative workflow on a phantom. Fourth, the influence of potential transponder migration and tissue deformation on the relative stability of transponders with respect to a rectal tumor is assessed in a rectal excision specimen. Last, as future outlook the influence of distortion by a da Vinci surgical system on the tracking accuracy of electromagnetic tracking systems is assessed.

Research design

In Chapter 3, a standardized assessment following the protocol of Franz et al. is performed. However, since intraoperative accuracy is dependent on both position and orientation accuracy, the protocol is extended to

orientation accuracy in the extended FOV. Furthermore, the influence of distortion by surgical tools inside the eFOV during navigation in rectal cancer surgery will be assessed. In addition, we included the NDI Polaris Spectra optical tracking system (Northern Digital Inc, Waterloo, Canada) as an absolute accuracy reference.

In Chapter 4, we investigate potential interference of alternating and pulsed magnetic field utilized by the Calypso GPS for the Body® Tracking system on critical operation room equipment. First, a comprehensive list of all equipment present during rectal cancer surgery was drafted. Second, this list was scores on the criteria: used during surgical navigation, electromagnetic interference is plausible and critical for patient safety. Third, functional output during EM tracking was separately assessed for all identified equipment and compared to reference measurements.

In Chapter 5, the feasibility of the proposed wireless setup will be assessed for the intraoperative phase based on usability and accuracy on a phantom. Compared to the current surgical navigation approach, the wireless surgical navigation setup utilizes a different software platform and is not able to track any surrounding structures, limiting the spatial orientation in the 3D model and correlation to the intraoperative setting by the surgeon. The visualization methods developed for this setup are mainly aimed to mitigate these limitations and provide an intuitive view of the surgical target area and surgical tool(s). The primary aim of this study is to assess the usability of a wireless surgical navigation setup for laparoscopic rectal cancer surgery as determined by questionnaires among participating surgeons using a phantom. A secondary aim is to determine the accuracy of the distance from the tumor border to the probe tip for laparoscopic rectal tumor margin assessment.

Chapter 6 aims to investigate potential migration and quantify relative rotations and translations in three ex vivo samples of rectosigmoid or tumor tissue with a third transponder simulating a tumor. Inter-transponder distances are assessed using cone beam computed tomography (CBCT) and EM data, while translations and rotations of the tumor simulating transponder in the virtual transponder coordinate system is assessed in static and dynamic experiments.

In Chapter 7, we evaluate the influence of two da Vinci telemanipulator systems – i.e. Si and Xi systems - on the tracking accuracy of the proposed Calypso GPS for the body system and the currently used NDI Aurora Tabletop field generator (TTFG) with an OTS reference. These systems are used since they enable positioning of the flat field generators (FG) on the operating table under the reclining patient, as implemented by Kok et al. for use of the NDI Aurora during surgical navigation in laparoscopic rectal cancer surgery [18]. During this study, the tumor sensors were located approximately 10 cm along the z-axis from the start of the FOV, therefore grid accuracy was assessed at this level (+- 2.5 cm) in the FOV of both EMTS. Furthermore, influence of arm position configurations was assessed as well as influence of converging robotic instruments on the sensor location.

References

[1] F. Bray, J. Ferlay, I. Soerjomataram, R. L. Siegel, L. A. Torre, and A. Jemal, “Global cancer statistics 2018: GLOBOCAN estimates of incidence and mortality worldwide for 36 cancers in 185 countries,” *CA. Cancer J. Clin.*, vol. 68, no. 6, pp. 394–424, Nov. 2018.

[2] Intergraal Kankercentrum Nederland (IKNL), “Incidentie darmkanker.” [Online]. Available: https://iknl.nl/kankersoorten/darmkanker/registratie/incidentie. [Accessed: 10-Apr-2021].

[3] Intergraal Kankercentrum Nederland (IKNL), “Overleving darmkanker.” [Online]. Available: https://iknl.nl/kankersoorten/darmkanker/registratie/overleving. [Accessed: 10-Apr-2021].

[4] Intergraal Kankercentrum Nederland (IKNL), “Sterfte darmkanker.” [Online]. Available: https://iknl.nl/kankersoorten/darmkanker/registratie/sterfte. [Accessed: 10-Apr-2021].

[5] P. Kumar and M. Clark, *Clinical Medicine*, Eight edit. Saunders, 2012.

[6] NVVH, “Colorectaal carcinoom (CRC),” *Richtlijnendatabase*, 2019. [Online]. Available: https://richtlijnendatabase.nl/richtlijn/colorectaal_carcinoom_crc/startpagina_-_crc.html. [Accessed: 29-Mar-2021].

[7] P. Rawla, T. Sunkara, and A. Barsouk, “Epidemiology of colorectal cancer: Incidence, mortality, survival, and risk factors,” *Prz. Gastroenterol.*, vol. 14, no. 2, pp. 89–103, 2019.

[8] Intergraal Kankercentrum Nederland (IKNL), “Behandeling darmkanker.” [Online]. Available: https://iknl.nl/kankersoorten/darmkanker/registratie/behandeling. [Accessed: 10-Apr-2021].

[9] R. Veldkamp *et al.*, “Laparoscopic surgery versus open surgery for colon cancer: Short-term outcomes of a randomised trial,” *Lancet Oncol.*, vol. 6, no. 7, pp. 477–484, Jul. 2005.

[10] H. J. Bonjer *et al.*, “A Randomized Trial of Laparoscopic versus Open Surgery for Rectal Cancer,” *N. Engl. J. Med.*, vol. 372, no. 14, pp. 1324–1332, 2015.

[11] DRCA, “Internationale vergelijking nationale darmkankeraudits,” *DICA*, 2017. [Online]. Available: https://dica.nl/jaarrapportage-2017/dcra. [Accessed: 15-Apr-2021].

[12] C. G. C. Pales, S. An, J. P. Cruz, K. Kim, and Y. Kim, “Postoperative bowel function after anal sphincter-

preserving rectal cancer surgery: Risks factors, diagnostic modalities, and management," *Annals of Coloproctology*, vol. 35, no. 4. Korean Society of Coloproctology, pp. 160–166, 2019.

[13] W. S. Lee *et al.*, "Risk factors and clinical outcome for anastomotic leakage after total mesorectal excision for rectal cancer," *World J. Surg.*, vol. 32, no. 6, pp. 1124–1129, Jun. 2008.

[14] A. S. Rickles *et al.*, "Rickles (2015) - High rate of positive circumferential resection margins following rectal cancer surgery.pdf," *Ann. Surg.*, vol. 262, no. 6, pp. 891–898, 2015.

[15] I. J. Adam *et al.*, "Role of circumferential margin involvement in the local recurrence of rectal cancer," *Lancet*, vol. 344, no. 8924, pp. 707–711, 1994.

[16] T. Nishikawa *et al.*, "Multivisceral resections for locally advanced colorectal cancer after preoperative treatment," *Mol. Clin. Oncol.*, pp. 493–498, Jan. 2018.

[17] J. Nijkamp *et al.*, "Prospective study on image-guided navigation surgery for pelvic malignancies," *J. Surg. Oncol.*, vol. 119, no. 4, pp. 510–517, Mar. 2019.

[18] E. N. D. Kok *et al.*, "Accurate surgical navigation with real-time tumor tracking in cancer surgery," *npj Precis. Oncol.*, vol. 4, no. 8, pp. 1–7, 2020.

[19] R. Eppenga, K. Kuhlmann, T. Ruers, and J. Nijkamp, "Accuracy assessment of wireless transponder tracking in the operating room environment," *Int. J. Comput. Assist. Radiol. Surg.*, vol. 13, no. 12, pp. 1937–1948, 2018.

[20] A. M. Franz *et al.*, "Standardized accuracy assessment of the calypso wireless transponder tracking system," *Phys. Med. Biol.*, vol. 59, no. 22, pp. 6797–6810, 2014.

[21] S. I. Patel, M. J. Souter, D. S. Warner, and M. A. Warner, "Equipment-related Electrocardiographic Artifacts," *Anesthesiology*, vol. 108, no. 1, pp. 138–148, 2008.

[22] K. Hodges, "IEC/EN 60601-1-2 Implications of the 4th edition- White Paper," Apr. 2018.

[23] International Commision on non-ionizing radiation protection (ICNIRP), "Guidlines for Limiting Exposure to Electromagnetic Fields (100 KHZ TO 300 GHZ)," *Health Phys.*, vol. 118, no. 5, pp. 483–524, 2020.

Chapter 2: Background

Background

Medical Background

Anatomy

The rectum, together with the anus, is the distal part of the large intestine and therefore the gastrointestinal tract. Passing through the pelvic floor, the rectum connects the sigmoid colon to the anus. Where the whole rectum lies extraperitoneal, the first part lies posterior to the peritoneum while the later part lies sub peritoneal. The rectum can be macroscopically distinguished from the colon by the absence of omental appendices, taenia coli and haustra. The sacral and anorectal flexure define the shape of the rectum and contribute to fecal continence. Furthermore, transverse folds in the internal rectum wall form three additional flexures, the superior, intermediate and inferior flexure also known as the valves of Houston, see Figure 1. The rectal wall itself is built up of an inner mucosal layer followed by submucosal, muscle and serous layers [1]. Since the rectum is the most distal part of the gastrointestinal tract before the anus, its function is to store the faces before excretion through the anal canal [2].

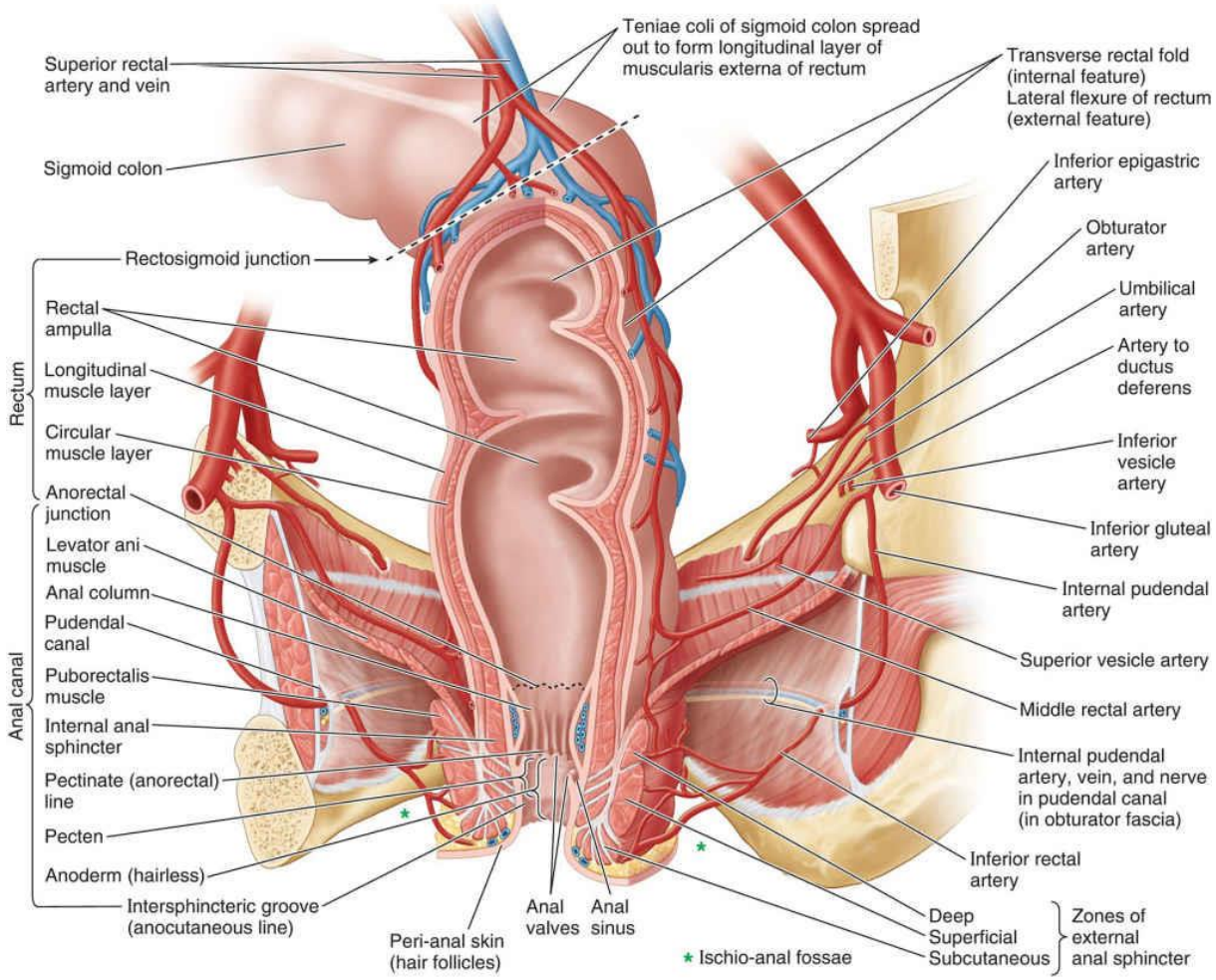

Figure 1 Posterior view of anterior pelvis, including the rectum and anal canal [2].

Vascularization and Innervation

The rectum is supplied of blood by three main arteries, the superior, middle and inferior rectal arteries. The superior rectal artery is the terminal continuation of the inferior mesenteric artery, whereas the middle rectal arty is a branch of the internal iliac artery and the inferior rectal artery is a branch of the internal pudendal artery, see Figure

1. The rectum is drained via the corresponding superior, middle and inferior rectal veins. The superior rectal vein empties into the portal venous system via the inferior mesenteric vein. The latter two rectal veins empty into the systemic venous system. The rectal venous plexus is drained by all three of the rectal veins and enables

communication between the portal and systemic systems. The rectal plexus is located directly proximal to the anal orifice. Lymph is drained from the rectum via the internal iliac and pararectal lymph nodes. The later drains into the inferior mesenteric lymph nodes, see Figure 2 [2], [3].

The rectum is both innervated by the sympathetic and parasympathetic system. Parasympathetic signals are conveyed from the S2-4 spinal cord level via pelvic splanchnic nerves and the pelvic plexus. Sympathetic innervation is supplied via the lumbar splanchnic nerves from T12-L2 and via the Superior rectal nerves and the Superior- and Inferior hypogastric plexus, see Figure 2. Somatic innervation is provided to the anal sphincter by the inferior anal (rectal) nerve, a branch of the pudendal nerve, and originates from S2-4 [2], [3].

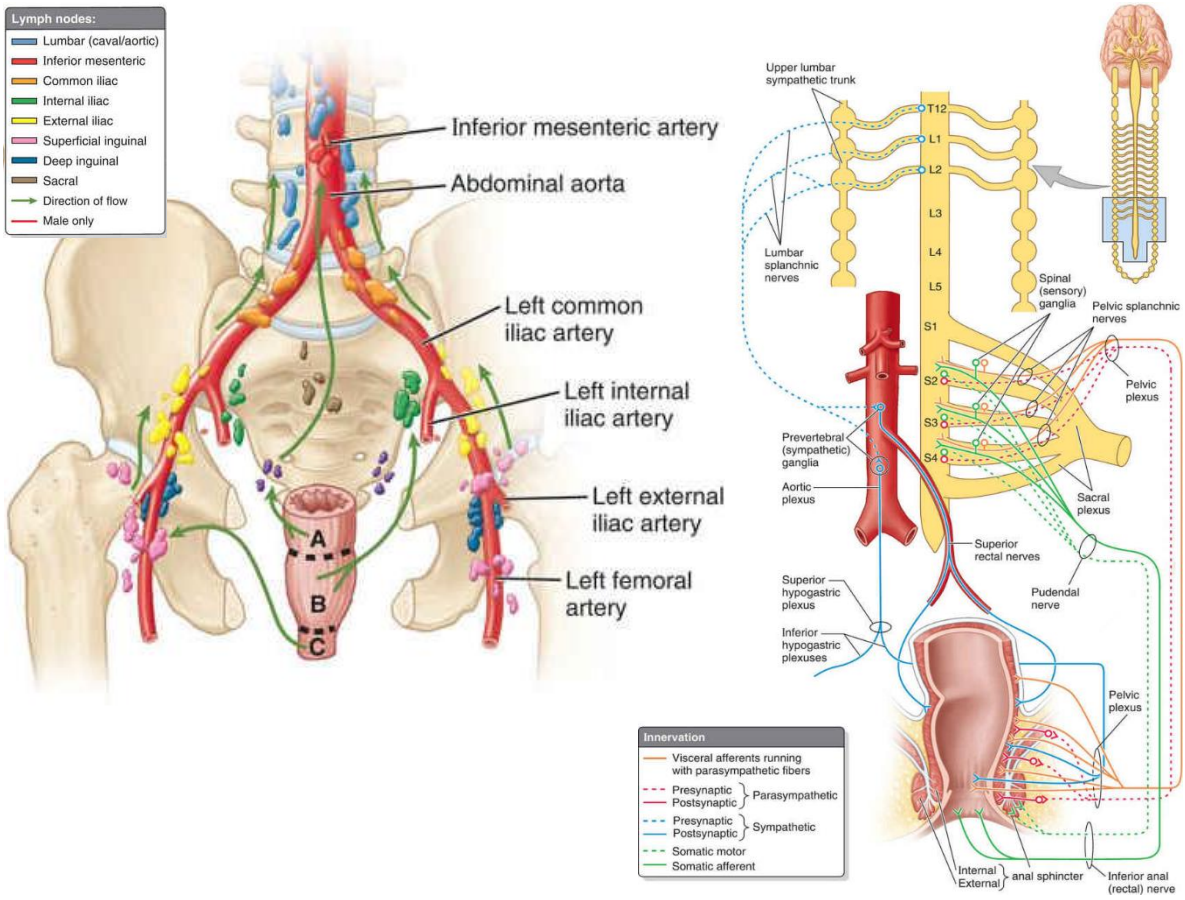

Figure 2 Anterior view of rectal lymphatic system (left). Innervation of the rectum and anal canal (right) [2].

Colorectal and Rectal Cancer

Colorectal cancer is the third most common cancer worldwide in 2018 with an incidence of 1.8 million annually [4]. Colorectal cancer is a common way to describe cancer of the colon, rectum and anus. When exclusively considering rectum cancer, it has an annual incidence of 704,000, ranking eight most common cancer and constituting 3.9 percent of all diagnosed cancers [4], [5].

In the Netherlands colorectal cancer amounts to more than 14.000 diagnosis in 2018, of which 4.500 diagnosis are rectum cancer [6]. Incidence of rectal cancer has more than doubled over the last three decades, while mainly

affecting older patients. More than 47% of patients are 70 years or older at time of diagnosis, while only 26% of patients is younger than 60 at diagnosis [6].

Survival rates of rectal cancer depend greatly on the stage at diagnosis with a 91% 5-year survival for stage I, dropping to 13% in stage IV [7]. Since 18% of new diagnosis are stage IV, rectal cancer contributes to more than 1000 deaths a year in the Netherlands [8]. However, 5-year survival rates have been increasing in the last decades due to advances in diagnostics and treatment of the disease.

There are multiple types of tumors which can originate in the rectum, including: carcinoid, gastrointestinal stromal tumors, lymphomas and sarcomas [9]. However, the single most prominent malignancy of the rectum is adenocarcinoma. Rectal adenocarcinomas originate in the mucosa of the rectal wall. Risk factors for this type of cancer include age, prior colorectal cancer, ulcerative colitis, crohn disease, genetic factors and dietary factors [9]. Furthermore, in 85% of cases at least eight to ten mutational events must accumulate before the disease reaches an invasive and metastatic potential. These mutations could involve: the APC gene, Ras oncogene, DCC gene and p53 tumor suppressor gene [1], [9].

Diagnosis and Staging

Rectal cancer presents with symptoms, such as a change in bowel habits, tenesmus, anaemic symptoms and the addition of blood or mucus to the stool [1]. When a patient presents with these symptoms, a digital rectal examination is essential and a colonoscopy is indicated [1], [10]. During this colonoscopy, which is the gold standard diagnostic test, a biopsy can be taken for histological conformation of malignancy. After conformation of a rectal tumor, the tumor grade and stadium is determined based on the TNM staging system, see Table 1 and Table 2 [11]. The primary tumor stage is determined using Magnetic Resonance Imaging (MRI) with Diffusion Weighted Imaging (DWI). Where MRI, Computed Tomography (CT) and Positron Emission Tomography (PET) can be utilized to examine local spread and lymphatic or distant metastases [1], [10]. A tumor is classified as a rectum tumor when the distal part is located distal of the sigmoid takeoff.

Table 1 TNM classification of colorectal tumor as described by the Union for International Cancer Control [11].

TNM Grade	Description according to grade
T1	Tumor invades the lamina propria or submucosa, ≤ 2 cm
T2	Tumor invades the muscularis propria, or > 2 cm
T3	Tumor invades the serosa or the perirectal tissue
T4	Tumor perforates the serosa or invades adjacent structures
T4a	Tumor invades nearby structures (other parts of colon or other organs)
T4b	Tumor perforates the serosa
N0	No lymph nodes containing tumor cells
N1	1-3 lymph nodes with tumor cells
N2	>3 lymph nodes with tumor cells
M0	No metastases to distant organs
M1	Metastases to distant organs
M1a	Metastases confined to one organ without peritoneal metastases
M1b	Metastasis in more than one organ
M1c	Metastasis to the peritoneum with or without other organ involvement

Table 2 Tumor stadium based on TNM classification. Tx and Nx involve all T- and N stages [11].

Stadium	*TNM*	*Description*
I	Tumor in situ, T1-2, N0, M0	Non-advanced tumor without metastases
II	T3-4, N0, M0	Locally advanced tumor without metastases
III	T1-4, N1-2, M0	Tumor with lymph node

		metastases
IV	Tx Nx M1	Tumor with metastases to distant organs

TREATMENT

Treatment of rectum carcinoma depends on several factors such as the stage of cancer, patient condition and patient preferences. The aim of treatment could differ between curative or palliative care. Worldwide, surgery is the primary curative option in non-metastasized rectal cancer, which accounts for 75% of all diagnoses [5]. In the Netherlands, as much as 95% of patients with stadium I-III rectal cancer get surgical treatment. For stadium II and III rectal cancer, 76% of patients received additional neoadjuvant radiotherapy and in 43% of cases also chemotherapy was given [12].

During surgical treatment, a total mesorectal excision (TME) is performed, which has been an important step forward in surgery of rectal carcinoma. By following the anatomical planes along the pelvic wall and organs, an excision can be achieved without damage to the rectal wall or the tumor. Since most resectable rectal carcinomas and potentially affected lymph nodes are located inside these mesorectal resection planes, a radical operation can be performed using this technique [10], [13].

The surgical procedure can be performed using an open or laparoscopic approach. A laparoscopic approach is widely used and accounts for 82% of colorectal surgery in the Netherlands in 2015 [14]. Laparoscopic surgery is associated with less blood loss, decreased pain and overall faster recovery, while no significant differences in postoperative mortality, morbidity and anastomotic leakage were found when compared to conventional open approach. However, laparoscopic surgery is associated with longer operations, long learning curve and higher costs. Studies on long term results have not yielded any significant differences [15], [16].

Rectal cancer surgery is commonly performed using the Low anterior resection (LAR) or Abdominoperineal Resection (APR) in combination with the aforementioned TME concept. APR surgery, where both rectum and anus are resected as can be seen in Figure 3, is performed when the distal border of the tumor is located close - order: cm - or inside of the anal sphincter. An LAR, where the rectum is resected after which the colon is attached to the anus, can be performed when a coloanal anastomosis is a surgical option and is usually preferred to APR since it will prevent a permanent colostomy [10]. However, this coloanal anastomosis is subject to anastomotic leakage in approximately 10% of patients, with increased risk for older patients or patients suffering from serious comorbidity. Furthermore, major bowel-, urinary-, and sexual dysfunctions, also known as LAR Syndrome (LARS), are experienced by 30%–80% patients after a LAR [17]. Due to these complications, studies indicate no clinically relevant or significant difference in Quality of Life between both interventions [18], [19].

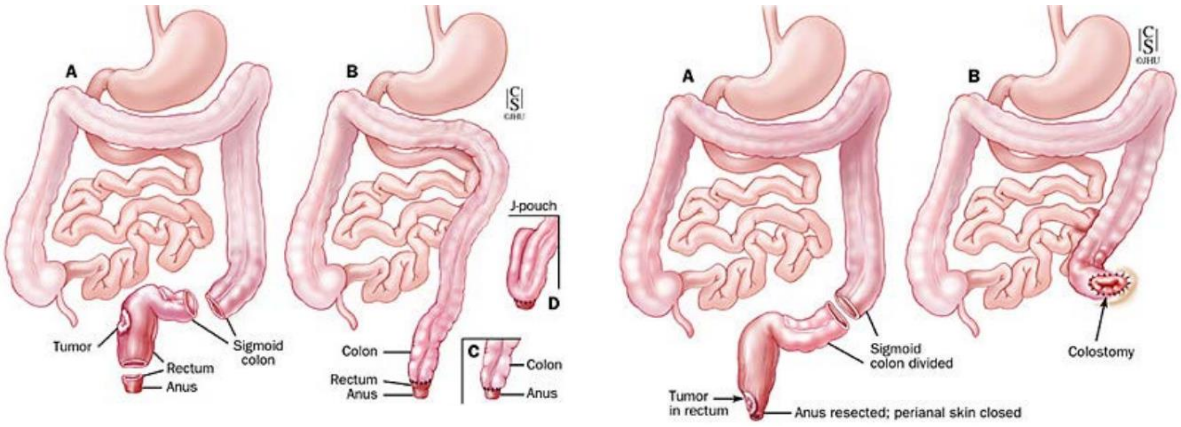

Figure 3 Surgical resection of a rectal tumor by (A) LAR and (B) APR [45].

CLINICAL PROBLEM

For oncological outcome, tumor localization and consequent margin assessment – i.e. distal, proximal and circumferential margin - is essential, since positive resection margin rates of 10-15% are observed after laparoscopic

rectal cancer surgery [20], [21], associated with local recurrence and overall poor survival [22]. During surgery, the surgeon must locate the tumor based on images of the laparoscopic camera in the narrow space of the pelvis without the possibility of intraoperative palpation. This is especially challenging when the target area is threatened and anatomical planes are disturbed due to the tumor ingrowth, previous surgery or fibrosis resulting from neoadjuvant radiotherapy [23]. On the other hand, an important risk factor for both anastomotic leakage and LARS is a low level of anastomosis [17], [24]. The level of anastomosis is based on the tumor location and distal resection margin. Therefore, tumor localization and intraoperative assessment of this margin can have direct and severe consequences on functional outcome.

Concluding, during laparoscopic rectal cancer surgery, tumor localization and consequent margin assessment are crucial for both oncological and functional outcome. To aid the surgeon in this challenging task, image guided surgery (IGS) is proposed. During IGS, preoperative imaging, showing relevant anatomy and the surgical target, is used to guide a surgeon during the intervention using tracked surgical instruments.

Technical background

The use of image guided surgery (IGS) has evolved rapidly over the past decades. Basically, preoperative imaging, such as MRI- and CT-scans, is made available for intraoperative guidance, allowing for planning an optimal approach, anticipate on the presence of critical anatomical structures and potentially increase surgical accuracy. Initially, IGS was adopted for Neuro, Head- and Neck- and Orthopedic procedures, since in these cases the surgical target area is somewhat rigid. As a result, tracking the anatomy is relatively simple, resulting in accurate implant placement and higher rates of complete tumor removal in oncological procedures [25], [26]. Besides these applications, IGS could be of great benefit to surgical procedures performed in non-rigid target areas.

Fundamentals of Tracking Systems in Surgery

All surgical navigation applications rely on an accurate tracking system to continuously monitor the pose of a sensor in a specified field of view (FOV). A pose represents an object in a three-dimensional (3D) space, giving the 3 degree of freedom (DOF) position – i.e. [x, y, z] - and 3DOF rotation, multiple representations are possible, e.g. rotation matrices and quaternions. A convenient method of representing the pose of an object is a transformation matrix: $T = \begin{bmatrix} R & t \\ 0 & 1 \end{bmatrix}$, where R is the rotation matrix and t is the position of the object . The cascading and inversion properties make this representation useful for surgical navigation.

A

B

Figure 4 Tracking systems for use in surgery. (A) The NDI Polaris spectra OTS (B) The NDI Aurora EMTS TTFG (left) and planar field generator (right) [43], [44].

Two main tracking systems can be distinguished for tracking during surgery, namely optical tracking systems (OTS) and electromagnetic tracking systems (EMTS). In OTS approaches a stereo view camera, such as the NDI Polaris spectra seen in Figure 4, is used to identify optical markers, commonly in a 4-marker configuration, and triangulate its pose. As seen Table 3, the optical markers are wireless and can be tracked with high accuracy - <0.17 mm -, however a direct line of sight to all optical markers is needed which is not feasible in lower abdominal surgery [26]. Contrarily, EMTS does not require a direct line of sight since it estimates the pose of sensors based on a known alternating electromagnetic field generated by a field generator (FG). A frequently used EMTS is the Northern

Digital Aurora system (Northern Digital Inc, Waterloo, Ontario, Canada), which is compatible with multiple FG's, such as the tabletop field generator (TTFG) and the planar FG, see figure 4.

Commonly, EM sensors use inductors to measure magnetic flux over time, subsequently the correlation between the magnetic flux and the distance to the source of the known field is the basis of pose estimation methods. Since the pose estimation methods rely on the accuracy of the known field, distortion of the electromagnetic field can cause tracking inaccuracies. There are three major sources of distortions in a magnetic field, being [27]:

- Ferromagnetic materials
- Eddy currents in conductive materials, induced by the magnetic field itself
- External currents inside the magnetic field, e.g. electronic devices

Hummel et al. [28] and Franz et al. [29] showed distortion effects of metallic cylinders on EMTS with positional errors up to 3.2 mm for the Calypso system (Varian Medical Systems Inc., USA), up to 4.2 mm for the NDI Aurora system (Northern Digital Inc, Canada) and up to 80 mm for the Ascension microBIRD (Ascension Technology Corp., USA). During an operation, multiple instruments and devices are used which could cause these distortions.

Table 3 Accuracy and limitations of Calypso EMST, NDI Aurora EMTS and NDI Polaris spectra OTS [29] [30].

Tracking system	Trueness	Precision	Direct line of sight needed	Wireless
Calypso system	0.1 mm	0.3 mm		Yes
NDI Aurora TTFG	0.4 mm	0.1 mm		
NDI Polaris spectra	0.2 mm	0.0 mm	Yes	Yes

Surgical Navigation at the NKI

At the Netherlands Cancer Institute (NKI), an IGS navigation technique has been developed and is currently applied as standard care for open tumor surgery in the lower abdominal and pelvic area [31], [32]. Here, contrast-enhanced CT-scans are acquired preoperatively and combined with other imaging data of the patient to create a 3D model of anatomical structure, such as bone, arteries, veins, ureters, nerves, lymph nodes and the tumor. The current navigation technique relies on the use of an EMTS to register the preoperative imaging to the intraoperative setting. Therefore, patient sensors are placed intraoperatively on the skin of the patient, one at the level of the anterior superior iliac spine and two at the spine in the lumbar curvature, and a subsequent cone beam CT (CBCT) is

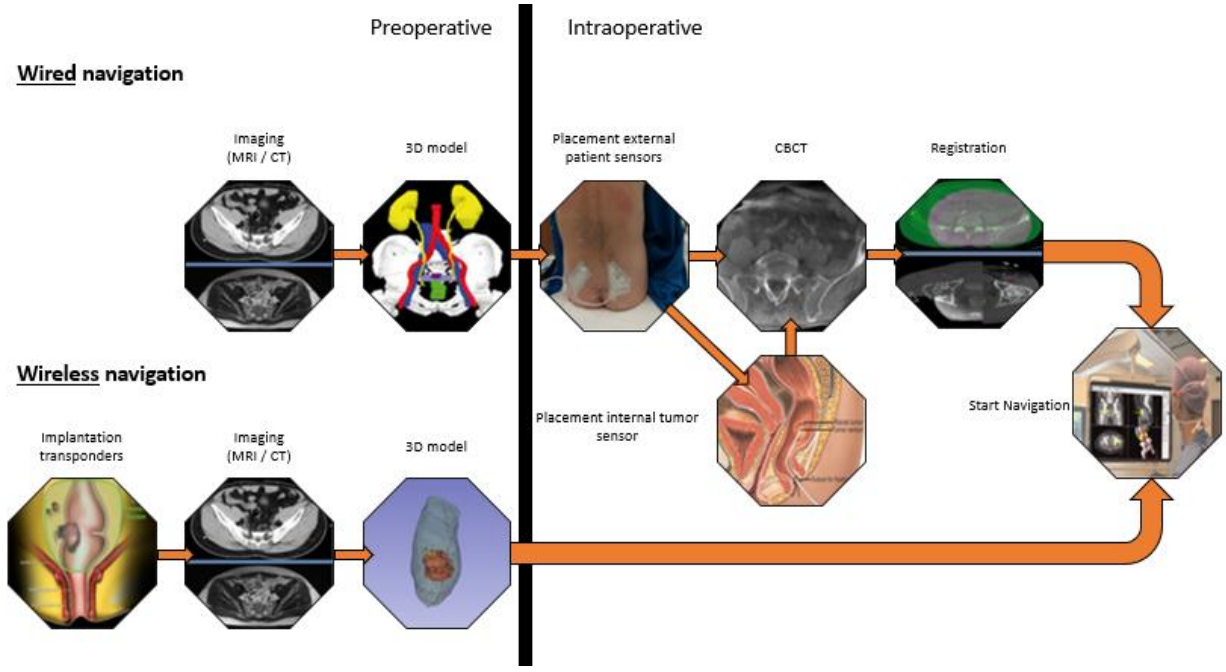

Figure 5 Workflow diagram of preoperative and intraoperative steps before start of navigation for current wired approach, including additional tumor sensor placement as implemented by Kok et al., and our proposed wireless navigation approach.

acquired, see Figure 5. In addition to the patient sensors, a surgical pointer or tools can be tracked by the EMTS. As shown in Figure 6, the intraoperative navigation user interface shows the position of the pointer in three orthogonal slices of the CT and in the 3D model. The surgeon can use the pointer and user interface for spatial orientation in the 3D model and correlation to the intraoperative setting.

Limitations of Current Navigation Setup

The surgical navigation setup, which is currently applied as standard care in the NKI, has two main limitations:

- Relative movement between patient sensors and target area
- Registration using CBCT

First, comparable to previous applications of IGS, accuracy of this surgical navigation technique hinges on a central assumption, being the rigid relation of the patient sensors, placed on the skin, and the tracked anatomical structures. There are to two types of errors impacting this assumption and therefore navigation accuracy. First, assuming rigidity of the surgical target area, the position of one or more of the patient sensors may change intraoperatively, for example by repositioning of the patient, tilt of the operating table into Trendelenburg, or skin incision and retractor placement. Currently, manual sensor position corrections are made to adjust for these errors. Second, assuming rigidity of the patient sensors, the position of anatomical structures may change. Most anatomical structures - e.g. vessel or lymph nodes - in the pelvis lay relatively rigid due to a close relation to pelvic bones and fascia. However, during rectal cancer surgery – i.e. TME – dissection of the tumor and mesorectum causes them to mobilize. A recent study by Kok et al. tried to solve this, next to tracking of surrounding structures using patient sensor on the skin, by placement of an additional EM sensor on the tumor using a proctoscope, resulting in a feasible, safe and accurate workflow [33].

Second, the workflow as proposed by Kok et al. showed high accuracies in tracking a mobilized rectum, however CBCT registration was still needed due to intraoperative placement of wired EM sensors. This CBCT is acquired to correlate the tumor- and patient sensors to the patient's anatomy. During acquisition, the patient receives additional radiation dose and surgical workflow is interrupted, since all surgical staff is required to leave the OR. Furthermore, a hybrid OR is needed hindering broader implementation of surgical navigation techniques.

In this study, we propose a novel wireless electromagnetic tracking setup for surgical navigation. Here, wireless transponders can be implanted preoperatively, enabling preoperative registration and eliminating the need for

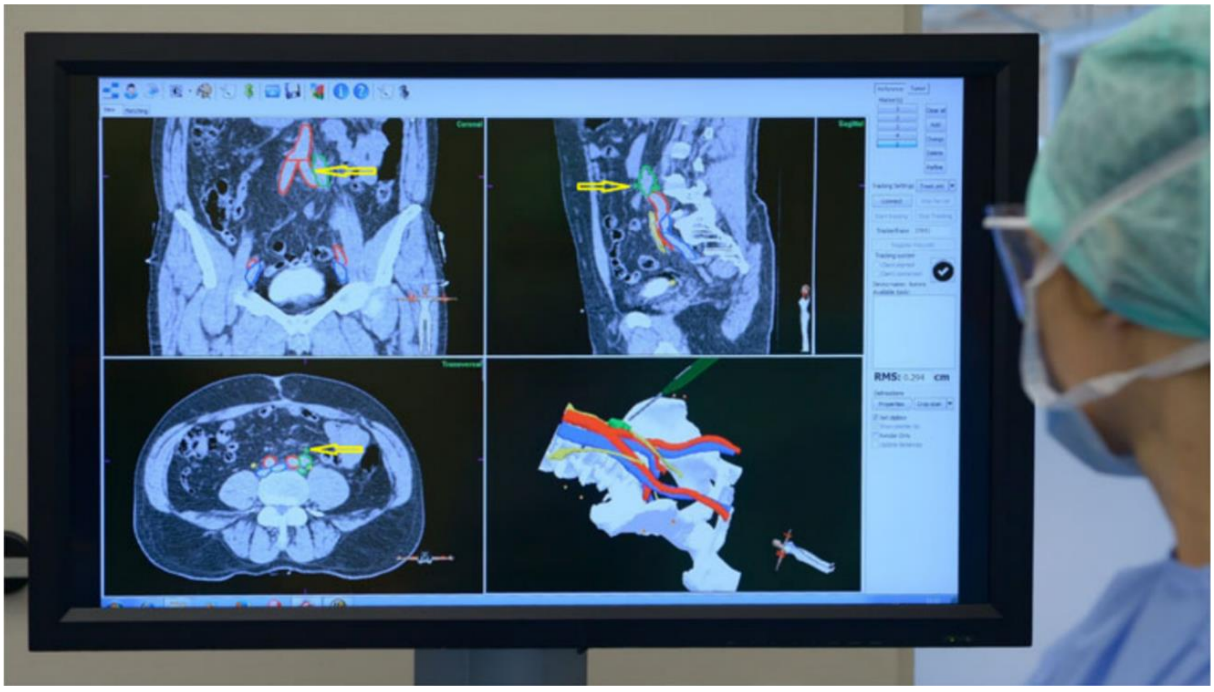

Figure 6 Intraoperative user interface of surgical navigation system at the NKI [33].

intraoperative CBCT imaging. Therefore, overcoming the limitations of the earlier wired EM tracking approaches for accurate navigation in rectal surgery [33]. This setup will allow for real-time tumor tracking and enable utilization of pre-operative imaging during surgery. The wireless EM tracking system, incorporated in the setup, has shown sub millimeter accuracy in both laboratory, radiotherapy and operation room (OR) environments [29], [34]. Comparable to the approach of Kok et al. wireless EM sensors can be implanted near the tumor for tracking of a mobilized rectum.

WIRELESS NAVIGATION SETUP

The proposed wireless navigation setup consists of multiple hardware components:

- Calypso's GPS for the Body®
- Implantable Beacon® Transponders
- Wireless tracked laparoscopic pointer
- Wireless tracked laparoscopic stapler
- Readout system

A B C

Figure 7 Overview of the components of wireless navigation setup: (A) Calypso GPS for the Body® Tracking system, (B) Wireless Beacon® Transponder, (C) Readout system on Navigation Trolley [42].

The readout system (Quad core 3.20 GHz Intel® Xeon® E-2104G with 16GB memory) is used for processing of the tracking data and visualization of the navigation using 3D Slicer and the "Image-guided navigation toolkit for 3D Slicer (SlicerIGT)" [35]. The setup incorporates the Calypso's GPS for the Body® system, see Figure 7, (Varian Medical Systems Inc., Palo Alto, California, USA) a readily available wireless EMTS developed for radiotherapy application. The clinical system can track a maximum of three 3DOF implantable wireless Beacon transponders with different excitation frequencies – i.e. 300, 400, 500 kHz -, a diameter of 1.85 mm and are 8 mm long. In the NKI, a modified research version was delivered by Varian that can be used in an operating room environment. Contrary to the clinical system, this research version allows for readout of a 5DOF transponder pose and extension of the field of view (eFOV; 27.5, 27.5, 22.5 cm), starting at 5.5 cm offset from the TA. The x- and y- axes of the eFOV define a parallel plane with regard to the TA while the z-axis is perpendicular, pointing away from the TA. The transponders inside the eFOV are excited at characteristic frequencies using an excitation signal generated by alternating current magnetic field, inducing a current in the transponder coil. Subsequently, the tracking system determines the 5DOF pose - position and orientation - based on the magnetic flux produced by transponder, which is sensed using a separate array of sensor coils inside the TA. The resulting transponder location can be determined with a trueness of 0.1 mm and precision 0.3 mm, see Table 3. Furthermore, Eppenga et al. concluded that two 5DOF beacon transponders can be combined into 6DOF virtual transponder and can be used to accurately track both position and orientation of a tumor during surgery [36].

The intraoperative tools – i.e. laparoscopic pointer and laparoscopic stapler - were developed in-house for use in *ex vivo* and *in vivo* experiments. The laparoscopic pointer, see Figure 8, consists of a polyoxymethylene shaft and cap of approximately 40 cm. A beacon transponder is positioned in the pointer cap, approximately 1 cm from the tip of pointer to minimize influence of orientation errors. The pointer can be used intraoperatively for spatial orientation in the 3D model and for localizing the tumor. Furthermore, it can be used to save the position or distance of surgical clips with respect to the tumor, by placing the tip of the pointer at the clip.

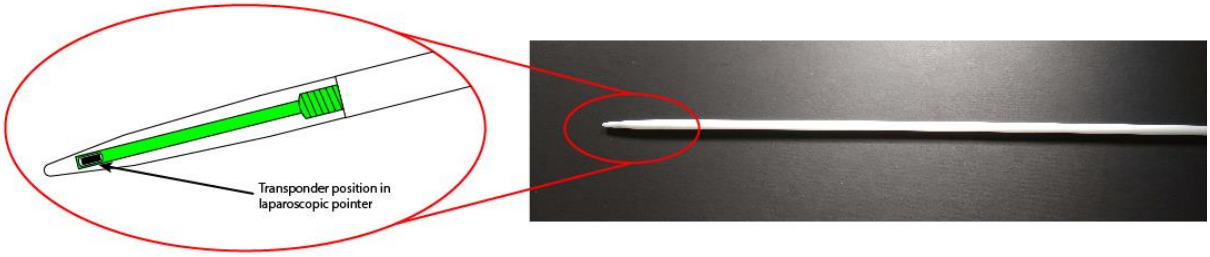

Figure 8 Wireless tracked laparoscopic pointer (right) and a schematic of design and transponder position (left).

The laparoscopic stapler is a Powered Echelon™ surgical stapler (Echelon Flex, Johnson & Johnson) with an in-house modified GST reload to fit a Beacon transponder. Since the transponders can be tracked in 5DOF, this tool is designed to track the stapler plane as illustrated in Figure 9. When placing the surgical stapler over the rectum during surgery, this allows the surgeon to determine the distance of this plane to the tumor and therefore aid in the estimation of the resection margin.

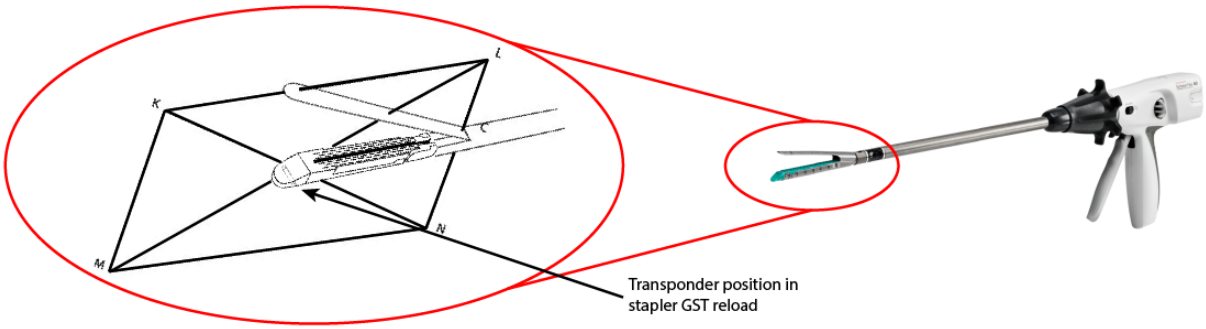

Figure 9 Wireless tracked laparoscopic stapler (right) and a schematic of the GST reload, transponder position and resulting tracked stapler plane KLMN (left).

Limitations of Wireless Navigation Setup

The main constraint of the wireless navigation setup is that the Calypso tracking system is limited to three transponders. In a surgical setting, one transponder is needed for use in a tracked surgical tool, e.g. Pointer or Stapler, and two sensors are available for 6DOF tumor tracking. Therefore, the setup, in contrast to the wired approach, is not able to track any surrounding structures, limiting the spatial orientation in the 3D model and correlation to the intraoperative setting by the surgeon.

The TTV sensor fusion algorithm based on data of two 5DOF transponders, as determined by the Calypso system, is accurate as shown by Eppenga et al. [36]. However, a z-axis direction reverse (ZDR) of the single 5DOF transponders is observed at specific positions and orientations in the eFOV. However, for sensor fusion into a 6DOF virtual transponder and visualization of the tracked tool, both accurate and stable 5DOF information is needed. Consequently, a detection and correction method is needed in order to cope with the ZDR.

Finally, there is some uncertainty surrounding the use of the Calypso system in the OR environment. For example, the transponders are designed for placement in prostate tissue before radiotherapy. Here, the system has demonstrated accurate target localization and allows reduction of irradiated volumes and facilitate safe dose escalation [37], [38]. It is unclear whether placement of the transponders in the rectal wall will yield the stability

needed for intraoperative navigation. Furthermore, promising results have been published for use of this system in the operating room, outlining sub millimeter accuracy and acceptable distortion effects of metallic cylinders (< 3.2 mm) on tracking accuracy in this proposed environment [29], [34]. However, distortion effects of surgical instruments or surgical robotics remain unclear. Furthermore, while Electromagnetic interference (EMI) is a relatively common issue in the OR [39]–[41], no information is published on EMI of EMTS on surrounding equipment.

Research Aim

The aim of this study is: to investigate the safety, accuracy and usability of a wireless surgical navigation setup for real-time rectal tumor tracking in laparoscopic rectal cancer surgery.

First, a standardized accuracy and distortion assessment of the Calypso wireless electromagnetic transponder tracking system is performed. Second, the potential EM interference of the Calypso system on critical operation room equipment is functionally assessed. Third, software for the navigation setup is developed and subsequently tested on usability and accuracy following the proposed intraoperative workflow on a phantom. Fourth, the influence of potential transponder migration and tissue deformation on the relative stability of transponders with respect to a rectal tumor is assessed in a rectal excision specimen. Last, as future outlook the influence of distortion by a da Vinci surgical system on the tracking accuracy of electromagnetic tracking systems is assessed.

REFERENCES

[1] P. Kumar and M. Clark, *Clinical Medicine*, Eight edit. Saunders, 2012.

[2] A. M. R. . Moore, Keith L.; Dalley, Arthur F.; Agur, K. Moore, A. Dalley, and A. Agur, *Clinically Oriented Anatomy*, Seventh ed. Baltimore: Wolters Kluwer, 2014.

[3] A. Agur and A. Dalley, *Grant's Atlas of Anatomy*, Thirteenth. Wolters Kluwer, 2013.

[4] F. Bray, J. Ferlay, I. Soerjomataram, R. L. Siegel, L. A. Torre, and A. Jemal, "Global cancer statistics 2018: GLOBOCAN estimates of incidence and mortality worldwide for 36 cancers in 185 countries," *CA. Cancer J. Clin.*, vol. 68, no. 6, pp. 394–424, Nov. 2018.

[5] P. Rawla, T. Sunkara, and A. Barsouk, "Epidemiology of colorectal cancer: Incidence, mortality, survival, and risk factors," *Prz. Gastroenterol.*, vol. 14, no. 2, pp. 89–103, 2019.

[6] Intergraal Kankercentrum Nederland (IKNL), "Incidentie darmkanker." [Online]. Available: https://iknl.nl/kankersoorten/darmkanker/registratie/incidentie. [Accessed: 10-Apr-2021].

[7] Intergraal Kankercentrum Nederland (IKNL), "Overleving darmkanker." [Online]. Available: https://iknl.nl/kankersoorten/darmkanker/registratie/overleving. [Accessed: 10-Apr-2021].

[8] NKR, "Sterfte Endeldarmkanker," 2019. [Online]. Available: https://iknl.nl/nkr-cijfers. [Accessed: 14-Apr-2021].

[9] R. Rubin and D. Strayer, *Rubin's Pathology*, Sixth edit. Wolters Kluwer, 2012.

[10] NVVH, "Colorectaal carcinoom (CRC)," *Richtlijnendatabase*, 2019. [Online]. Available: https://richtlijnendatabase.nl/richtlijn/colorectaal_carcinoom_crc/startpagina_-_crc.html. [Accessed: 29-Mar-2021].

[11] C. W. James D. Brierley, Mary K. Gospodarowicz, *TNM Classification of Malignant Tumours*, Eight edit. Wiley, 2016.

[12] Intergraal Kankercentrum Nederland (IKNL), "Behandeling darmkanker." [Online]. Available: https://iknl.nl/kankersoorten/darmkanker/registratie/behandeling. [Accessed: 10-Apr-2021].

[13] "Colorectal cancer NICE guideline," 2020.

[14] DRCA, "Internationale vergelijking nationale darmkankeraudits," *DICA*, 2017. [Online]. Available: https://dica.nl/jaarrapportage-2017/dcra. [Accessed: 15-Apr-2021].

[15] M. M. Reza, J. A. Blasco, E. Andradas, R. Cantero, and J. Mayol, "Systematic review of laparoscopic versus open surgery for colorectal cancer," *British Journal of Surgery*, vol. 93, no. 8. Br J Surg, pp. 921–928, Aug-2006.

[16] S. Vennix *et al.*, "Laparoscopic versus open total mesorectal excision for rectal cancer," *Cochrane Database of Systematic Reviews*, vol. 2014, no. 4. John Wiley and Sons Ltd, 15-Apr-2014.

[17] C. G. C. Pales, S. An, J. P. Cruz, K. Kim, and Y. Kim, "Postoperative bowel function after anal sphincter-preserving rectal cancer surgery: Risks factors, diagnostic modalities, and management," *Annals of Coloproctology*, vol. 35, no. 4. Korean Society of Coloproctology, pp. 160–166, 2019.

[18] J. Pachler and P. Wille-Jørgensen, "Quality of life after rectal resection for cancer, with or without permanent colostomy.," in *Cochrane Database of Systematic Reviews*, no. 2, John Wiley & Sons, Ltd, 2005.

[19] M. G. Guren *et al.*, "Quality of life and functional outcome following anterior or abdominoperineal resection for rectal cancer," *Eur. J. Surg. Oncol.*, vol. 31, no. 7, pp. 735–742, Sep. 2005.

[20] H. J. Bonjer *et al.*, "A Randomized Trial of Laparoscopic versus Open Surgery for Rectal Cancer," *N. Engl. J. Med.*, vol. 372, no. 14, pp. 1324–1332, 2015.

[21] A. S. Rickles *et al.*, "Rickles (2015) - High rate of positive circumferential resection margins following rectal cancer surgery.pdf," *Ann. Surg.*, vol. 262, no. 6, pp. 891–898, 2015.

[22] I. J. Adam *et al.*, "Role of circumferential margin involvement in the local recurrence of rectal cancer," *Lancet*, vol. 344, no. 8924, pp. 707–711, 1994.

[23] T. Nishikawa *et al.*, "Multivisceral resections for locally advanced colorectal cancer after preoperative treatment," *Mol. Clin. Oncol.*, pp. 493–498, Jan. 2018.

[24] W. S. Lee *et al.*, "Risk factors and clinical outcome for anastomotic leakage after total mesorectal excision for rectal cancer," *World J. Surg.*, vol. 32, no. 6, pp. 1124–1129, Jun. 2008.

[25] C. Senft, A. Bink, K. Franz, H. Vatter, T. Gasser, and V. Seifert, "Intraoperative MRI guidance and extent of resection in glioma surgery: A randomised, controlled trial," *Lancet Oncol.*, vol. 12, no. 11, pp. 997–1003, 2011.

[26] M. J. Tormenti, D. B. Kostov, P. A. Gardner, A. S. Kanter, R. M. Spiro, and D. O. Okonkwo, "Intraoperative computed tomography image-guided navigation for posterior thoracolumbar spinal instrumentation in spinal deformity surgery," *Neurosurg. Focus*, vol. 28, no. 3, pp. 1–6, 2010.

[27] A. M. Franz, T. Haidegger, W. Birkfellner, K. Cleary, T. M. Peters, and L. Maier-Hein, "Electromagnetic

tracking in medicine -A review of technology, validation, and applications," *IEEE Trans. Med. Imaging*, vol. 33, no. 8, pp. 1702–1725, 2014.
[28] J. B. Hummel *et al.*, "Design and application of an assessment protocol for electromagnetic tracking systems," *Med. Phys.*, vol. 32, no. 7, pp. 2371–2379, 2005.
[29] A. M. Franz *et al.*, "Standardized accuracy assessment of the calypso wireless transponder tracking system," *Phys. Med. Biol.*, vol. 59, no. 22, pp. 6797–6810, 2014.
[30] R. Elfring, M. de la Fuente, and K. Radermacher, "Assessment of optical localizer accuracy for computer aided surgery systems," *Comput. Aided Surg.*, vol. 15, no. 1–3, pp. 1–12, Feb. 2010.
[31] J. Nijkamp *et al.*, "Prospective study on image-guided navigation surgery for pelvic malignancies," *J. Surg. Oncol.*, vol. 119, no. 4, pp. 510–517, Mar. 2019.
[32] G. Delso, A. Martinez-Möller, R. A. Bundschuh, S. G. Nekolla, and S. I. Ziegler, "The effect of limited MR field of view in MR/PET attenuation correction," *Med. Phys.*, vol. 37, no. 6, pp. 2804–2812, 2010.
[33] E. N. D. Kok *et al.*, "Accurate surgical navigation with real-time tumor tracking in cancer surgery," *npj Precis. Oncol.*, vol. 4, no. 8, pp. 1–7, 2020.
[34] R. Eppenga, K. Kuhlmann, T. Ruers, and J. Nijkamp, "Accuracy assessment of wireless transponder tracking in the operating room environment," *Int. J. Comput. Assist. Radiol. Surg.*, vol. 13, no. 12, pp. 1937–1948, 2018.
[35] A. Fedorov *et al.*, "3D Slicer as an Image Computing Platform for the Quantitative Imaging Network," *Magn Reson Imaging*, vol. 30, no. 9, pp. 1323–1341, 2012.
[36] R. Eppenga, K. Kuhlmann, T. Ruers, and J. Nijkamp, "Accuracy assessment of target tracking using two 5-degrees-of-freedom wireless transponders," *Int. J. Comput. Assist. Radiol. Surg.*, vol. 15, no. 2, pp. 369–377, 2019.
[37] T. R. Willoughby *et al.*, "Target localization and real-time tracking using the Calypso 4D localization system in patients with localized prostate cancer," *Int. J. Radiat. Oncol. Biol. Phys.*, vol. 65, no. 2, pp. 528–534, Jun. 2006.
[38] J. A. Tanyi *et al.*, "Assessment of planning target volume margins for intensity-modulated radiotherapy of the prostate gland: Role of daily inter- and intrafraction motion," *Int. J. Radiat. Oncol. Biol. Phys.*, vol. 78, no. 5, pp. 1579–1585, Dec. 2010.
[39] S. I. Patel, M. J. Souter, D. S. Warner, and M. A. Warner, "Equipment-related Electrocardiographic Artifacts," *Anesthesiology*, vol. 108, no. 1, pp. 138–148, 2008.
[40] K. Hodges, "IEC/EN 60601-1-2 Implications of the 4th edition- White Paper," Apr. 2018.
[41] International Commision on non-ionizing radiation protection (ICNIRP), "Guidlines for Limiting Exposure to Electromagnetic Fields (100 KHZ TO 300 GHZ)," *Health Phys.*, vol. 118, no. 5, pp. 483–524, 2020.
[42] Varian Medical Systems Inc., "Calypso," 2021. [Online]. Available: https://www.varian.com/products/radiotherapy/real-time-tracking-motion-management/calypso. [Accessed: 03-May-2021].
[43] Northern Digital Inc., "Aurora Field Generators." [Online]. Available: https://www.ndigital.com/products/aurora/aurora-field-generators/. [Accessed: 04-Sep-2020].
[44] "Neuronavigation Product Catalog PowerMAG View! Content Content."
[45] M. A. Choti, "Management of Rectal Cancer," Baltimore.

Chapter 3: Accuracy Assessment of Wireless Navigation Setup

Accuracy Assessment of Wireless Navigation Setup

Standardized accuracy and distortion assessment of the Calypso wireless electromagnetic transponder tracking system for use in laparoscopic rectal cancer surgery.

I. INTRODUCTION

Rectal cancer is the eight most common cancer worldwide with an annual incidence of 704,000, constituting 3.9 percent of all diagnosed cancers [1]. Worldwide, surgery is the primary curative option in non-metastasized rectal cancer, which accounts for 75% of all diagnoses [2]. In the Netherlands, as much as 95% of patients with stadium I-III rectal cancer get surgical treatment [3]. In recent decades, laparoscopic surgery has progressively replaced open rectal surgery due to favorable short-term outcomes, such as less pain, reduced blood loss, and improved recovery time [4], [5]. However, laparoscopic rectal cancer surgery is associated with positive resection margin rates of 10-15% [5], [6], while larger margins are shown to negatively impact functional outcome [7], [8]. Therefore, this indicates a need for accurate tumor localization and margin assessment during rectal cancer surgery. To this end, a new wireless surgical navigation setup is proposed, where preoperative imaging, showing relevant anatomy and the surgical target, is used intraoperatively to guide a surgeon using tracked surgical instruments.

During laparoscopic rectal cancer surgery, the wireless surgical navigation setup can be utilized to actively track the tumor location and correlate the preoperative imaging to the intraoperative setting. The 6 degree of freedom (DOF) position and orientation of the tumor can be determined by placing wireless transponders close to the tumor [9], [10]. For successful implementation of this new wireless navigation setup, which incorporates the Calypso wireless transponder tracking system (Varian Medical Systems Inc., USA), an intraoperative accuracy below 1 cm should be achieved. To attain this sub- centimeter threshold for tumor tracking, the 6DOF position and orientation of the tumor has to be determined accurately.

Basically, the intraoperative accuracy is affected by the trueness and precision with which the used tracking system can track the position and orientation of the transponders. In turn, this tracking accuracy can be affected by distortions of the magnetic field, which is utilized by the Calypso system for tracking of the transponders. There are three major sources of distortions in a magnetic field, being: 'Ferromagnetic materials'; 'Eddy currents in conductive materials, induced by the magnetic field itself'; and 'External currents inside the magnetic field, e.g. electronic devices' [11]. During an operation, multiple instruments and devices are used which could cause these distortions. Therefore, it is important to quantify the tracking accuracy of the setup and the influence of surgical instruments and devices on this accuracy.

Franz et al. has proposed a standardized assessment protocol for such accuracy assessments for use with the field of view (FOV; 14 cm × 14 cm × 19 cm) of the commercially available Calypso system. The Frantz protocol is based on a standardized board setup [12]. The clinical available Calypso system – opposite from the research system that is used for the wireless navigation setup – only provides 3DOF position information. Therefore, the Franz-protocol was limited to position accuracy assessment. Subsequently, both Franz et al., as well as Eppenga et al., have demonstrated sub millimeter position accuracy of the Calypso tracking system in both laboratory, radiotherapy and operation room conditions using this adapted protocol [10], [12]. Distortion measurements, carried out as part of the Franz-protocol, assessed influence of different metal cylinders at several distances between the tracking array and transponder. This assessment indicates that the influence of these materials is generally highest when close – i.e. 3.7 cm - to the transponder, leading to inaccuracies of up to 3.2 mm.

Next to the clinical Calypso system, a research version of the Calypso transponder tracking system is available in the Netherlands Cancer Institute (NKI). This system can acquire 5DOF position and orientation data of three transponders in an extended field of view (eFOV; 27.5 cm x 27.5 cm x 22.5 cm). Eppenga et al. concluded that sub-millimeter accuracy can be attained in this eFOV [10]. Furthermore, the additional orientation information can be used for fusion of 5DOF data of two transponders into a single 6DOF sensor, required for accurate intraoperative tumor tracking [9]. These sensor fusion methods rely on accuracy of the orientation data, increasing the importance of orientation accuracy in the eFOV for intraoperative accuracy. In this paper, Eppenga et al. showed orientation accuracy for specific relative orientations of the transponders at a stationary location in the eFOV.

In this study, a standardized assessment following the protocol of Franz et al. is performed. However, since intraoperative accuracy is dependent on both position and orientation accuracy, the protocol is extended to orientation accuracy in the eFOV. Furthermore, the influence of distortion by surgical tools inside the eFOV during navigation in rectal cancer surgery will be assessed. In addition, we included the NDI Polaris Spectra optical tracking system (Northern Digital Inc, Waterloo, Canada) as an absolute accuracy reference.

II. METHODS AND MATERIALS

A. *Calypso tracking system*

The Electromagnetic tracking system (EMTS) consists of an EM Tracking Array (TA), a readout system and three 5DOF

implantable wireless Beacon transponders with different excitation frequencies – i.e. 300, 400, 500 kHz -, a diameter of 1.85 mm and 8 mm long. The tracking system has an eFOV of 27.5 x 27.5 x 22.5 cm (in x-, y-, z-direction), starting at 5.5 cm offset from the TA, in which the Beacon transponders can be tracked. The x- and y- axes define a parallel plane with regard to the TA while the z-axis is perpendicular, pointing away from the TA. The transponders inside the eFOV are excited at characteristic frequencies using an excitation signal generated by alternating current magnetic field, inducing a current in the transponder coil. Subsequently, the tracking system determines the 5DOF pose - position and orientation - based on the magnetic flux produced by transponder, which is sensed using a separate array of sensor coils inside the TA. Single transponder position trueness has been reported at 0.1 mm, while precision has been reported at 0.3 mm standard deviation [12]. The z-axis direction reversal detection and correction algorithm, described in Appendix A is applied on the orientation data. Furthermore, the TTV sensor fusion method proposed by Eppenga et al. is implemented to fuse 5DOF pose of two transponders into a single 6DOF virtual transponder [9].

B. *Measurement Setup*

The standardized accuracy assessments were performed in the operating room of the NKI, being the proposed operational environment of the Calypso system. Here, measurements were performed using a sleeve, incasing the TA, stackable height adapter boxes, and a Hummel board -depicted in Figure 1-, for accurate, stable and reproducible positioning of transponders in the eFOV. To enable sensor fusion, the two 5DOF wireless Beacon transponders were positioned in an approximate 90-degree angle to each other, embedded in a transponder phantom size 10 x 10 x 4 cm.

For absolute accuracy measurements, the optical tracking system (OTS), NDI Polaris Spectra (Northern Digital Inc, Waterloo, Canada) is used. The OTS utilizes passive reflective markers, commonly in a 4-marker configuration, which can be tracked with a Root Mean Square Error (RMSE) of <0.17 mm [13]. These passive reflective markers were rigidly attached to the transponder phantom. To avoid any influence on the accuracy by camera movement, an optical tracker was rigidly attached to the TA as reference.

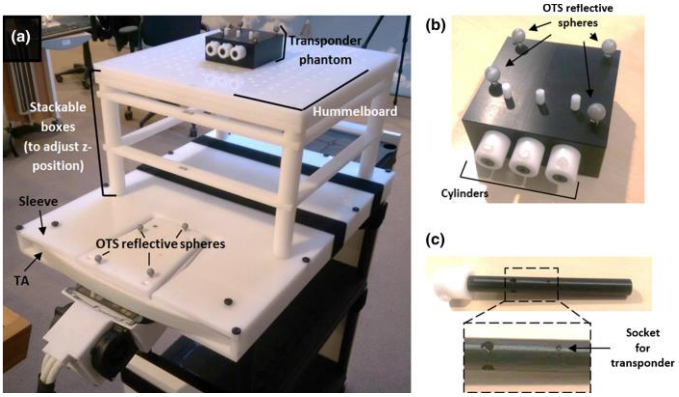

Figure 1 Pictures of the measurement setup (a), the transponder phantom (b) and one cylinders of the transponder phantom (c) as reprinted with permission from Eppenga et al. [10]

The acquisition protocol of Franz et al. was applied with the transponder phantom on five different levels (z = 5.5, 10.5, 15.5, 20.5 and 25.5 cm), in order to sample the eFOV. On each level, EMTS and OTS measurements were taken at 5 x 6 = 30 positions for a total of 150 measurement locations in the eFOV. All locations were interspaced with 5 cm in each orthogonal direction. For each recorded location, the sensor fusion algorithm – Appendix B - is used to determine the 6DOF pose of the transponder phantom in EM coordinates using MATLAB (MATLAB, version R2019a, Natick, Massachusetts: The MathWorks Inc.). For each measurement location, 150 samples were recorded at an average sample rate of 50 Hz for EMTS and OTS. Each sample consisted of the following pose information:

- The 5DOF pose of two EM transponders (*Tx*, x = 1, 2) expressed in the EMT coordinate system ${}^{EMT}T_{Tx}$
- The 6DOF pose of the optical reference sensor rigidly attached to the TA expressed in the optical coordinate system ${}^{OT}T_{TA}$
- The 6DOF pose of the transponder phantom expressed in the optical coordinate system ${}^{OT}T_{Phantom}$

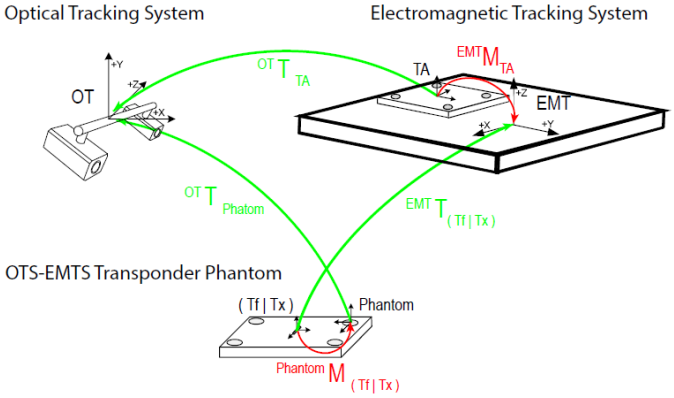

Figure 2 The basic EMTS-OTS setup containing measured and calculated transformations. The transformations from the Transponder Phantom to the EMTS transponder and from the Tracking Array to EM Tracker (both red) are initially unknown and can be computed by the hand-eye calibration procedure. The other mappings can change dynamically in real-time and are reported by the tracking systems.

All poses were represented by 4 x 4 transformation matrix T and communicated through OpenIGTLink TRANSFORM messages. The superscript OT or EMT implies the coordinate system in which the specific pose is given, e.g., Optical Tracker or EM Tracker. The subscript specifies the tool or transponder of which the pose is expressed in this coordinate system. Therefore, ${}^{EMT}T_{T1}$ is the pose of the first transponder expressed in the EMT coordinate system. The 5DOF EMT transponder data, ${}^{EMT}T_{T1}$ and ${}^{EMT}T_{T2}$, was fused to a 6DOF transformation matrix: ${}^{EMT}T_{Tf}$. The pose of the transponder phantom was calculated with respect to the TA reference sensor using:

$$ {}^{TA}_{OTS}T_{Phantom} = {}^{TA}T_{OT}\ {}^{OT}T_{Phantom} $$

$$= {}^{OT}T_{TA}^{-1}\ {}^{OT}T_{Phantom} \quad (3.1)$$

The additional subscript, OTS, highlights the fact that this measurement originates from the optical tracking system.

For readout of the EMTS system, specialized readout software, provided by the manufacturer, was used. The readout of the OTS hardware was performed using PlusServer from the Plus Toolkit (https://plustoolkit.github.io/) [14]. Subsequently, all data was received and analyzed using MATLAB.

C. Surgical Equipment

The different surgical instruments and devices that are used during laparoscopic rectal cancer surgery in the NKI are listed in Appendix E and scored for:

- Used during navigation section of a surgical procedure
- Used inside of the EM tracking volume
- Containing possibly distorting components

Scoring resulted in five surgical instruments that could negatively influence the tracking accuracy and thus the navigation accuracy. These surgical instruments are tested for possible distortion of EM field:

- Powered laparoscopic stapler (Echelon Flex, Johnson & Johnson)
- Ultrasonic shears (Harmonic ace, Johnson & Johnson)
- Laparoscopic sealer (Ligasure Maryland, Covidien)
- Video Laparoscope system (Evis Exera III, Olympus)
- Laparoscopic fenestrated forceps

Exempt the laparoscope system, it is assumed that all instruments can be held passive during navigation section of a surgical procedure, therefore the instruments were tested in a passive mode. The surgical fenestrated forceps was tested since it was assumed to be representative for all reusable non-electronic surgical tools.

D. EMTS-OTS Calibration

The calibration between the EMTS and OTS was described by the transformation matrix ${}^{EMT}M_{TA}$, transforming the optical TA marker to the EMT coordinate system – Figure 2 -. A second static transformation was estimated ${}^{Phantom}M_{Tf}$, transforming the fused EM sensor to the optical transponder phantom. Calibration was performed in two steps. First, hand-eye calibration – Appendix C - was used for initial estimation of these transformation matrices [15], [16]. To this end, a combined EMTS-OTS dataset was collected at three levels (z = 10.5, 13 and 15.5 cm) with 5 sampled poses per level for a total of 15 measurement poses. For increased robustness and precision of the calibration, the position and orientation of the combined sensor was varied as much as possible, resulting in measurement locations in the center and corners of each level. For each pose, 20 values were acquired and subsequently averaged.

Second, an optimization algorithm - Levenberg- Marquardt; Appendix D - was applied using the calibration dataset, resulting in a final transformation estimation [17]. The final static calibration is used to estimate an absolute reference dataset of the fused transponder pose in EMT coordinates, based on optical measurements, using:

$${}^{EMT}_{OTS}T_{Tf} = {}^{EMT}M_{TA}\ {}^{TA}_{OTS}T_{Phantom}\ {}^{Phantom}M_{Tf} \quad (3.2)$$

Accuracy of the calibration is assessed using the Fiducial Registration Error (FRE) of the calibration dataset – i.e. grid matching error between ${}^{EMT}_{OTS}T_{Tf}$ and ${}^{EMT}T_{Tf}$ -.

E. Data Evaluation

Relative trueness

The relative position and orientation trueness will be estimated by comparing adjoining measurement locations in the known 3D grid. Exclusively, ${}^{EMT}T_{Tf} = \begin{bmatrix} {}^{EMT}R_{Tf} & {}^{EMT}t_{Tf} \\ 0 & 1 \end{bmatrix}$ information is used for this relative trueness calculation. Before evaluation, ${}^{EMT}R_{Tf}$ was transformed to a quaternion representation (${}^{EMT}q_{Tf}$).

For position trueness, the mean position, ${}^{EMT}\bar{t}_{Tf}(i)$, over the 150 samples was calculated per measurement location (i=1..150). Subsequently, the 5 cm distances are computed between adjoining measurement locations for each level. All possible 5 cm distances were calculated using (3.3), resulting in 4 x 6 = 24 distance values in the rows of the grid and 5 x 5 = 25 in the columns, for a total of 49 distances per level in the z-direction.

$$Diff_{pos}(i) = \left\| {}^{EMT}\bar{t}_{Tf}(i) - {}^{EMT}\bar{t}_{Tf}(i+1) \right\|_2 \quad (3.3)$$

Where $|...|_2$ denotes the Euclidian norm and i represents the measurement location. The error is calculated by subtracting the distance measurements from the known physical distance ($Diff_{pos\_ref} = 5\ cm$) between the measurement locations using:

$$Err_{pos}(i) = Diff_{pos}(i) - Diff_{pos\_ref} \quad (3.4)$$

For relative orientation trueness, the mean orientation, ${}^{EMT}\bar{q}_{Tf}(i)$, over the 150 samples is calculated per measurement location (i=1..150), using the quaternion averaging method proposed by Markley et al. [18].

Table 1 Results of position accuracy evaluation

	Precision	Relative trueness	Absolute trueness	Grid matching error
5th Level (Highest - 110 invalid)	2.72 mm	0.29 mm	1.35 mm	0.53 mm
4th Level (1 invalid)	0.69 mm	0.13 mm	1.04 mm	0.30 mm
3rd Level (0 invalid)	0.17 mm	0.12 mm	0.84 mm	0.22 mm
2nd Level (0 invalid)	0.06 mm	0.14 mm	0.94 mm	0.24 mm
1st Level (Lowest - 2 invalid)	0.04 mm	0.18 mm	0.95 mm	0.28 mm
Overall	1.26 mm	0.18 mm	1.04 mm	0.38 mm

Subsequently, the orientation difference ($Diff_{or}$) in degrees between adjoining measurement locations was calculated using:

$$Diff_{or}(i) = \frac{180}{\pi} \cdot 2 \cdot arcsin\left(\left\| vec\left({}^{EMT}\bar{q}_{Tf}(i) * {}^{EMT}\bar{q}_{Tf}(i+1)^{-1}\right)\right\|\right) \quad (3.5)$$

Here, $vec\left({}^{EMT}\bar{q}_{Tf} * {}^{EMT}\bar{q}_{Tf}{}^{-1}\right)$ implies the vector part of the quaternion product [19]. The error is calculated by subtracting the orientation measurements from the known difference between orientations ($Diff_{or\_ref} = 0\,^{\circ}$) :

$$Err_{or}(i) = Diff_{or}(i) - Diff_{or\_ref} \quad (3.6)$$

Similar to position error, resulting in a total of 49 orientation error values per level in the z-direction.

Both relative position and orientation errors are summarized by calculating the RMSE per level and for the entire field of view.

$$\text{RMSE} = \sqrt{\frac{1}{N}\sum_{i}^{N} Err_{(pos\,|\,or)}(i)^2} \quad (3.7)$$

Grid matching error

As proposed by Maier-Hein et al., the grid matching error was calculated [20]. The grid accuracy was determined by matching each set of 36 mean grid positions per level and a complete set of 150 mean positions to a set of reference positions of the known 3D grid. The optimal transformation was estimated using the Procrustes algorithm and transformed grid positions (${}^{EMT}T_{ref}$) were compared to the measured positions. Position error was computed using:

$$Err_{pos}(i) = \left\| {}^{EMT}\bar{t}_{Tf}(i) - {}^{EMT}t_{ref}(i)\right\|_2 \quad (3.8)$$

While orientation error was calculated using:

$$Err_{or}(i) = \frac{180}{\pi} \cdot 2 \cdot arcsin\left(\left\| vec\left({}^{EMT}\bar{q}_{Tf}(i) * {}^{EMT}q_{ref}(i)^{-1}\right)\right\|\right) \quad (3.9)$$

The error was specified both per level and the entire tracking volume using the RMSE (3.7).

Absolute trueness

For absolute position and orientation error calculations, the optical reference ${}^{EMT}_{OTS}T_{Tf}$, as calculated by (3.2), and ${}^{EMT}T_{Tf}$ were compared. For position trueness, the mean position of both systems, ${}^{EMT}_{OTS}\bar{t}_{Tf}(i)$ and ${}^{EMT}\bar{t}_{Tf}(i)$, over the 150 samples was calculated per measurement location (i=1..150). Subsequently, the absolute position error was computed:

$$Err_{pos}(i) = \left\| {}^{EMT}\bar{t}_{Tf}(i) - {}^{EMT}_{OTS}\bar{t}_{Tf}(i)\right\|_2 \quad (3.10)$$

Similarly, for orientation trueness, the mean orientation of both systems, ${}^{EMT}_{OTS}\bar{q}_{Tf}(i)$ and ${}^{EMT}\bar{q}_{Tf}(i)$, was calculated. The error was defined as:

$$Err_{or}(i) = \frac{180}{\pi} \cdot 2 \cdot arcsin\left(\left\| vec\left({}^{EMT}\bar{q}_{Tf}(i) * {}^{EMT}_{OTS}\bar{q}_{Tf}(i)^{-1}\right)\right\|\right) \quad (3.11)$$

Precision

The jitter error – defined as the standard deviation - was calculated for both position and orientation as a measure of precision:

$$Jitter_{pos}(i) = \sqrt{\frac{1}{N}\sum_{j=1}^{N}\left\| {}^{EMT}t_{Tf}(i,j) - {}^{EMT}\bar{t}_{Tf}(i)\right\|_2^2} \quad (3.12)$$

$$Diff_{or}(i,j) = \frac{180}{\pi} \cdot 2 \cdot arcsin\left(\left\| vec\left({}^{EMT}q_{Tf}(i,j) * {}^{EMT}\bar{q}_{Tf}(i)^{-1}\right)\right\|\right) \quad (3.13)$$

$$Jitter_{or}(i) = \sqrt{\frac{1}{N}\sum_{j=1}^{N}\left\| Diff_{or}(i,j)\right\|_2^2} \quad (3.14)$$

Where j represent the number of samples per measurement location. The Jitter error was specified both per level and the entire tracking volume using the RMSE (3.7).

Distortion

Distortion measurements with surgical instruments were performed in the center of the x- y- plane at a fixed distance along the z-axis, z = 13 cm. Instruments were placed between the TA and transponder phantom at a distance of 3.7 cm from the transponders, being a clinically relevant distance and the position where most significant distortions were found by Franz et al. [12]. The distortion measurements dataset consisted of 150 (j=1..150) measurements at a single measurement location (i=1) for all five measured instruments (k=1..5). The measured transforms, ${}^{EMT}T_{Tf}(k,j)$, were compared to a distortion free reference (DFR) EMTS measurement ${}^{EMT}T_{Tf-DFR}(j)$, the absolute pose as estimated by OTS ${}^{EMT}_{OTS}T_{Tf}(k,j)$ and jitter was calculated.

The relative error was calculated using:

$$Err_{pos}(k) = \left\| {}^{EMT}\bar{t}_{Tf}(k) - {}^{EMT}\bar{t}_{Tf-DFR}\right\|_2 \quad (3.15)$$

Table 2 Results of orientation accuracy evaluation

	Precision	Relative trueness	Absolute trueness
5th Level (Highest)	1.63 °	0.38 °	0.43 °
4th Level	0.50 °	0.24 °	0.37 °
3rd Level	0.15 °	0.25 °	0.35 °
2nd Level	0.07 °	0.28 °	0.32 °
1st Level (Lowest)	0.04 °	0.31 °	0.35 °
Overall	0.76 °	0.29 °	0.37 °

$$Err_{or}(k) = \frac{180}{\pi} \cdot 2 \cdot arcsin\left(\left\| vec\left({}^{EMT}\bar{q}_{Tf}(k) * {}^{EMT}q_{Tf-DFR}{}^{-1}\right)\right\|\right) \quad (3.16)$$

An absolute error was calculated using (3.10) and (3.11). Jitter error was computed for position and orientation data as a measure of precision using (3.12, 3.13, 3.14).

III. RESULTS

Calibration between the EMTS and OTS systems resulted in a FRE of 0.37 mm and 0.48°.

Position accuracy evaluation

Results of position data evaluation are listed in Table 1. All error values for precision and trueness are highest on the 5th level – i.e. furthest from the TA-. Furthermore, the number of invalid samples was highest on the 5th level although invalid samples were seen on the 1st and 4th level (<1% of all transponder samples), all were excluded from further analysis. Grid matching resulted in an overall error of 0.38 mm and the error is illustrated in Figure 3 as the 3D plot of the mean measured positions and the corresponding points in the known 3D grid. When taken over all 5 cm distances (49 × 5 = 245 distances) in the eFOV a relative RMSE of 0.18 mm was observed. Figure 4 shows a box-and-whisker plot of these errors by level; outliers can be seen on the 2nd, 3rd and 5th levels. However, all median error values are below 0.2 mm. Concerning precision, the jitter error over all 5 × 30 = 150 measurement locations was 1.26 mm.

Orientation accuracy evaluation

Results of orientation data evaluation are listed in Table 2. Similar to position error values, precision and trueness errors are highest on the 5th level. In addition, Figure 4 shows a box-and-whisker plot of relative trueness errors by level; outliers can be seen on the 1st, 2nd and 3rd levels. However, all median error values are below 0.5°, while the overall relative RMSE was 0.29° and absolute RMSE was 0.37°. Concerning precision, the jitter error over all 5 × 30 = 150 measurement locations was 0.76°.

Distortion data evaluation

Influence of distortion of surgical instruments on precision, absolute, and relative trueness, is shown per instrument in Figure 5 and Figure 6. Positioning of the Powered laparoscopic stapler near the transponders resulted in the largest trueness and precision errors of both position and orientation, exempt absolute orientation error. Deviations from DFR were seen up to 0.78 mm and 0.51°, while the maximum precision errors – over *j*=1…150 samples - were 0.21 mm and 0.14°.

IV. DISCUSSION

A standardized assessment protocol was used to assess transponder position accuracy, comparable to Franz et al. [12]. Results are promising, generally accuracy values stay below 1mm. As described for previously assessed EMTS, such as the NDI Aurora, the accuracy decreases with an increased distance to the TA [20], [21]. However compared to these EMTS, a higher jitter error (2.72 mm) was observed on the highest level in the eFOV of the Calypso system. Contrastingly, the trueness of the Calypso was higher with a relative trueness RMSE of 0.18 mm (NDI Aurora: 1.0 mm; Ascension microBIRD: 1.1 mm) [21]. Grid matching errors were low for the Calypso system at 0.38 mm, which was comparable to results of Franz et al. [12]. Compared to these studies, we also assessed orientation accuracy in the eFOV and influence of distortion by surgical instruments on the tracking accuracy.

No previous studies assessed the orientation accuracy in the entire eFOV, while the standardized Franz protocol was even limited to position accuracy. Therefore, no direct reference was available for orientation accuracy in the eFOV of the Calypso system. However, Hummel et al. assessed rotation trueness at the center of the FOV resulting in relative errors of 0.8° for NDI Aurora and 0.04° for Ascension microBIRD [20], [21]. Relative orientation trueness, as measured over the eFOV, was therefore comparable for the Calypso system (0.29°). Comparable to position accuracy, the orientation

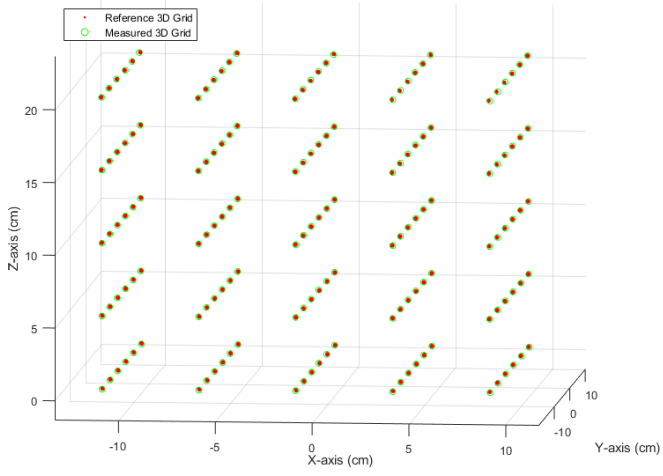

Figure 3 Results of grid accuracy; 3D plot of all measured positions, averaged over 150 values per position (green), and reference 3D grid (red)

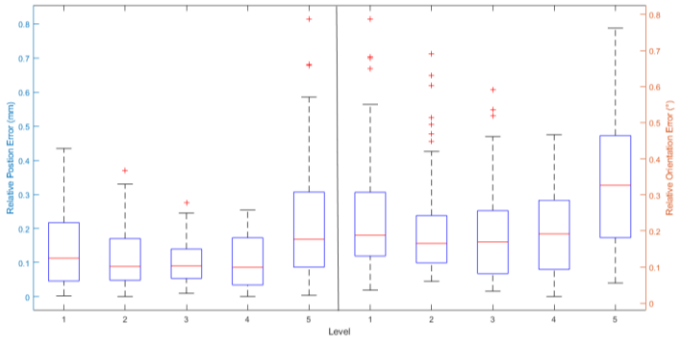

Figure 4 Results of relative position and orientation errors as specified using a box-and-whisker plot over 49 error values per measured level. On each box, the central mark indicates the median, and the bottom and top edges of the box indicate the 25th and 75th percentiles, respectively. The whiskers extend to the most extreme data points not considered outliers (1.5 times the interquartile range from the box), and the outliers are plotted individually using the '+' symbol

accuracy decreased with increased distance to the TA. Clinically, in an ideal case, transponders are positioned at the distal border of a tumor for tumor tracking. Given a mean rectal tumor diameter of 4.5 cm, as reported by Kornprat et al., an orientation trueness error of 0.29° would result in a positional error at the proximal tumor border of 0.23 mm [22]. At the distal resection margin – i.e. 1 cm from distal tumor border and therefore the transponder – this position error would be 0.05 mm, whereas at the proximal resection margin – i.e. 5 cm from proximal tumor border and therefore 9.5 cm from the transponder – the orientation error would translate to a deviation of 0.48 mm. This error range is comparable to position trueness errors. This indicates the importance of orientation accuracy for rectal tumor tracking.

Regarding the surgical instrument distortion assessment, the laparoscopic stapler showed the highest impact on tracking accuracy, resulting in deviations from DFR of 0.78 mm and 0.51° error. All other surgical instruments showed comparable results with deviations ranging from 0.06 mm – 0.18 mm and 0.01° - 0.12°. Also precision was affected most by the laparoscopic stapler, whereas all other instruments showed comparable results to precision of the DFR. The impact of these surgical tools on the tracking accuracy is therefore low when compared to the standardized assessments performed with metallic cylinders resulting in errors up to 3.2 mm for the Calypso system (NDI Aurora: up to 4.2 mm; Ascension microBIRD: up to 80 mm) [12], [21].

Jitter errors of both orientation and position data could pose issues with real time tumor tracking applications. Therefore, alignment of the more precise lower levels of eFOV with the target area would be ideal. However, while positioning of the Calypso system and TA in radiotherapy is relatively trivial. During laparoscopic surgery, the operating area is occluded by surgical instruments – e.g. trocars, laparoscopic instruments –, the surgeon, surgical assistant and equipment, e.g. anesthesiology setup or surgical supply carts . Therefore,

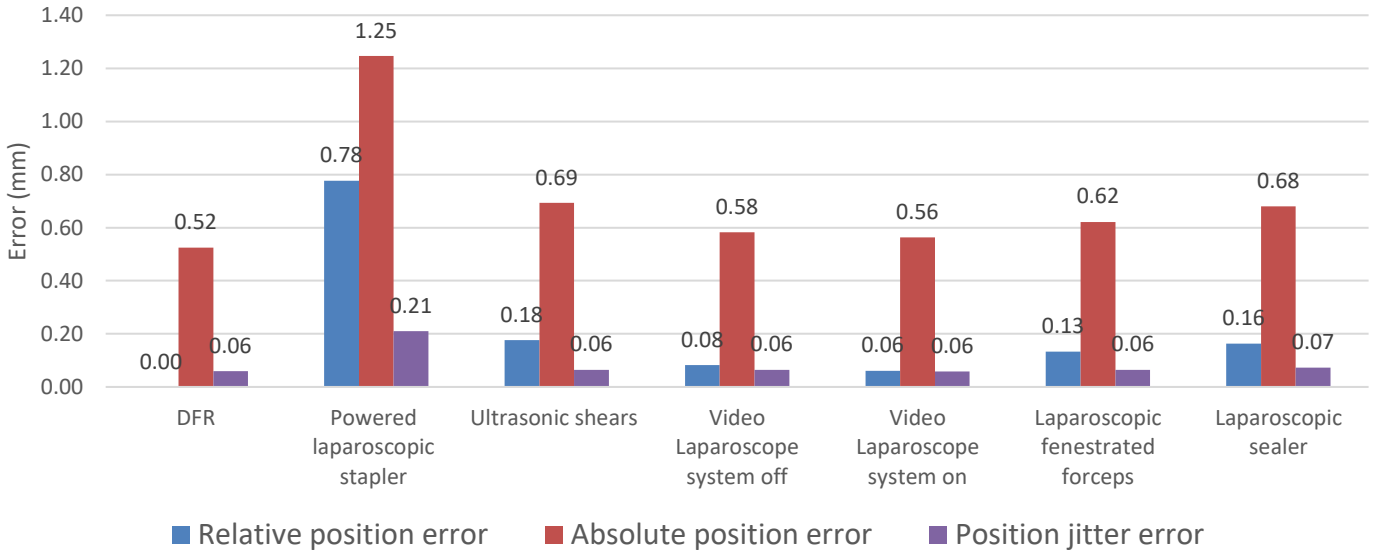

Figure 5 Results of position evaluation of distortion effects by surgical instruments.

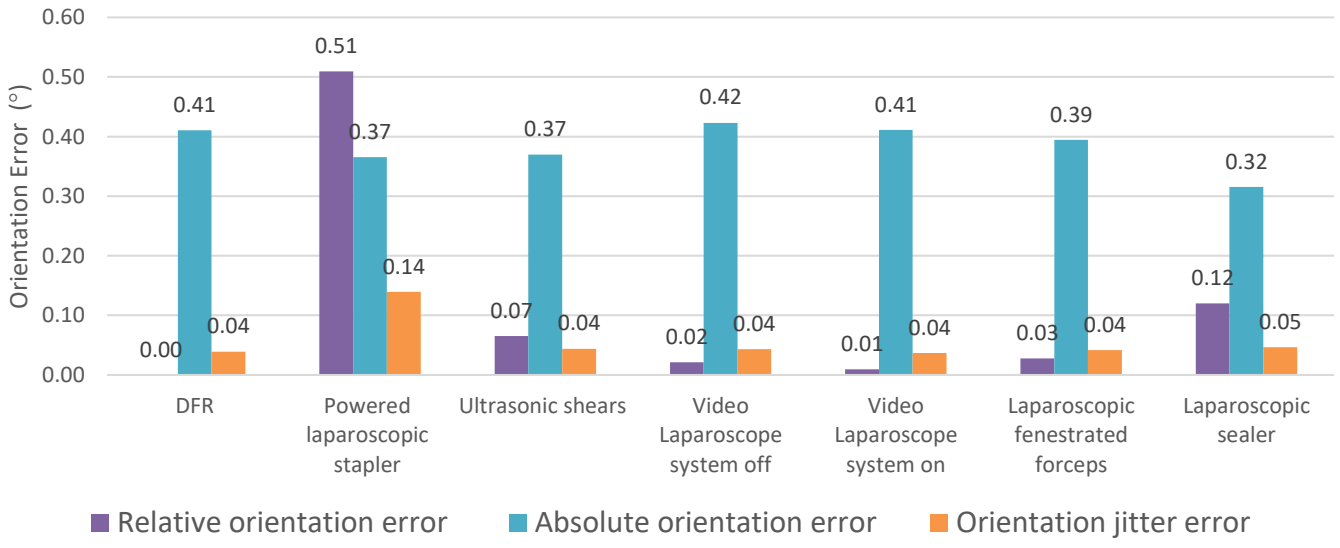

Figure 6 Results of orientation evaluation of distortion effects by surgical instruments

positioning of the Calypso system and aligning the TA and eFOV with the target area could prove a challenging task. Mitigating the decreased precision by adding constraints to positioning of the TA - i.e. aligning the more precise lower levels of the eFOV with the target - is therefore not feasible. Alternatively, filtering of these errors using a Savitzky-Golay or Kalman filter is proposed.

For clinical application, the maximum of three tracked transponders may prove challenging. In laparoscopic rectal cancer surgery, navigation will be used primarily for tumor localization and subsequent resection margin assessment. However, for spatial orientation and correlation of navigation information to the intraoperative setting, display of surrounding structures such as bone, arteries, veins and ureters may prove useful. Kok et al. showed feasibility and accuracy of a navigation approach using such 3D models, correlated to the intraoperative setting using EM sensors placed on the skin. Since the Calypso system is limited in tracking a maximum of three transponders, where two are needed for tumor tracking and one for a tracked tool, hybrid tracking possibilities – e.g. addition of an OTS to the navigation setup - could be a suitable alternative. The absolute accuracy values show the accuracy with which these systems can be calibrated, and the secondary structures can be shown, being approximately 1 mm an 0.4°.

The operating table system also met all scoring criteria of the surgical equipment for distortion analysis. However, it was excluded from this assessment since it was extensively tested by Eppenga et al. [10], showing high absolute errors (> 10 mm) while relative errors remained below 1 mm. This means that relative distances are not highly impacted by the operating table, and when only the Calypso system is used in a navigation setup – opposed to a hybrid tracking setup – it can be used accurately without a need for calibration. However the large absolute error implies a calibration step is needed when a secondary tracking system – e.g. OTS – is added to the tracking setup, which may prove useful for tracking of surrounding organs.

In conclusion, this study showed that the Calypso system can provide position and orientation of a 6DOF virtual transponder in the eFOV with high accuracy as well as high robustness to distortions of surgical equipment in an ideal clinical environment. Future work includes integration in clinical workflow.

V. REFERENCES

[1] F. Bray, J. Ferlay, I. Soerjomataram, R. L. Siegel, L. A. Torre, and A. Jemal, "Global cancer statistics 2018: GLOBOCAN estimates of incidence and mortality worldwide for 36 cancers in 185 countries," *CA. Cancer J. Clin.*, vol. 68, no. 6, pp. 394–424, Nov. 2018.

[2] P. Rawla, T. Sunkara, and A. Barsouk, "Epidemiology of colorectal cancer: Incidence, mortality, survival, and risk factors," *Prz. Gastroenterol.*, vol. 14, no. 2, pp. 89–103, 2019.

[3] Intergraal Kankercentrum Nederland (IKNL), "Behandeling darmkanker." [Online]. Available: https://iknl.nl/kankersoorten/darmkanker/registratie/behandeling. [Accessed: 10-Apr-2021].

[4] R. Veldkamp *et al.*, "Laparoscopic surgery versus open surgery for colon cancer: Short-term outcomes of a randomised trial," *Lancet Oncol.*, vol. 6, no. 7, pp. 477–484, Jul. 2005.

[5] H. J. Bonjer *et al.*, "A Randomized Trial of Laparoscopic versus Open Surgery for Rectal Cancer," *N. Engl. J. Med.*, vol. 372, no. 14, pp. 1324–1332, 2015.

[6] A. S. Rickles *et al.*, "Rickles (2015) - High rate of positive circumferential resection margins following rectal cancer surgery.pdf," *Ann. Surg.*, vol. 262, no. 6, pp. 891–898, 2015.

[7] C. G. C. Pales, S. An, J. P. Cruz, K. Kim, and Y. Kim, "Postoperative bowel function after anal sphincter-preserving rectal cancer surgery: Risks factors, diagnostic modalities, and management," *Annals of Coloproctology*, vol. 35, no. 4. Korean Society of Coloproctology, pp. 160–166, 2019.

[8] W. S. Lee *et al.*, "Risk factors and clinical outcome for anastomotic leakage after total mesorectal excision for rectal cancer," *World J. Surg.*, vol. 32, no. 6, pp. 1124–1129, Jun. 2008.

[9] R. Eppenga, K. Kuhlmann, T. Ruers, and J. Nijkamp, "Accuracy assessment of target tracking using two 5-degrees-of-freedom wireless transponders," *Int. J. Comput. Assist. Radiol. Surg.*, vol. 15, no. 2, pp. 369–377, 2019.

[10] R. Eppenga, K. Kuhlmann, T. Ruers, and J. Nijkamp, "Accuracy assessment of wireless transponder tracking in the operating room environment," *Int. J. Comput. Assist. Radiol. Surg.*, vol. 13, no. 12, pp. 1937–1948, 2018.

[11] A. M. Franz, T. Haidegger, W. Birkfellner, K. Cleary, T. M. Peters, and L. Maier-Hein, "Electromagnetic tracking in medicine -A review of technology, validation, and applications," *IEEE Trans. Med. Imaging*, vol. 33, no. 8, pp. 1702–1725, 2014.

[12] A. M. Franz *et al.*, "Standardized accuracy assessment of the calypso wireless transponder tracking system," *Phys. Med. Biol.*, vol. 59, no. 22, pp. 6797–6810, 2014.

[13] R. Elfring, M. de la Fuente, and K. Radermacher, "Assessment of optical localizer accuracy for computer aided surgery systems," *Comput. Aided Surg.*, vol. 15, no. 1–3, pp. 1–12, Feb. 2010.

[14] T. Ungi, A. Lasso, C. Pinter, A. Rankin, T. Heffter, and G. Fichtinger, "PLUS: Open-Source Toolkit for Ultrasound-Guided Intervention Systems," *IEEE Trans. Biomed. Eng.*, 2014.

[15] F. C. Park and B. J. Martin, "Robot sensor calibration: solving AX=XB on the Euclidean group," *IEEE Trans. Robot. Autom.*, vol. 10, no. 5, pp. 717–721, 1994.

[16] M. Shah, R. D. Eastman, and T. Hong, "An overview of robot-sensor calibration methods for evaluation of perception systems," in *Performance Metrics for Intelligent Systems (PerMIS) Workshop*, 2012, pp. 15–20.

[17] M. Feuerstein, T. Reichl, J. Vogel, J. Traub, and N.

NAVAB, “New approaches to online estimation of electromagnetic tracking errors for laparoscopic ultrasonography,” *Comput. Aided Surg.*, vol. 13, no. 5, pp. 311–323, Jan. 2008.

[18] F. L. Markley, Y. Cheng, J. L. Crassidis, and Y. Oshman, “Averaging Quaternions,” *J. Guid. Control. Dyn.*, vol. 30, no. 4, pp. 1193–1197, Jul. 2007.

[19] F. L. Markley, “How do I calculate the smallest angle between two quaternions?” [Online]. Available: / www . researchgate . net / post / How _ do _ I _ calculate _ the _ smallest _ angle _ between _ two _ quaternions. [Accessed: 10-Sep-2020].

[20] L. Maier-Hein and A. M. Franz, “Standerdized assesment of new electromagnetic field generators in an interventional radiology setting,” *Med. Phys.*, vol. 39, no. 6, pp. 3424–3434, 2012.

[21] J. B. Hummel *et al.*, “Design and application of an assessment protocol for electromagnetic tracking systems,” *Med. Phys.*, vol. 32, no. 7, pp. 2371–2379, 2005.

[22] P. Kornprat, M. J. Pollheimer, R. A. Lindtner, and A. Schlemmer, “Value of Tumor Size as a Prognostic Variable in Colorectal Cancer A Critical Reappraisal,” vol. 34, no. 1, pp. 43–49, 2011.

Chapter 4: Electromagnetic Interference of Calypso System

Electromagnetic Interference of Calypso System

Functional assessment of potential interference of the Calypso Electromagnetic Tracking System on critical operation room equipment

I. INTRODUCTION

Rectal cancer is the eight most common cancer worldwide with an annual incidence of 704,000, constituting 3.9 percent of all diagnosed cancers [1]. Worldwide, surgery is the primary curative option in non-metastasized rectal cancer, which accounts for 75% of all diagnoses [2]. In the Netherlands, as much as 95% of patients with stadium I-III rectal cancer get surgical treatment [3]. In recent decades, laparoscopic surgery has progressively replaced open rectal surgery due to favorable short-term outcomes, such as less pain, reduced blood loss, and improved recovery time [4], [5]. However, laparoscopic rectal cancer surgery is associated with positive resection margin rates of 10-15% [5], [6], while larger margins are shown to negatively impact functional outcome [7], [8]. Therefore, indicating a need for accurate tumor localization and margin assessment during rectal cancer surgery.

To aid a surgeon in this challenging task, surgical navigation is proposed, where preoperative imaging, showing relevant anatomy and the surgical target, is used intraoperatively to guide a surgeon using tracked surgical instruments. This allows for planning an optimal approach, anticipate on the presence of critical anatomical structures to potentially increase surgical accuracy [9]. Recently, feasibility and safety of real time rectal tumor tracking for surgical navigation, using a wired electromagnetic (EM) tracking system, was reported [9]. However, this system requires intraoperative placement of sensors and intraoperative imaging for registration, hindering and extending surgical workflow. Therefore, we propose a wireless electromagnetic tracking setup for surgical navigation, where wireless transponders can be placed preoperatively eliminating the need for intraoperative sensor placement and imaging.

Our proposed setup incorporates the Calypso GPS for the Body® Tracking system. Clinical implementation in its intended use market, radiotherapy, has demonstrated accurate target localization and allows reduction of irradiated volumes and facilitate safe dose escalation [10], [11]. Furthermore, promising results have been published for use of this system in the operating room, outlining sub millimeter accuracy and acceptable distortion effects (< 3.2 mm) on tracking accuracy in this proposed environment [12], [13]. In order to track the transponders inside a specified field of view, they are excited at characteristic frequencies using an excitation signal generated by an alternating current (AC) electromagnetic (EM) field. However, EM fields may cause electromagnetic interference (EMI) in other equipment, as observed in preclinical experiments at the Netherlands Cancer Institute (NKI). Here, heating of operating table components was observed, indicating possible EMI.

EMI is a relatively common issue, influencing surgical equipment [14]–[16]. EMI of a dynamic magnetic field, during Magnetic resonance imaging, has been reported mimicking atrial flutter and ventricular tachycardia or fibrillation [14], [17]. Furthermore, loss of pulsoximeter waveform may be associated with the use of high energy electrocautery [14]. Even cell phone use has been reported as a cause of false positive arrhythmia on electrocardiogram [18]. Therefore, EMI could negatively influence patient monitoring and patient safety during surgery.

In this study, we investigate potential interference of alternating and pulsed magnetic field utilized by the Calypso GPS for the Body® Tracking system on critical operation room equipment. First, a comprehensive list of all equipment present during rectal cancer surgery was drafted. Second, this list was scores on the criteria: used during surgical navigation, electromagnetic interference is plausible, critical for patient safety and with no suitable alternatives. Third, functional output during EM tracking was separately assessed for all identified equipment and compared to reference measurements.

II. METHODS AND MATERIALS

A. Electromagnetic tracking system

The Calypso electromagnetic tracking system (EMTS) consists of an EM Tracking Array (TA), a readout system and three 5 degree of freedom (DOF) implantable wireless Beacon transponders with different excitation frequencies – i.e. 300, 400, 500 kHz-, a diameter of 1.85 mm and 8 mm long. The clinically approved system, compliant to EM Compatibility standard [15], is used in radiation oncology and has an extended field of view (eFOV) of 27.5 x 27.5 x 22.5 cm, starting at 5.5cm offset from the TA, in which the Beacon transponders can be tracked. The x- and y- axes define the horizontal plane with regard to the TA while the z-axis is perpendicular, pointing away from the TA. The transponders inside the eFOV are excited at characteristic frequencies using an excitation signal generated by alternating current magnetic field, inducing a current in the transponder coil. Subsequently, the tracking system determines the 5DOF pose - position and orientation - based on the magnetic flux produced by transponder, which is sensed using a separate array of sensor coils inside the TA.

The magnetic field generated for excitation of the transponders is similar to the one depicted in Figure 1. Four excitation coils are configured to simultaneously receive one

of the alternating electrical signals at a selected phase to generate a magnetic field. The magnetic fields from the excitation coils combine to form a spatially adjustable EM field for excitation of the transponders. The excitation volume in which the transponders are excited, starts at 5.5 cm from the TA to ensure the desired (anti-) parallel field. As magnetic field strength is proportional to the magnetic flux density: B (tesla), the magnetic field strength is highest close to the excitation coils. Therefore, the influence of the generated field on surgical equipment will decrease with distance to the TA.

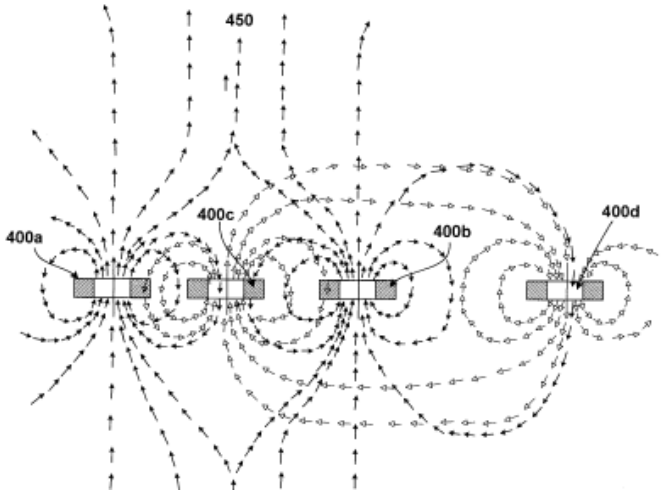

Figure 1 A magnetic field diagram, depicting two sets of generator coils producing magnetic fields of different shapes. Coils 400a and 400b are activated simultaneously and generate a parallel field 450. When the first pair is deactivated and coils 400c and 400d are activated, they together produce anti-parallel field 460. Several, combinations can be used to produce varying magnetic fields [25].

B. Operating room equipment

The different surgical instruments and devices that are used during laparoscopic rectal cancer surgery in the NKI are listed in Appendix E and scored for: used during surgical navigation, electromagnetic interference is plausible, critical for patient safety and no suitable alternatives. Scoring resulted in four surgical devices that could be negatively influenced by EMI from the EMTS:

- Operating table system (Magnus, Maquet)
- ECG Measurement System (Intellivue, Philips)
- Syringe pumps (Alaris plus, Carefusion)
- Video laparoscope system (Evis Exera III, Olympus)

C. Measurement setup

The functional output assessments were performed in the operating room of the NKI, being the proposed operational environment of the Calypso system. Here measurements were performed for all identified surgical devices in two settings:

- Inactive EMTS
- Active EMTS

The first setting was taken as reference, while the second setting was used to assess the influence of continuous tracking of three 5DOF transponders within eFOV. For activation of the EMTS, specialized software (Calypso Surgical Tracking Tool, Version 1.0.8.0, Varian Medica Systems Inc., USA) was used on the readout system.

Operating table system

The operating table system utilizes carbon fiber plates, because of the weight, strength and radiolucent characteristics. Heating of Maquet padded plate (1180.11B1) and the Maquet CF Plate (1180.44AC), designed for intraoperative Computed Tomography imaging, was assessed.

During consecutive measurements, the Maquet padded plate and the Maquet CF Plate were attached to the operating table system. Subsequently, a thermal sensor was attached directly on the plates and the operating table mattress was positioned to prevent cooling due to air (air temperature 19°C). The TA was position parallel to the operating table and centered above the temperature sensor at a distance of 10 cm, see Figure 2.

As inactive EMTS setting, a single reference value was taken before initialization of the EMTS (t=0). For the active tracking setting, assessment of temperature was performed at two-minute interval during a measurement period of 30 minutes. Evaluation of heating was based on the slope of a fitted trendline of all 15 values during this measurement period.

Due to sensor interference and heating during Maquet CF plate assessment, additional measurements were performed. First, during initial measurements, an extra temperature value was taken at five-minute interval with the tracking array temporarily switched off, in order to track plate heating without sensor interference. Second, an additional pose of the TA, similar to proposed clinical pose for laparoscopic rectal cancer surgery – Figure 3 -, was assessed.

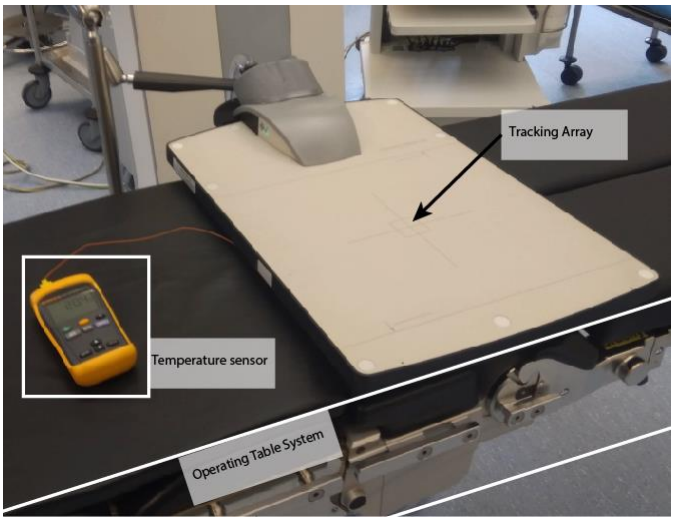

Figure 2 Measurement setup for operating table system heating assessment

ECG Measurement System

Intraoperatively, the electrocardiogram (ECG) measurement system (Intellivue, Philips) is used for rhythm monitoring of patients with a three-lead ECG – i.e. heart rate and relative changes in morphology of ECG waves and complexes -. Assessment of the ECG Measurement System was performed using three healthy male volunteers. While on the operating

table, three electrodes were placed on the volunteers and connected to the ECG measurement system and the TA was positioned according to proposed clinical pose for rectal cancer surgery, as can be seen in Figure 3. Subsequently, a 30-second three-lead ECG signal was recorded for the inactive and active EMTS settings. An additional third setting, where the system was activated during the 30 second measurement period, was used to assess influence of initialization of the EMTS on the ECG measurement system. The acquired ECG signals were assessed based on heart rate (bpm) and apparent morphological changes in the P wave, QRS complex and T wave.

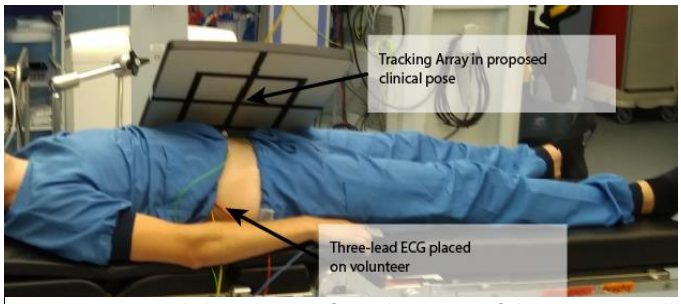

Figure 3 Proposed clinical pose of TA; the center of the TA is vertically aligned with the iliac crest and tilted in an approximate 45-degree angle over the transversal axis of the TA.

Syringe pump

A syringe pump, used for accurate intraoperative drug administration, was assessed based on functional output in a high flow setting. During the measurements, the tracking array was positioned perpendicular to the operating table along the lateral side with the center of the eFOV positioned at the intersection between the table and the divided leg section. The syringe pump was centered in the EMTS eFOV with the syringe along the z-axis and subsequently placed 1.5 m horizontally in the direction of the headrest, as depicted in Figure 4. A water filled syringe was placed in the pump and set to a high flow of 400 ml/h for 5 minutes, which was repeated three times for each setting. The water was collected in a receiving bin and subsequently the mass was measured and compared to a total expected mass of 33 g, as calculated using:

$$m_{output} = t * Q_{water} * \rho_{water} \quad (4.1)$$

Wherein t is the measurement time (h), m_{output} is the mass (g) of the output , Q_{water} is volumetric flow rate (ml/h) of water set on the syringe pump and ρ_{water} is the water density at 20° Celsius in (g/ml).

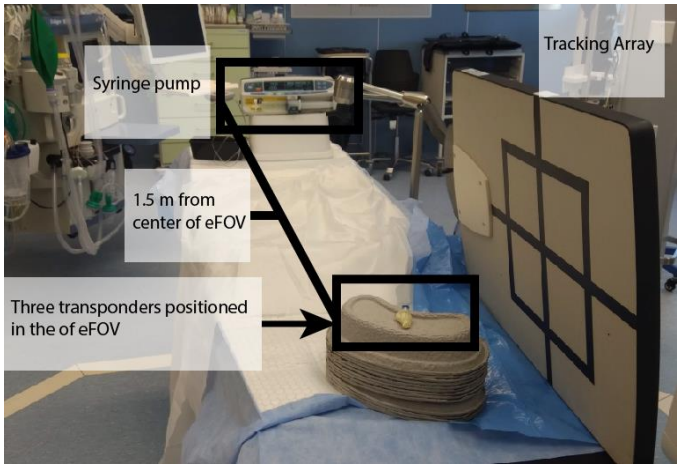

Figure 4 Syringe pump test setup. The pump is located 1.5 meter horizontally with regard to the center of the tracking array.

Video laparoscope system

The video laparoscope system was dynamically assessed on image quality by two observers. During the measurements, the tracking array was positioned perpendicular to the operating table along the lateral side. Subsequently, the FOV of the video laparoscope was aligned with the eFOV of the EMTS and multiple objects were placed in the combined FOV, as seen in Figure 5. During measurements of both settings, image distortions and morphological changes of the video stream were noted when apparent.

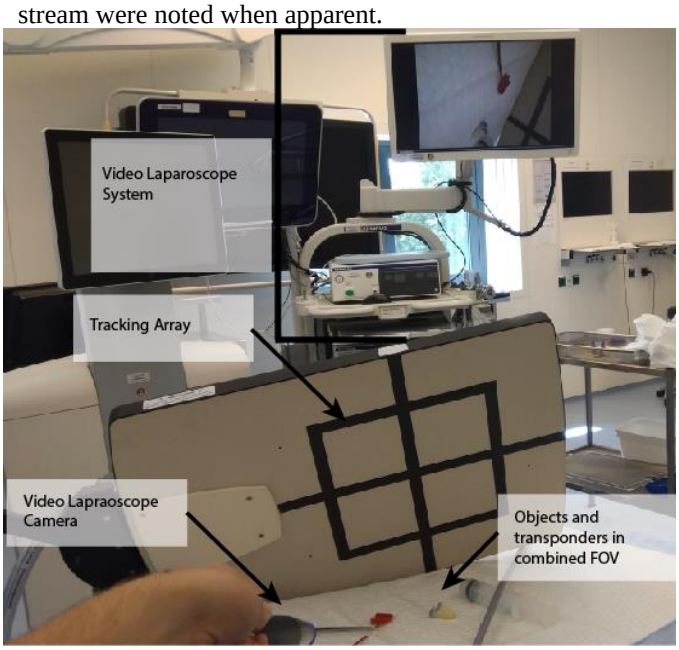

Figure 5 Test setup for laparoscope testing. Objects are placed in the laparoscope field of view and image quality is dynamically assessed on the system monitor.

III. RESULTS

Operating table system

During measurements, the temperature of the Maquet padded plate fluctuated between 20.1° and 20.07° Celsius with a slope of -0.0019°/min, see Figure 6. For the Maquet CF Plate, the temperature ranged from 21.0° to 27.9° Celsius for an upward trendline with a slope of 0.24°/min.

The additional measurements for the Maquet CF Plate, where the EMTS was temporarily switched off, showed a temperature increase from 21.0 to 25.8 degrees Celsius resulting in an upward trendline with a slope of 0.16°/min. When the TA was positioned according to our proposed clinical pose, temperature varied between 21.7 and 21.9° Celsius during the measurement period.

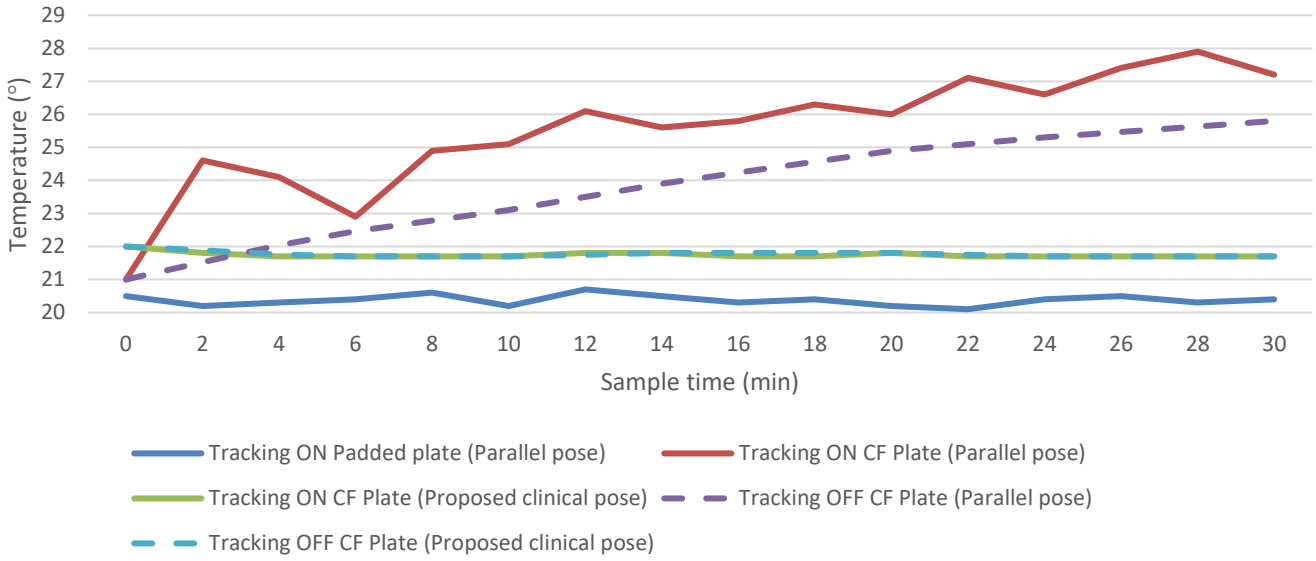

Figure 6 Temperature of Padded plate and CF Plate during measurement period, where the TA was positioned in proposed clinical pose or parallel pose. Samples were taken in two-minute interval for 'Tracking on' measurements and five-minute interval for 'Tracking off'.

ECG Measurement System

The ECGs of a healthy volunteer for the three different EMTS settings can be seen in Figure 7. For each separate volunteer, the morphology of the waves and complexes appear similar within and between the ECG's recorded per setting. For the first volunteer, heart rate was 38 beats per minute (bpm) in the first and third setting, and 40 during the second setting. The second volunteer registered a heart rate of 36 bpm in all settings
and the third volunteer registered 42bpm in the first setting and 38bpm during the latter two settings.

Syringe Pump

Measurements with an inactive TA had a range in mass of 33-33.5g. Alternatively, the maximum deviation from expected 33 g output was 0.5 g – i.e. 1.5 % -, when measuring with an inactive EMTS. Contrarily, all measurements with an active EMTS resulted in a measured mass of 33.0 g – i.e. equal to expected mass -.

Video laparoscope system

For both settings, the video laparoscope showed no apparent distortions or morphological changes in the laparoscopic image when observing the objects in the combined FOV.

IV. DISCUSSION

Operating table system

The operating table system is essential for patient support and positioning during surgery and therefore patient safety. However, electromagnetic fields can cause eddy currents along carbon fibers, with heating of these plates as result [19], [20]. Therefore, measurements were performed to assess potential heating of carbon fiber parts of the operating table system. The commonly used Maquet padded plate (1180.11B1) did not show indications of heating during the 30-minute measurement period, measurements were influenced by sensor interference. Contrarily, heating of the Maquet CF plate was observed during the 30-minute measurement period when the TA was placed perpendicular to the CF plate at a distance of 10 cm. The Maquet CF plate did not show heating during the measurement period when the TA was positioned according to our proposed clinical pose. Generally, the Maquet CF plate is used to enable acquisition of intraoperative CBCT, which is essential for registration of intraoperatively placed sensors to a preoperative three-dimensional (3D) model as shown by Kok et al. [9]. Since the Calypso electromagnetic tracking system uses wireless transponders which can be incorporated in the preoperative 3D model, the Maquet CF plate could be substituted for the commonly used Maquet padded plate. However, no issues are expected regarding heating of the operating table system during implementation of this electromagnetic tracking system for surgical navigation with our proposed clinical TA pose and the Maquet padded plate.

In future studies, it could be beneficial to position the TA in close proximity to the Maquet CF plate, e.g. incorporate the TA in the operating table system. For example, for optimizing positioning with regard to workflow and compatibility during laparoscopic and robot assisted surgery or for additional intraoperative CBCT imaging. In that case, shorter active tracking periods, electromagnetic shielding, cooling solutions or different material composition of the operating table plates could be considered to minimize heating due to active tracking. Furthermore, it should be considered that the influence of carbon and metallic components of the operating table system on electromagnetic tracking accuracy increase with a decreasing distance between the two, as has been shown by Eppenga et al. [12]. Therefore, careful consideration is advised when changes are made regarding the intraoperative setup for surgical navigation using the Calypso system.

ECG system

During surgery, a three channel ECG is continuously monitored. Together with parameters such as temperature, blood pressure, oxygen saturation and ventilation, it is used to monitor a patient during surgery. However, a three lead ECG may only be used for rhythm monitoring and is inadequate to

Figure 7 Recorded ECG of a volunteer during three measurements settings; 1. Inactive EMTS; 2. Initialization of EMTS; 3. Active EMTS.

determine for example ST elevation. Changes of ECG complexes compared to a normal ECG can for example be due to lead placement and sensitive to patient or lead movements. Therefore, in clinical practice no decisions may be derived from this 3 three channel ECG information. It may only be used for sinus rhythm monitoring and changes between complexes could be cause to prompt a 12 lead ECG for accurate diagnostics. Furthermore, influence of active EM tracking on the ECG was not observed during measurements. Compared to for example characteristic EMI from electrocautery devices, influence of EMTS for online ECG monitoring is deemed neglectable [14].

Syringe Pump

During surgery, syringe pumps are continuously used to administer for example sedatives and opioids to the patient. Precise drug administration is critical for prevention of complications and improve patient outcome [21]. EMI of the syringe pumps was deemed plausible since they are powered by an electromotor. However, no changes were observed in functional output of the syringe pumps. Furthermore, during laparoscopic rectal cancer surgery the syringe pumps are positioned further from the TA compared to our experimental setup. Therefore, inference during surgery is deemed unlikely.

Video laparoscope system

The video laparoscope system is used for visualization of the surgical target area and therefore essential for surgical success and patient safety [22]. For the Video Laparoscope system no apparent distortions or morphological changes were observed in the laparoscopic image. Small relative changes could not be assessed using this setup.

Recommendations

The Calypso system utilizes an alternating and pulsed magnetic field to uniquely identify a transponder within the excitation volume. This field is created by four coils, which together form a temporally and spatially adjustable excitation field, with the magnetic field strength decreasing with distance to the TA . Therefore, the influence of this field could vary for every application, device, position and orientation. In this study, functional output tests were conducted where equipment was placed in a similar orientation and, whenever possible, closer than under normal working conditions. For our proposed application and pose, no indications of EMI were observed. Furthermore, the Calypso system is already implemented in the technically demanding radiation therapy setting. During these procedures, multiple devices, comparable to the surgical setting, are in use and no evidence for EMI is mentioned in literature [10], [11], [23]. Also for comparable wired EMTS, no signs of EMI are reported as well as any adverse events correlated to the use of EMTS and surgical navigation [9], [24]. However, for clinical implementation of the Calypso system, monitoring of any signs of EMI is recommended. Also, care should be taken with equipment prone to eddy currents, e.g. carbon fibers, when close to the TA. Finally, prolonged and repeated exposure of the surgical equipment to the EMTS was not assessed.

Concluding, no signs of EMI were found for our proposed navigation setup for laparoscopic rectal cancer surgery, however monitoring of signs of EMI during clinical implementation is recommended.

V. REFERENCES

[1] F. Bray, J. Ferlay, I. Soerjomataram, R. L. Siegel, L. A. Torre, and A. Jemal, “Global cancer statistics 2018: GLOBOCAN estimates of incidence and mortality worldwide for 36 cancers in 185 countries,” *CA. Cancer J. Clin.*, vol. 68, no. 6, pp. 394–424, Nov. 2018.

[2] P. Rawla, T. Sunkara, and A. Barsouk, “Epidemiology of colorectal cancer: Incidence, mortality, survival, and risk factors,” *Prz. Gastroenterol.*, vol. 14, no. 2, pp. 89–103, 2019.

[3] Intergraal Kankercentrum Nederland (IKNL), “Behandeling darmkanker.” [Online]. Available: https://iknl.nl/kankersoorten/darmkanker/registratie/behandeling. [Accessed: 10-Apr-2021].

[4] R. Veldkamp *et al.*, “Laparoscopic surgery versus open surgery for colon cancer: Short-term outcomes of a randomised trial,” *Lancet Oncol.*, vol. 6, no. 7, pp. 477–484, Jul. 2005.

[5] H. J. Bonjer *et al.*, “A Randomized Trial of Laparoscopic versus Open Surgery for Rectal Cancer,” *N. Engl. J. Med.*, vol. 372, no. 14, pp. 1324–1332, 2015.

[6] A. S. Rickles *et al.*, “Rickles (2015) - High rate of positive circumferential resection margins following rectal cancer surgery.pdf,” *Ann. Surg.*, vol. 262, no. 6, pp. 891–898, 2015.

[7] C. G. C. Pales, S. An, J. P. Cruz, K. Kim, and Y. Kim,

"Postoperative bowel function after anal sphincter-preserving rectal cancer surgery: Risks factors, diagnostic modalities, and management," *Annals of Coloproctology*, vol. 35, no. 4. Korean Society of Coloproctology, pp. 160–166, 2019.

[8] W. S. Lee *et al.*, "Risk factors and clinical outcome for anastomotic leakage after total mesorectal excision for rectal cancer," *World J. Surg.*, vol. 32, no. 6, pp. 1124–1129, Jun. 2008.

[9] E. N. D. Kok *et al.*, "Accurate surgical navigation with real-time tumor tracking in cancer surgery," *npj Precis. Oncol.*, vol. 4, no. 8, pp. 1–7, 2020.

[10] T. R. Willoughby *et al.*, "Target localization and real-time tracking using the Calypso 4D localization system in patients with localized prostate cancer," *Int. J. Radiat. Oncol. Biol. Phys.*, vol. 65, no. 2, pp. 528–534, Jun. 2006.

[11] J. A. Tanyi *et al.*, "Assessment of planning target volume margins for intensity-modulated radiotherapy of the prostate gland: Role of daily inter- and intrafraction motion," *Int. J. Radiat. Oncol. Biol. Phys.*, vol. 78, no. 5, pp. 1579–1585, Dec. 2010.

[12] R. Eppenga, K. Kuhlmann, T. Ruers, and J. Nijkamp, "Accuracy assessment of wireless transponder tracking in the operating room environment," *Int. J. Comput. Assist. Radiol. Surg.*, vol. 13, no. 12, pp. 1937–1948, 2018.

[13] A. M. Franz *et al.*, "Standardized accuracy assessment of the calypso wireless transponder tracking system," *Phys. Med. Biol.*, vol. 59, no. 22, pp. 6797–6810, 2014.

[14] S. I. Patel, M. J. Souter, D. S. Warner, and M. A. Warner, "Equipment-related Electrocardiographic Artifacts," *Anesthesiology*, vol. 108, no. 1, pp. 138–148, 2008.

[15] K. Hodges, "IEC/EN 60601-1-2 Implications of the 4th edition- White Paper," Apr. 2018.

[16] International Commision on non-ionizing radiation protection (ICNIRP), "Guidlines for Limiting Exposure to Electromagnetic Fields (100 KHZ TO 300 GHZ)," *Health Phys.*, vol. 118, no. 5, pp. 483–524, 2020.

[17] M. K. Laudon, J. G. Webster, R. Frayne, and T. M. Grist, "Minimizing interference from magnetic resonance imagers during electrocardiography," *IEEE Trans. Biomed. Eng.*, vol. 45, no. 2, pp. 160–164, Feb. 1998.

[18] F. Van den Brande and P. Martens, "A false positive arrhythmia on electrocardiogram induced by a cell phone," *Eur. J. Emerg. Med.*, vol. 10, no. 4, 2003.

[19] R. Yang and Y. He, "Eddy current pulsed phase thermography considering volumetric induction heating for delamination evaluation in carbon fiber reinforced polymers," *Appl. Phys. Lett.*, vol. 106, no. 23, p. 234103, Jun. 2015.

[20] Y. He, R. Yang, H. Zhang, D. Zhou, and G. Wang, "Volume or inside heating thermography using electromagnetic excitation for advanced composite materials," *Int. J. Therm. Sci.*, vol. 111, pp. 41–49, Jan. 2017.

[21] J. Steadman, B. Catalani, C. Sharp, and L. Cooper, "Life-threatening perioperative anesthetic complications: Major issues surrounding perioperative morbidity and mortality," *Trauma Surgery and Acute Care Open*, vol. 2, no. 1. BMJ Publishing Group, 01-Jan-2017.

[22] B. Zhao *et al.*, "Comparison of short-term surgical outcome between 3D and 2D laparoscopy surgery for gastrointestinal cancer: a systematic review and meta-analysis," *Langenbeck's Archives of Surgery*, vol. 405, no. 1. Springer, pp. 1–12, 01-Feb-2020.

[23] A. P. Shah *et al.*, "Real-Time Tumor Tracking in the Lung Using an Electromagnetic Tracking System," *Int. J. Radiat. Oncol.*, vol. 86, no. 3, pp. 477–483, Jul. 2013.

[24] J. Nijkamp *et al.*, "Prospective study on image-guided navigation surgery for pelvic malignancies," *J. Surg. Oncol.*, vol. 119, no. 4, pp. 510–517, Mar. 2019.

[25] G. de Brunner, "Multi-Field Magnetic Tracking," CA 2733621, 2017.

Chapter 5: Usability of a Wireless Navigation Setup

Usability of a Wireless Navigation Setup

Usability Assessment of a Wireless Navigation Setup for Laparoscopic Rectal Cancer Surgery: A Phantom Study

I. Introduction

Rectal cancer is the eight most common cancer worldwide with an annual incidence of 704,000, constituting 3.9 percent of all diagnosed cancers [1]. Worldwide, surgery is the primary curative option in non-metastasized rectal cancer, which accounts for 75% of all diagnoses [2]. In the Netherlands, as much as 95% of patients with stadium I-III rectal cancer get surgical treatment [3]. In recent decades, laparoscopic surgery has progressively replaced open rectal surgery due to favorable short-term outcomes, such as less pain, reduced blood loss, and improved recovery time [4], [5]. However, laparoscopic rectal cancer surgery is associated with positive resection margin (RM) rates of 10-15% [4], [6], while larger margins are shown to negatively impact functional outcome [7], [8]. Therefore, indicating a need for accurate tumor localization and margin assessment during rectal cancer surgery.

Surgical navigation systems can be used to integrate preoperative imaging, showing relevant anatomy and the surgical target into the surgical procedure, providing intraoperative guidance using tracked surgical instruments. A surgical navigation setup incorporates a tracking system to actively track the tumor location and correlate the preoperative imaging to the intraoperative setting. Consequently, this information could be used to accurately determine for example the distal RM - i.e. 1 cm from distal tumor border - and therefore potentially decrease positive RM and improve patient outcome.

For successful implementation of surgical navigation setup an intraoperative accuracy below 1 cm should be achieved. Kok et al. proposed a navigation approach using an electromagnetic tracking system (EMTS), which has demonstrated feasibility and an intraoperative accuracy of 3 mm [9]. During rectal cancer surgery, wired electromagnetic sensors were placed on the skin and tumor and registered to a three-dimensional (3D) model of patient specific anatomy. Subsequently, a tracked tool was visualized relative to the 3D model allowing oncological surgeons to obtain real-time accurate information on tumor location, as well as on critical surrounding organs. However, their system has two main disadvantages: positioning and securing the tumor sensor against the rectal tumor during surgery can be impractical, and an intraoperative cone beam computed tomography (CBCT) scan is needed for registration resulting in additional radiation exposure and surgical workflow interruption.

In this study, we present a novel wireless surgical navigation setup, improving workflow by eliminating the need for intraoperative sensor placement and imaging. Before surgery, two tumor transponders are implanted near the distal border of the tumor in the rectal wall. Subsequently, the position and orientation of the transponders can be determined with a high accuracy with respect to a tracking array (TA), providing real-time information about tumor location and orientation [10], [11].

However, in contrast to the previous wired approach, the wireless navigation setup is limited to tracking of three transponders. In a surgical setting, one transponder is needed for use in a tracked surgical tool, e.g. Pointer or Stapler, and two sensors are available for 6DOF tumor tracking [11]. Therefore, the setup is not able to track any surrounding structures, limiting the spatial orientation in the 3D model and correlation to the intraoperative setting by the surgeon. In addition, in our proposed setup the TA in positioned in a tilted pose above the patient further limiting intuitive visualization. The visualization methods used in this setup, are aimed to mitigate these limitations and provide an intuitive view of the surgical target area and surgical tool using application specific camera views. Furthermore, the shortest distance from the tracked tool to the tumor, being clinically relevant for RM estimation, are calculated and displayed in real-time.

In this study, the feasibility of the proposed wireless setup was assessed for the intraoperative phase based on usability and accuracy on a phantom. Where the primary aim is to assess the usability of a wireless surgical navigation setup for laparoscopic rectal cancer surgery as determined by questionnaires among participating surgeons using a phantom. While the secondary aim to determine the accuracy of the distance from the tumor border to the probe tip and the cutting plane of a stapler for laparoscopic rectal tumor RM assessment.

II. Methods and Materials

A. Surgical navigation setup

The surgical navigation setup consists of an EMTS, a readout system, a tracked laparoscopic pointer, a tracked laparoscopic stapler, an inertial measurement unit (IMU) and three 5DOF implantable wireless Beacon transponders with different excitation frequencies – i.e. 300, 400, 500 kHz -, a diameter of 1.85 mm and 8 mm long. The readout system (Quad core 3.20 GHz Intel® Xeon® E-2104G with 16GB memory) is used for processing of the tracking data and visualization of the navigation using 3D Slicer, the “Image-guided navigation toolkit for 3D Slicer (SlicerIGT)” and the Python command line interface [12]. The laparoscopic pointer, with a diameter of 6 mm and 40 cm long, was developed in-house and consists of a polyoxymethylene shaft and cap. A transponder is positioned in the pointer cap, approximately 1 cm from the tip of pointer, to minimize influence of

orientation errors, and secured in place with polyurethane casting resin, see Figure 1. The laparoscopic stapler is a Powered Echelon™ surgical stapler (Echelon Flex, Johnson & Johnson) with an in-house modified GST reload to fit a 5DOF transponder, enabling tracking of the stapler cutting plane.

The incorporated EMTS, the Calypso GPS for the body (Varian Medical Systems Inc., Palo Alto, California, USA), has an eFOV of 27.5 x 27.5 x 22.5 cm (in x-, y-, z-direction), starting at 5.5 cm offset from the tracking array (TA), in which the Beacon transponders can be tracked. The x- and y- axes define a parallel plane with regard to the TA while the z-axis is perpendicular, pointing away from the TA. The IMU is rigidly attached to the TA for tilt correction of visualization. The transponders inside the eFOV are excited at characteristic frequencies using an excitation signal generated by alternating current magnetic field, inducing a current in the transponder coil. Subsequently, the tracking system determines the 5DOF pose - position and orientation - based on the magnetic flux produced by transponder, which is sensed using a separate array of sensor coils inside the TA. Transponder position trueness has been reported at 0.2 mm, while precision has been reported at 1.3 mm standard deviation in Chapter 3. The z-axis direction reversal detection and correction algorithm, described in Appendix A is applied on the orientation data. Furthermore, the TTV sensor fusion method proposed by Eppenga et al. is implemented to fuse 5DOF pose of two transponders into a single 6DOF virtual transponder [11].

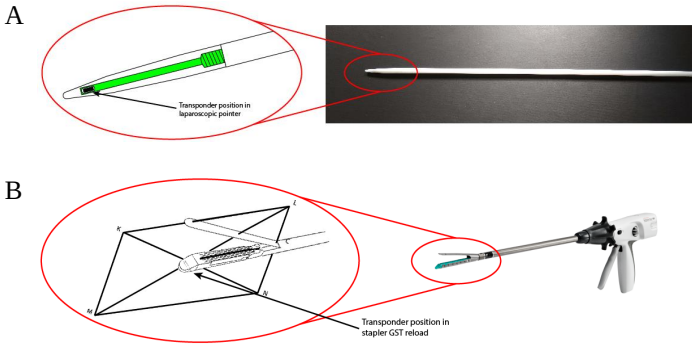

Figure 1 (A) Image of the wireless tracked laparoscopic pointer (right) and a schematic of design and transponder position (left); (B) Image of the wireless tracked laparoscopic stapler (right) and a schematic of the GST reload, transponder position and resulting tracked cutting plane KLMN of laparoscopic stapler (left).

B. Measurement Setup

Experiments were performed in the operating room of the NKI, being the proposed operational environment of the navigation setup. Here measurements were performed on a distortion free table using a sleeve, incasing the TA, and a Hummel board -depicted in Figure 2, for stable positioning of phantom in the eFOV. A laparoscope and laparoscopy simulator are used to simulate a surgical situation. Furthermore, a multimodal rectum-and-mesorectal-fat-mimicking phantom was developed based on plastisol melting techniques described by Ungi et al. [13]. The hollow cylindric phantom mimics a view of the rectum from the abdominal cavity as approached during a laparoscopic total mesorectal excision (TME). A silicon-based tumor, with an approximate maximal diameter of 4 cm, minimal diameter of 2.5 cm and height of 1.8 cm, is embedded in the middle of the phantom. The phantom was placed in the laparoscopy simulator parallel to the x- y-plane in the eFOV of the Calypso system, at an approximate 7.5 cm distance from the TA.

This study followed the proposed clinical workflow for wireless navigation in laparoscopic rectal cancer surgery at the Netherlands Cancer Institute (NKI) (study: N20WRS). During the preoperative phase, a pre-loaded needle with a 5DOF 17G Beacon® Transponder is inserted into the phantom, near the distal border of the tumor, within the intended resection, and the transponder is pushed out into the tissue. This is repeated for the second transponder, considering the sensor fusion algorithm accuracy may be negatively affected when the angle between the z-axes of the two transponders – i.e. length axis - approach 0° [11]. Subsequently, a clinical CT-scan of the phantom is acquired – 38 mAs, 120 kV, 1 mm slice thickness - and used to create a 3D model of the transponders and tumor using 3D Slicer. In addition to the proposed clinical workflow, the rectal wall of the phantom, which is assumed to be rigid with respect to the transponders, is segmented during this study as a tracked anatomical reference. During intraoperative phase, a laparoscope was used for visualization of the target area, while the navigation setup was used to verify the tumor location and intended RM. Usability of the current wireless

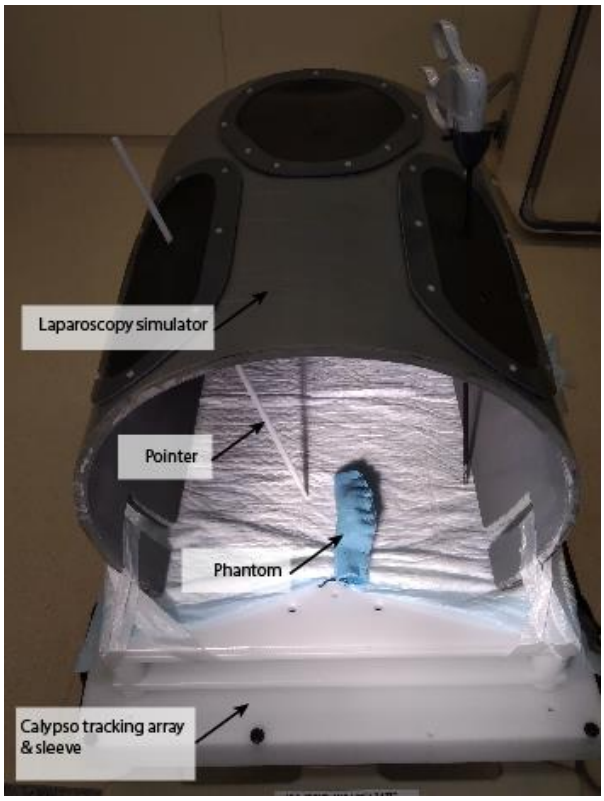

Figure 2 Picture of measurement setup for phantom experiments.

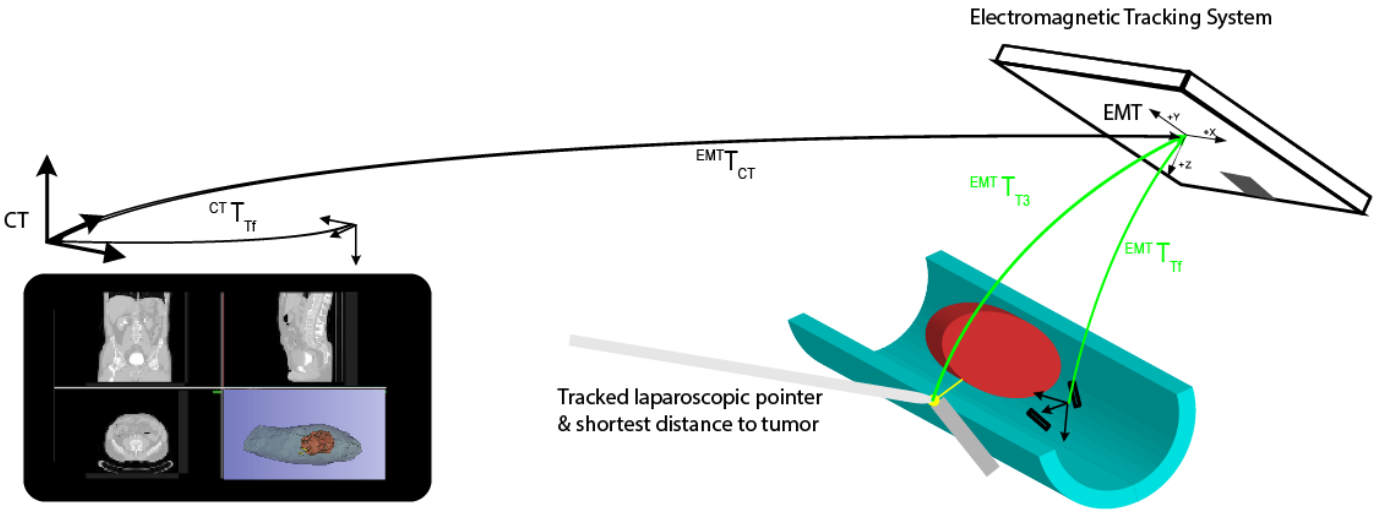

Figure 3 Schematic CT-EMTS setup for phantom measurements. Representation of phantom model, received transforms and shortest distance as calculated for accuracy evaluation.

surgical navigation setup, was assessed using the System Usability Scale (SUS), based on questionnaires filled in by two participating oncologic surgeons.

During experiments, samples were received, processed and displayed in real-time at a sample rate of 25Hz. i.e. 8 Hz per sensor being the maximum frequency of the EMTS. Each sample consisted of the following pose information:

- The 5DOF pose of three EM transponders (*Tx*, *x* = 1, 2, 3) expressed in the EMT coordinate system ${}^{EMT}T_{Tx}$

All poses were represented by a 4 x 4 transformation matrix T and communicated through OpenIGTLink TRANSFORM messages. The superscript EMT implies the coordinate system in which the specific pose is given, e.g., EM Tracker. The subscript specifies the tool or transponder of which the pose is expressed in this coordinate system. Therefore, ${}^{EMT}T_{T1}$ is the pose of the first transponder expressed in the EMT coordinate system. The 5DOF data of the 300 Hz and 400 Hz transponder (${}^{EMT}T_{T1}$ and ${}^{EMT}T_{T2}$), being the tumor tracker transponders, was fused to a 6DOF transformation matrix: ${}^{EMT}T_{Tf}$, see Appendix X. 500 Hz transponders (${}^{EMT}T_{T3}$) were placed in both the tracked pointer and stapler, which can be used interchangeably. Specialized readout software, provided by the manufacturer, was used for readout of the EMTS system.

For CT-EMT registration, virtual cylinder models were registered to the transponder models in CT coordinates, resulting in a 5DOF representation. Subsequently, the sensor fusion algorithm is used to determine a 6DOF virtual transponder in CT coordinates (${}^{CT}T_{Tf}$), see Figure 3, which is then registered to EMT :

$$ {}^{EMT}T_{CT} = {}^{EMT}T_{Tf}\,{}^{CT}T_{Tf}^{-1} = {}^{EMT}T_{Tf}\,{}^{Tf}T_{CT} \qquad (5.1) $$

Consequently, the 3D model, expressed as surface points in CT coordinates (${}^{CT}model$), can be transformed using:

$$ {}^{EMT}model = {}^{EMT}T_{CT}\;{}^{CT}model \qquad (5.2) $$

C. *Visualization*

The pointer is represented in the 3D visualization using a custom made 1:1 scale model. Since the stapler can be tracked in 5DOF, the virtual cutting plane is displayed using a circle with a diameter corresponding to the stapler anvil and a protruding cylinder model indicating the transponder pose. If the cutting plane and rectal wall model overlap, this is visualized with a red resection plane.

A custom layout with dual 3D view is used in 3D Slicer for visualization, showing a static laparoscope port view and a dynamic cutting plane view. For the static view, two points (${}^{EMT}p_1$, ${}^{EMT}p_2$) are placed with the pointer through the laparoscope camera port aiming at the target lesion, the first point cranial and the second caudal in the EM FOV, see Figure 4. Subsequently, using the tilt vector of the TA, as determined by the rigidly attached IMU sensor, and an adjustable zoom variable the first 6DOF camera pose is defined, see Figure 5. Since the virtual cutting plane is mostly orthogonal to this first view, a second view is used in conjunction with the tracked stapler. This dynamic view is

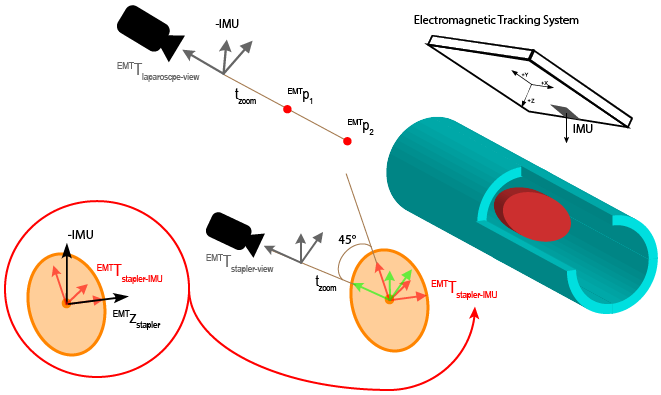

Figure 4 Schematic representation of camera poses; the static laparoscope port view is determined using two points along the view axis and IMU vector (top); the initial coordinate system of the dynamic cutting plane view is based on stapler transponder vector and IMU data (bottom left) and subsequently rotated 45 ° around transponder axis and translated.

based on the ZDR corrected transponder vector ($^{EMT}z_{T3}$). This vector normal to the cutting plane, is combined with the tilt vector of the TA – as determined by IMU, and assumed not to be (anti-) parallel to $^{EMT}z_{T3}$ - to define a 6DOF pose, which is subsequently rotated 45° around the transponder axis to achieve an oblique view angle, see Figure 6.

The shortest distance from either the pointer tip or cutting plane to a point on the tumor model surface are calculated and displayed in accordance with the used tool – Python implementation in Appendix G -. For pointer tip to tumor model distances (d), the Euclidian norm of the vectors between the pointer position ($^{EMT}t_{T3} = {}^{EMT}p$) and the position of model surface points ($^{EMT}model$), as transformed to EMT coordinate system using 5.2, is calculated:

$$d\left({}^{EMT}model, {}^{EMT}p\right) = \left\| {}^{EMT}model - {}^{EMT}p \right\| \qquad (5.3)$$

For cutting plane to tumor model distance, the projections of the transformed model surface points ($^{EMT}model$) on the cutting plane are calculated (^{EMT}p) and subsequently the Euclidian norm to the corresponding model surface points is determined using 5.3. For both, only the shortest distance is displayed.

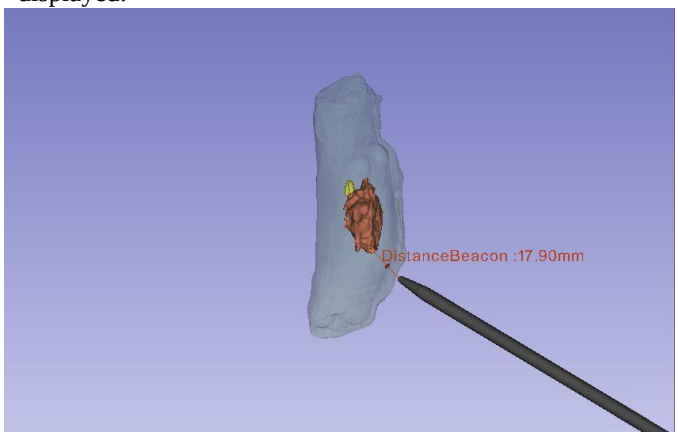

Figure 5 Intraoperative 3D visualization showing laparoscope port view of phantom and laparoscopic pointer.

D. Accuracy Evaluation

During experiments, accuracy of the navigation setup was determined by correlation of the position of the distal tumor margin, as determined with navigation setup and marked by surgical clips, with the position of the clips as determined with a post-operative CT. At each of the four placed clips, the shortest distance to the tumor was be recorded five times by placing the pointer at the base of the clip and recording 20 subsequent distance values - approximately 2.5 seconds at 8 Hz per transponder -. Subsequently, the interquartile range (IQR) over each 20 distance values was calculated, as well as over the 100 values per clip determining a precision error for pointer placement. The mean distance over 20 values per measurement and 100 values per clip, was compared to the absolute CT reference and reported as a mean absolute error (mm).

III. RESULTS

The SUS-score for the wireless surgical navigation setup was 77.5, additionally surgeons indicated the technology could contribute to more decisive action during surgery. Furthermore, when comparing the setup to surgery without surgical navigation, surgeons indicated a more positive experience for effective tumor localization and RM estimation, while no negative experiences were reported.

In total four clips were placed during experiments with a mean absolute distance error of 1.32 mm (range: 0.06 mm - 3.51 mm), whereas errors per clip are specified in Figure 7.

Figure 7 shows results of IQR evaluation, where IQR over the 20 distance values per measurement ranged from 0.07 mm to 1.63 mm, while IQR over all 100 values per clip ranged from 0.91 mm to 1.96 mm.

IV. DISCUSSION

In this study, a novel wireless navigation setup is presented for real-time tumor tracking during laparoscopic rectal cancer surgery. Our preliminary work on a phantom model suggests improvement in accurate tumor localization and RM assessment. Furthermore, participating surgeons were enthusiastic about usability and indicate potential for more decisive action based on the navigation setup, most notably for distal resection margin assessment. Therefore, the presented wireless navigation setup shows potential for use during rectal cancer surgery, aiming to reduce positive RM while sparing healthy tissue.

However this study was conducted in a controlled setting, with optimal TA positioning. Where, Chapter 3 showed precision errors increase drastically near the top the field up to 2.72 mm and 1.63° – i.e. furthest away from the TA -. Therefore alignment of the more precise lower levels of eFOV with the target area, as performed in this study, would be ideal. However, during laparoscopic surgery, the operating area is occluded by surgical instruments – e.g. trocars, laparoscopic instruments –, the surgeon, surgical assistant and equipment – e.g. anesthesiology setup or surgical supply carts -. Therefore, positioning of the Calypso system and aligning the TA and eFOV with the target area, could prove a challenging task. Mitigating the decreased precision by adding constraints to positioning of the TA - i.e. aligning the more precise lower levels of the eFOV with the target - is therefore not feasible. It is therefore recommended to assess navigation data based on multiple data samples instead of single values. Alternatively, filtering of these errors using a Savitzky-Golay or Kalman filter is proposed.

The most comparable study was performed for navigation in breast conserving surgery by Janssen et al. [14]. They showed improved resection of complex tumors with navigation guidance even with large tissue deformations during surgery. A SUS score of 68.5 was obtained for their system, considered above average. Our wireless navigation setup showed higher perceived usability of 77.5, which is higher than 70% of all products tested with SUS scores, indicating good usability [15], [16]. However, direct

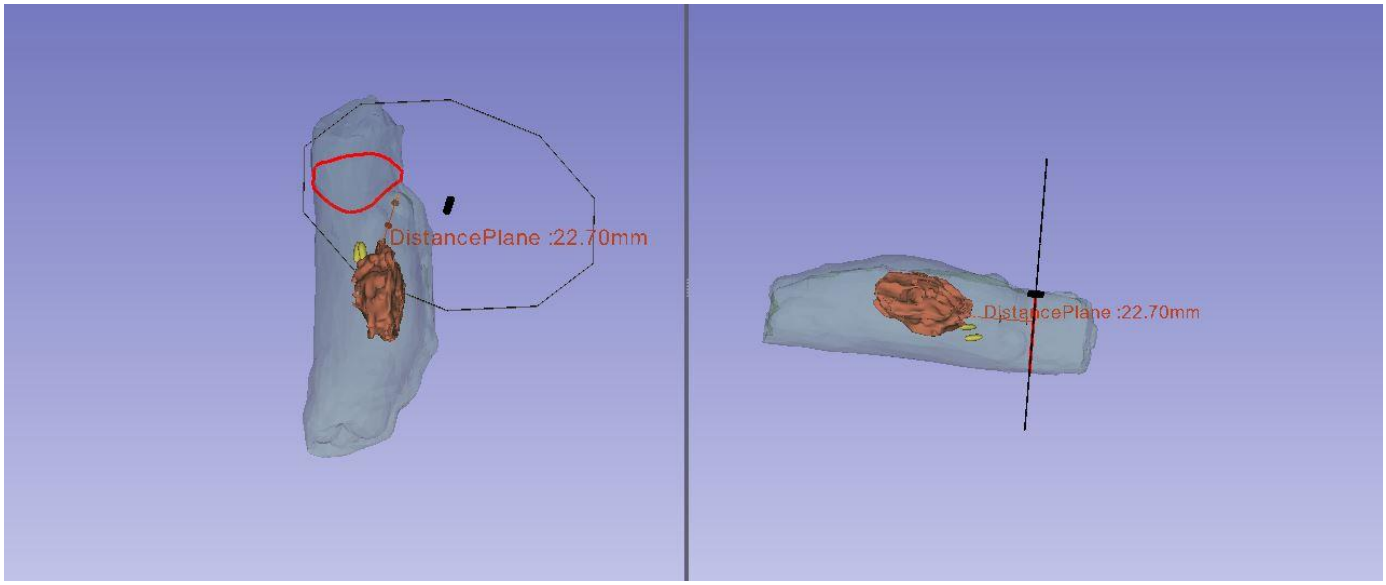

Figure 6 Intraoperative 3D visualization showing laparoscope port view and cutting plane view of phantom and laparoscopic stapler.

comparison is challenging, as application of the wireless navigation differ. Furthermore, they used a hybrid optical-EM tracking system, where 6DOF tumor tracking is based on position data of three tumor transponders while optical markers are used for surgical tool tracking. Therefore, their system, as the setup presented here, has the major advantage of being wireless, eliminating the need for intraoperative sensor placement and CBCT acquisition needed for comparable wired navigation systems. During acquisition, the patient receives additional radiation dose and surgical workflow is interrupted, since all surgical staff is required to leave the OR.

Such a wired surgical navigation setup was proposed by Kok et al. for rectal cancer surgery [9]. Next to intraoperative tumor tracking, they tracked surrounding structures using patient sensor on the skin resulting in a feasible, safe and accurate workflow. In contrast to our proposed setup, this enables tracking of surrounding structures, such as bones and vessels, offering increased spatial orientation in the 3D model and correlation to the intraoperative setting. In addition, in our proposed setup the TA in positioned in a tilted pose above the patient further limiting intuitive visualization. This combination of limiting factors was mitigated by use of an IMU and application specific camera views – i.e. laparoscope view and stapler view -.

For accurate visualization, tracking accuracy of the EMTS is essential. This accuracy decreases when further from the TA and is affected by distortions – Chapter 3 -. However, when incorporating the transponders in a rigid body, e.g. laparoscopic stapler and pointer, a third form of error is introduced by the transponder quality. As explained in Appendix E, deviations between the sensor coil and transponder capsule were observed up to 3.43°. Given the 400 mm long pointer an error of up to 23.97 mm could be observed, which is a visualization error and due to the design only translates to positional error at the tip of 0.06 mm. However, for an anvil length of 60 mm, this results in positional errors of up to 3.60 mm at the end of the anvil which could translate to errors in RM assessment. Furthermore, such errors can affect the perceived usability and reliability of a setup. Therefore, a tool to assess these errors is proposed in Appendix E, so transponders with the smallest deviations can be used in tracked surgical instruments.

During surgery, the aim of using a surgical navigation setup is to give the surgeon accurate real-time information on tumor location and consequently determine the RM. Therefore, the surgeon needs to correlate the navigation information to the intraoperative setting. Here we used application specific camera views, which could be complemented with display of CT and MRI images based on the location of the pointer tip. Additionally a partial model of the rectal wall, where it is assumed to be rigid to the transponders, was added in this study as a tracked anatomical reference. However, when starting with the eventual resection of the rectum, using a surgical stapler, the rectum is significantly deformed and display of the rigid model is therefore invalid. Subsequently, visualization should be restricted to transponder and tool poses. Since the transponders are placed distal to the tumor and RM has been determined before resection, this visualization still yields most important information.

As for successful implementation of this wireless navigation setup, a multidisciplinary collaboration is essential. The preoperative workflow, starts with acquisition of a high quality MRI used for tumor delineation due to its high soft tissue contrast [17]. Since the transponder cause small signal voids on MRI images, the MRI has to be acquired before implantation of the transponders in the rectum and CT is the most appropriate imaging technique to localize the transponders after. Subsequently, registration of the MRI and CT images is required for their combined information to be

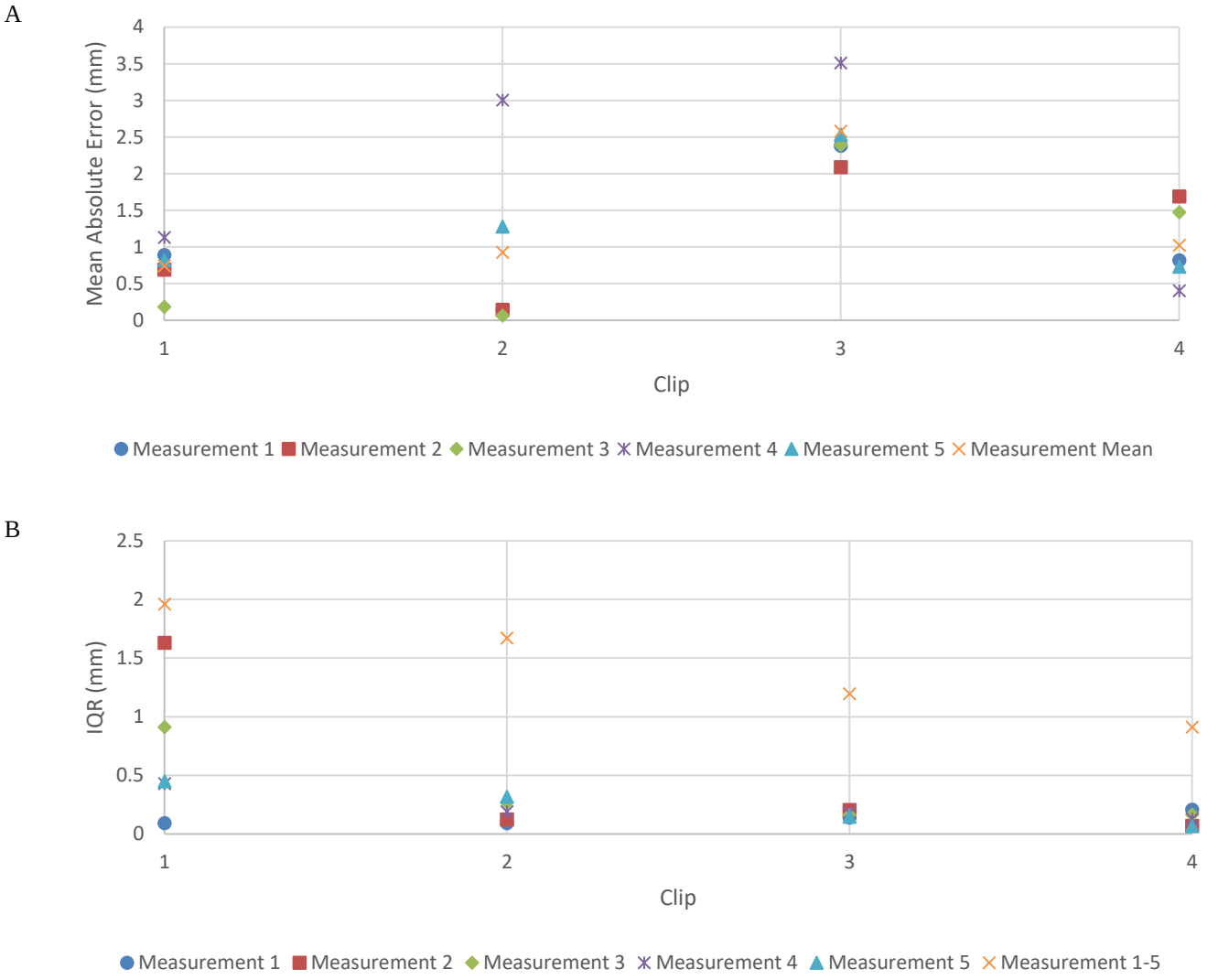

Figure 7 Results of accuracy evaluation over 20 values per measurement and 100 values per clip; showing mean absoluter error (A) and IQR (B).

used by navigation experts for localization of the implanted transponders relative to the tumor borders and create a 3D model. Our study was limited to acquisition of CT images, however for clinical implementation an accurate MRI-CT registration method is needed.

The wireless surgical navigation setup assumes the two transponders to be representative for the tumor pose. Migration and tissue deformation may cause this assumption to be invalid. In our phantom setup, we observed deformation due to pointer and stapler placement, influencing both accurate visualization and distance calculations. Beacon transponders are shown to be positionally stable in prostate tissue and no migration was observed in breast tissue for comparable fiducials [18], [19]. However, these studies focused on positional accuracy, while also orientational stability is needed in our application. Furthermore, the layered rectal wall might pose different challenges, compared to glandular and connective tissue of the prostate and breast, in migration and deformation. Therefore, it is recommended to study potential tissue deformation and migration of transponders in *ex vivo* setting.

In conclusion, this study shows good usability and accuracy of a novel wireless navigation setup for real-time tumor tracking during laparoscopic rectal cancer surgery on a phantom. However, it is recommended to study potential tissue deformation and migration of transponders in *ex vivo* setting before clinical implementation of this setup.

V. REFERENCES

[1] F. Bray, J. Ferlay, I. Soerjomataram, R. L. Siegel, L. A. Torre, and A. Jemal, "Global cancer statistics 2018: GLOBOCAN estimates of incidence and mortality worldwide for 36 cancers in 185 countries," *CA. Cancer J. Clin.*, vol. 68, no. 6, pp. 394–424, Nov. 2018.

[2] P. Rawla, T. Sunkara, and A. Barsouk, "Epidemiology of colorectal cancer: Incidence, mortality, survival, and risk factors," *Prz. Gastroenterol.*, vol. 14, no. 2,

pp. 89–103, 2019.

[3] Intergraal Kankercentrum Nederland (IKNL), "Behandeling darmkanker." [Online]. Available: https://iknl.nl/kankersoorten/darmkanker/registratie/behandeling. [Accessed: 10-Apr-2021].

[4] H. J. Bonjer *et al.*, "A Randomized Trial of Laparoscopic versus Open Surgery for Rectal Cancer," *N. Engl. J. Med.*, vol. 372, no. 14, pp. 1324–1332, 2015.

[5] R. Veldkamp *et al.*, "Laparoscopic surgery versus open surgery for colon cancer: Short-term outcomes of a randomised trial," *Lancet Oncol.*, vol. 6, no. 7, pp. 477–484, Jul. 2005.

[6] A. S. Rickles *et al.*, "Rickles (2015) - High rate of positive circumferential resection margins following rectal cancer surgery.pdf," *Ann. Surg.*, vol. 262, no. 6, pp. 891–898, 2015.

[7] C. G. C. Pales, S. An, J. P. Cruz, K. Kim, and Y. Kim, "Postoperative bowel function after anal sphincter-preserving rectal cancer surgery: Risks factors, diagnostic modalities, and management," *Annals of Coloproctology*, vol. 35, no. 4. Korean Society of Coloproctology, pp. 160–166, 2019.

[8] W. S. Lee *et al.*, "Risk factors and clinical outcome for anastomotic leakage after total mesorectal excision for rectal cancer," *World J. Surg.*, vol. 32, no. 6, pp. 1124–1129, Jun. 2008.

[9] E. N. D. Kok *et al.*, "Accurate surgical navigation with real-time tumor tracking in cancer surgery," *npj Precis. Oncol.*, vol. 4, no. 8, pp. 1–7, 2020.

[10] R. Eppenga, K. Kuhlmann, T. Ruers, and J. Nijkamp, "Accuracy assessment of wireless transponder tracking in the operating room environment," *Int. J. Comput. Assist. Radiol. Surg.*, vol. 13, no. 12, pp. 1937–1948, 2018.

[11] R. Eppenga, K. Kuhlmann, T. Ruers, and J. Nijkamp, "Accuracy assessment of target tracking using two 5-degrees-of-freedom wireless transponders," *Int. J. Comput. Assist. Radiol. Surg.*, vol. 15, no. 2, pp. 369–377, 2019.

[12] A. Fedorov *et al.*, "3D Slicer as an Image Computing Platform for the Quantitative Imaging Network," *Magn Reson Imaging*, vol. 30, no. 9, pp. 1323–1341, 2012.

[13] T. Ungi *et al.*, "Navigated Breast Tumor Excision Using Electromagnetically Tracked Ultrasound and Surgical Instruments," *IEEE Trans. Biomed. Eng.*, vol. 63, no. 3, pp. 600–606, Mar. 2016.

[14] N. Janssen *et al.*, "Real-time wireless tumor tracking during breast conserving surgery," *Int. J. Comput. Assist. Radiol. Surg.*, vol. 13, no. 4, pp. 531–539, 2018.

[15] J. Sauro, *A Practical Guide to the System Usability Scale: Background, Benchmarks & Best Practices*. Denver: CreateSpace Independent Publishing Platform, 2011.

[16] J. Brooke, "SUS: A quick and dirty usability scale," *Usability Eval. Ind.*, vol. 189, Nov. 1995.

[17] NVVH, "Colorectaal carcinoom (CRC)," *Richtlijnendatabase*, 2019. [Online]. Available: https://richtlijnendatabase.nl/richtlijn/colorectaal_carcinoom_crc/startpagina_-_crc.html. [Accessed: 29-Mar-2021].

[18] D. W. Litzenberg *et al.*, "Positional Stability of Electromagnetic Transponders Used for Prostate Localization and Continuous, Real-Time Tracking," *Int. J. Radiat. Oncol. Biol. Phys.*, vol. 68, no. 4, pp. 1199–1206, Jul. 2007.

[19] T. Alderliesten, C. E. Loo, K. E. Pengel, E. J. T. Rutgers, K. G. A. Gilhuijs, and M. J. T. F. D. Vrancken Peeters, "Radioactive seed localization of breast lesions: An adequate localization method without seed migration," *Breast J.*, vol. 17, no. 6, pp. 594–601, Nov. 2011.

Chapter 6: Transponder Stability in Ex Vivo Specimen

Transponder Stability in *Ex Vivo* Specimen

Assessment of Positional and Orientational Stability of Electromagnetic Transponders in *Ex Vivo* Rectosigmoid and Tumor Specimen

I. INTRODUCTION

Rectal cancer is the eight most common cancer worldwide with an annual incidence of 704.000, constituting 3.9 percent of all diagnosed cancers [1]. Worldwide, surgery is the primary curative option in non-metastasized rectal cancer, which accounts for 75% of all diagnoses [2]. In the Netherlands, as much as 95% of patients with stadium I-III rectal cancer get surgical treatment [3]. In recent decades, laparoscopic surgery has progressively replaced open rectal surgery due to favorable short-term outcomes, such as less pain, reduced blood loss, and improved recovery time [4], [5]. However, laparoscopic rectal cancer surgery is associated with positive resection margin (RM) rates of 10-15% [5], [6], while larger margins are shown to negatively impact functional outcome [7], [8]. Therefore, indicating a need for accurate tumor localization and margin assessment during rectal cancer surgery. To this end, a new wireless surgical navigation setup is proposed, where preoperative imaging, showing relevant anatomy and the surgical target, is used intraoperatively to guide a surgeon using tracked surgical instruments.

In this study, we present a novel wireless surgical navigation setup, improving workflow by eliminating the need for intraoperative sensor placement and imaging. A surgical navigation setup incorporates a tracking system to actively track the tumor pose and correlate the preoperative imaging to the intraoperative setting. Before surgery, two tumor transponders are implanted near the distal border of the tumor in the rectal wall. Subsequently, the position and orientation of the transponders can be determined with a high accuracy with respect to a tracking array (TA), providing real-time information about tumor location and orientation [9], [10]. Consequently, this information could be used to accurately determine for example the distal RM - i.e. 1 cm from distal tumor border - and therefore potentially decrease positive RM and improve patient outcome.

For use in rectal cancer surgery, the transponders are expected to be implanted in the rectal wall, distal (order mm) to a tumor, or in tumor itself. Subsequently, the 5 degree of freedom (DOF) information of the two transponders will be fused into single 6DOF virtual transponder, subsequently a three-dimensional model of the tumor is expressed in this virtual coordinate system. Therefore, the relation between the two transponders and the tumor is assumed to be rigid. However, it remains unclear whether the transponders will remain sufficiently rigid in the rectal tissue. For example, migration of one or both transponders may occur, while tissue deformation may lead to relative rotations and/ or translations.

Transponders are shown to be positionally stable in prostate tissue with a root mean square error of inter-transponder distances of 1.5 mm (std: ≤1.2 mm) for up to 1 month [11]. Migration of 0.9 mm (std: 1.0 mm) was observed in breast tissue when comparable fiducials were in-situ for 60 days [12]. However, these studies focused on positional stability, while also orientational stability is needed in our application. Furthermore, the layered rectal wall might pose different challenges, compared to glandular and connective tissue of the prostate and breast, in migration and deformation.

This study will aim to investigate potential migration and quantify relative rotations and translations in three *ex vivo* samples of rectosigmoid or tumor tissue with a third transponder simulating a tumor. Intertransponder distances are assessed using cone beam computed tomography (CBCT) and EM data, while translations and rotations of the tumor simulating transponder in the virtual transponder coordinate system is assessed in static and dynamic experiments.

II. METHODS AND MATERIALS

A. Surgical Navigation Setup

The Electromagnetic tracking system (EMTS) consists of an EM Tracking Array (TA), a readout system and three 5DOF implantable wireless Beacon transponders with different excitation frequencies – i.e. 300, 400, 500 kHz -, a diameter of 1.85 mm and 8 mm long. The tracking system has an extended field of view (eFOV) of 27.5 x 27.5 x 22.5 cm (in x-, y-, z-direction), starting at 5.5 cm offset from the TA, in which the transponders can be tracked. The x- and y- axes define a parallel plane with regard to the TA while the z-axis is perpendicular, pointing away from the TA. The transponders inside the eFOV are excited at characteristic frequencies using an excitation signal generated by alternating current magnetic field, inducing a current in the transponder coil. Subsequently, the tracking system determines the 5DOF pose - position and orientation - based on the magnetic flux produced by transponder, which is sensed using a separate array of sensor coils inside the TA. Single transponder position trueness has been reported at 0.2 mm in Chapter 3, while precision has been reported at 1.3 mm standard deviation. The z-axis direction reversal detection and correction algorithm, described in Appendix A is applied on the orientation data. Furthermore, the TTV sensor fusion method proposed by Eppenga et al. is implemented to fuse 5DOF pose of two transponders into a single 6DOF virtual transponder [9].

B. Measurement setup

Experiments were performed using a separate EM and C-arm measurement setup in the operating room of the NKI, being the proposed operational environment of the navigation setup. Here, EM measurements were performed on a distortion

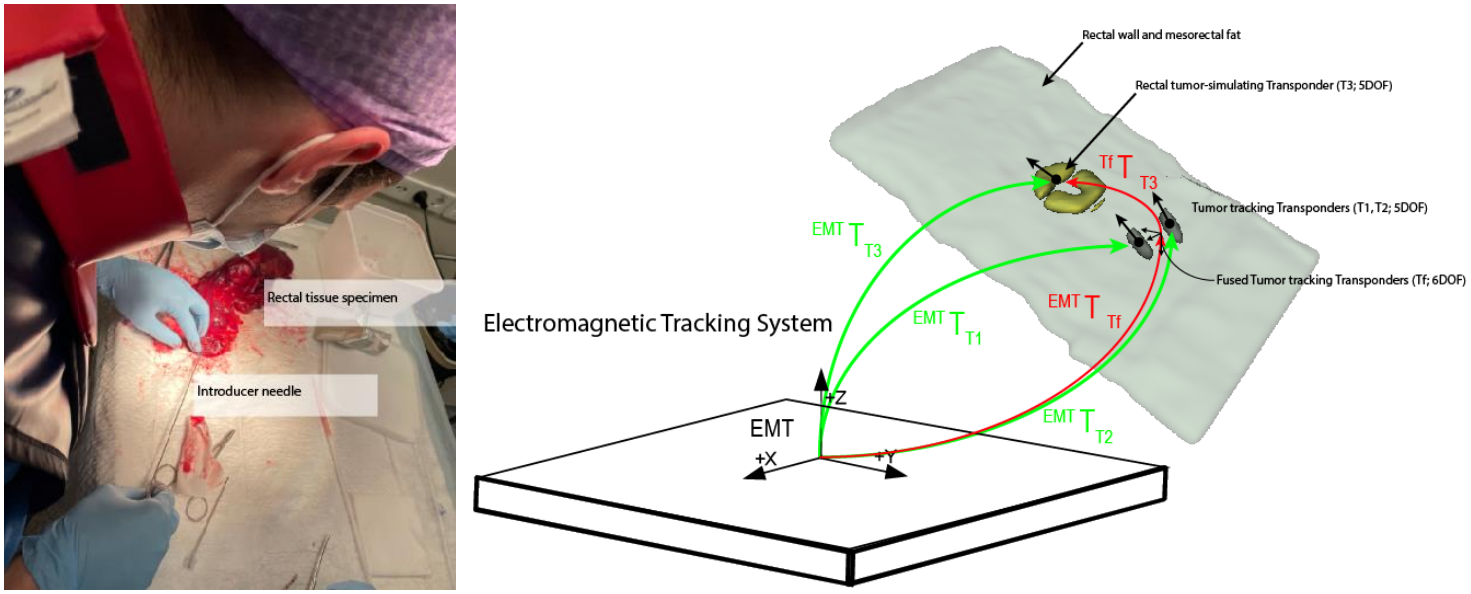

Figure 1 Implantation of transponders in the ex vivo specimen using a preloaded introducer needle (left), The schematic EMTS setup containing measured and calculated transformations (right). The transformations from the EMTS to the transponders (green) can change dynamically in real-time and are reported by the tracking system. The other mappings (both red) are initially unknown and are computed.

free table using a sleeve, incasing the TA, and a detachable

Hummel board, for stable positioning of *ex vivo* specimen parallel to the x- y-plane in the eFOV, at an approximate 7.5 cm distance from the TA. The detachable board is used to transition between the EM and C-arm setup. The C-arm setup consists of a radiolucent carbon fiber imaging table (Magnus, Maquet) on which the detachable board is placed inside the FOV of the mobile 3D C-arm (Ziehm Vision RFD 3D, Ziehm Imaging GmbH) for image acquisition.

This study workflow was comparable to the proposed preoperative workflow for wireless navigation in laparoscopic rectal cancer surgery at the Netherlands Cancer Institute (NKI) (study: N20WRS). Three *ex vivo* specimen were evaluated, the first two being rectosigmoid tissue, while the third consisted of a colon carcinoma metastasis. During the preoperative phase, a pre-loaded needle with a 5DOF 17G Beacon® Transponder was inserted into the rectosigmoid wall for the rectosigmoid specimen and into the tumor in the tumor specimen, subsequently the transponder was pushed out into the tissue, see Figure 1. This was repeated for the second transponder, considering the sensor fusion algorithm accuracy may be negatively affected when the angle between the z-axes of the two transponders – i.e. length axis - approach 0° [9]. In contrast to the workflow for wireless navigation, in this experiment a third tumor-simulating transponder is placed approximately 10 mm from the two tumor tracking transponders.

During the experiment, dynamic and static measurements were taken for each specimen. During static measurements, first a CBCT acquisition – 18 mAs, 60 kV, 0.6 mm slice thickness - is made and subsequently 150 EM samples are recorded after transition from the C-arm to the EM setup. During dynamic measurements, the specimen is manipulated three times, simulating forces present pre- and intraoperatively, and subsequently placed in a similar orientation on the board while EM data is acquired continuously. In total, three dynamic measurements are performed per specimen, with a static measurement before and after each, resulting in four static measurements per specimen.

During experiments, samples were recorded at a sample rate of 25Hz. i.e. 8 Hz per sensor being the maximum frequency of the EMTS. Each sample, see Figure 1, consisted of the following pose information:

- The 5DOF pose of three EM transponders (*Tx*, *x* = 1, 2, 3) expressed in the EMT coordinate system ${}^{EMT}T_{Tx}$

Specialized readout software, provided by the manufacturer, was used for readout of the EMTS system. All poses were represented by a 4 x 4 transformation matrix T and communicated through OpenIGTLink TRANSFORM messages. Subsequently, the data is received, evaluated, and stored in MATLAB (MATLAB, version R2019a, Natick, Massachusetts: The MathWorks Inc.) in 4 x 4 x *j* x *i* matrices, where *j* represent the number of samples per measurement and *i* represents the measurement number – e.g. 1..3 for dynamic measurements and 1..4 for static measurements -. The superscript EMT implies the coordinate system in which the specific pose is given, e.g. EM Tracker. The subscript specifies the tool or transponder of which the pose is expressed in this coordinate system. Therefore, ${}^{EMT}T_{T1}$ is the pose of the first transponder expressed in the EMT coordinate system. The 5DOF data of the 300 Hz and 400 Hz transponder (${}^{EMT}T_{T1}$ and ${}^{EMT}T_{T2}$), being the tumor tracker transponders, was fused to a 6DOF virtual transponder - Appendix B - represented by a transformation matrix: ${}^{EMT}T_{Tf}$. The 500 Hz 5DOF transponder (${}^{EMT}T_{T3}$), being the tumor-simulating transponder, was subsequently expressed in this virtual coordinate system (${}^{Tf}_{EMTS}T_{T3}$), using:

$$ {}^{Tf}_{EMTS}T_{T3} = {}^{Tf}T_{EMT}\ {}^{EMT}T_{T3} = {}^{EMT}T_{Tf}^{-1}\ {}^{EMT}T_{T3} \quad (6.1) $$

The additional subscript, EMTS, highlights the fact that this measurement originates from the EM tracking system. The distance between the tumor-simulating transponder and the 6DOF virtual transponder is reported.

C. Data Evaluation

Intertransponder distance

The mean position over the 150 samples was calculated per transponder ($^{EMT}\bar{t}_{Tx}$, x = 1, 2, 3) for all static measurements (i=1..4). Subsequently, three distances between the implanted markers per measurement were calculated, using:

$$ Dist_{Tx\to T(x+1)}(i) = \left\| {}^{EMT}\bar{t}_{Tx}(i) - {}^{EMT}\bar{t}_{T(x+1)}(i) \right\|_2 \quad (6.2) $$

Where $|\dots|_2$ denotes the Euclidian norm.

The difference in distance between all four static sets was calculated resulting in six intertransponder distance error values per distance for a total of 18 per specimen.

$$ Err_{pos} = Dist_{Tx\to T(x+1)}(i) - Dist_{Tx\to T(x+1)}(i+1) \quad (6.3) $$

All intertransponder distance errors were summarized by calculating the root mean square error (RMSE) per specimen, using:

$$ \text{RMSE} = \sqrt{\frac{1}{N}\sum_i^N Err_{(pos\,|\,or)}(i)^2} \quad (6.4) $$

Similair, after extraction of the transponder position from the CBCT images, the intertransponder distance error was calculated.

Static measurement

Static measurements were evaluated on relative position and orientation accuracy as determined by comparing $ {}^{Tf}_{EMTS}T_{T3} = \begin{bmatrix} {}^{Tf}_{EMTS}x_{T3} & {}^{Tf}_{EMTS}y_{T3} & {}^{Tf}_{EMTS}z_{T3} & {}^{Tf}_{EMTS}t_{T3} \\ 0 & 0 & 0 & 1 \end{bmatrix}$ between all four acquired datasets.

For position accuracy, the mean position, $ {}^{Tf}_{EMTS}\bar{t}_{T3}$, over the 150 samples was calculated. Subsequently, all possible distances between the four static measurements per specimen were calculated, resulting in six relative position error values:

$$ Err_{pos}(i) = \left\| {}^{Tf}_{EMTS}\bar{t}_{T3}(i) - {}^{Tf}_{EMTS}\bar{t}_{T3}(i+1) \right\|_2 \quad (6.5) $$

For orientation accuracy, the mean z-vector, $ {}^{Tf}_{EMTS}\bar{z}_{T3}$, over the 150 samples was calculated. Subsequently, all possible angles between the four static measurements per specimen were calculated, resulting in six relative orientation error values. The angle between these vectors (p = $ {}^{Tf}_{EMTS}\bar{z}_{T3}(i)$, q = $ {}^{Tf}_{EMTS}\bar{z}_{T3}(i+1)$) was calculated using the inner product:

$$ Err_{or}(i) = \arccos\left(\frac{(p,q)}{\|p\|\|q\|}\right) \quad (6.6) $$

Both relative position and orientation errors are summarized by calculating the RMSE per specimen, using (6.4).

Dynamic measurement

Dynamic measurements were evaluated on relative position as determined by comparing the continuous data stream ($ {}^{Tf}_{EMTS}T_{T3}(j,i)$, j = 1…N, i = 1 … 3) to the corresponding mean static EM measurement ($ {}^{Tf}_{EMTS}\bar{T}_{T3}(i)$, i = 1..3) as reference, using:

$$ Err_{pos}(i) = \left\| {}^{Tf}_{EMTS}\bar{t}_{T3}(i) - {}^{Tf}_{EMTS}t_{T3}(j,i) \right\|_2 \quad (6.7) $$

Orientation accuracy was defined as the angle between the vectors (p = $ {}^{Tf}_{EMTS}\bar{z}_{T3}(i)$, q = $ {}^{Tf}_{EMTS}z_{T3}(j,i)$) as calculated using (6.6)

III. RESULTS

Distance between the tumor-simulating transponder and the 6DOF virtual transponder was 7.7 mm for the first specimen, 16.3 mm for the second specimen and 10.5 mm for the third specimen.

Intertransponder distance

RMSE of intertransponder distance evaluation based on EM and CBCT data are listed in Table 1. The rectosigmoid specimen – i.e. Specimen 1&2 – showed higher errors of up to 10.8 mm and 11.5° compared to a maximum of 0.3 mm and 0.4° for the specimen where transponders were implanted in tumor tissue.

Table 1 Results of intertransponder distance evaluation

	EM RMSE (range)	CBCT RMSE (range)
Specimen 1	1.2 mm (0.0 – 2.8)	1.3 mm (0.0 – 2.7)
Specimen 2	5.8 mm (0.1 – 10.8)	6.0 mm (0.1 – 11.5)
Specimen 3	0.1 mm (0.0 - 0.3)	0.2 mm (0.0 - 0.4)

Static measurement

Results of relative position and orientation data evaluation are listed in Table 2. Comparing the corresponding static EM measurements for the rectosigmoid specimen resulted in relative position errors between 1.5 mm and 23.7 mm, while orientation errors ranged from 12.8° up to 108.5°. Considering, the tumor tissue specimen – i.e. Specimen 3 - resulted in relative position errors between 0.1 mm and 0.2 mm, while orientation errors ranged from 0.3° to 0.9°.

Table 2 Results of relative position and orientation data evaluation of static measurements

	Relative Position RMSE (range)	Relative Orientation RMSE (range)
Specimen 1	2.7 mm (1.5 - 4.1)	33.4° (16.1 - 48.7)
Specimen 2	19.1 mm (2.5 - 23.7)	83.9° (12.8 - 108.5)
Specimen 3	0.2 mm (0.1 - 0.2)	0.7° (0.3 - 0.9)

Dynamic measurement

All position and orientation error values per specimen are visualized using a boxplot in Figure 3.

The first specimen resulted in a median positional error 3.2 mm with an IQR of 2.8 mm, while the median orientation error was 32.5° with an IQR of 32.4°.

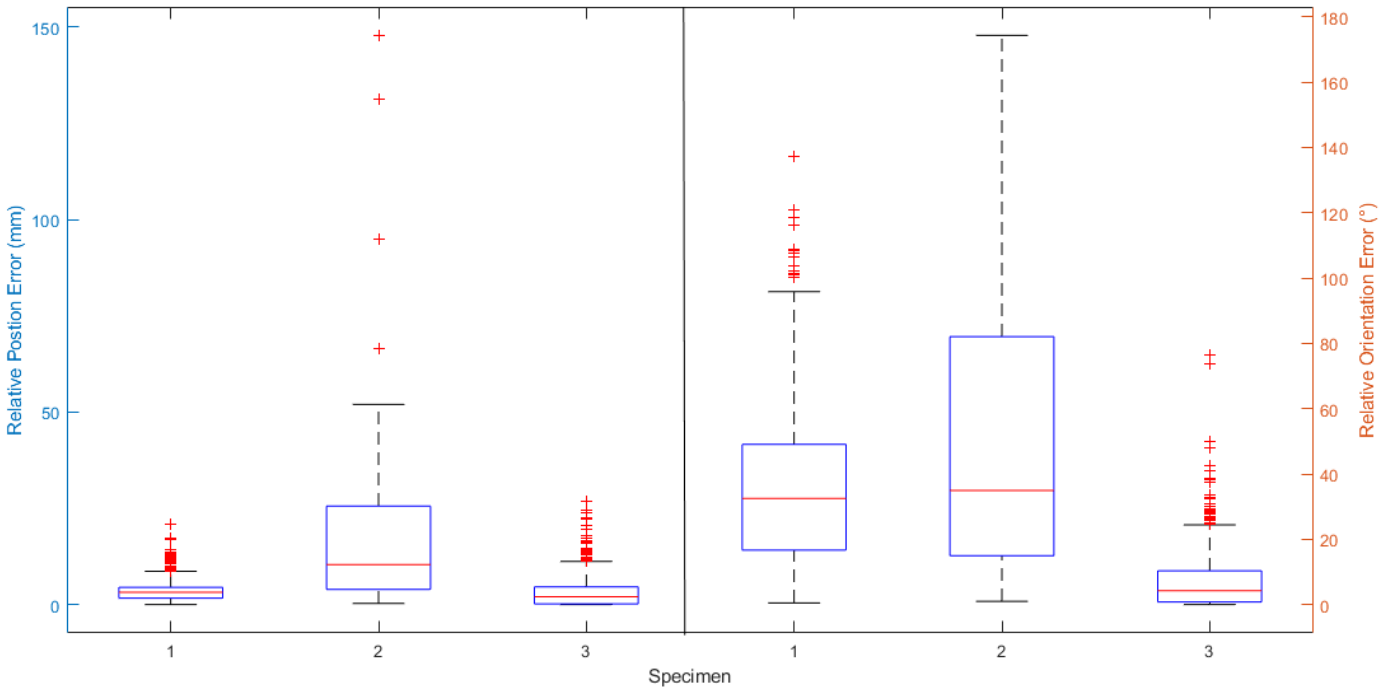

Figure 2 Results of dynamic measurements depicting the relative position and orientation errors as specified using a box-and-whisker plot over all error values per measured specimen. On each box, the central mark indicates the median, and the bottom and top edges of the box indicate the 25th and 75th percentiles, respectively. The whiskers extend to the most extreme data points not considered outliers (1.5 times the interquartile range from the box), and the outliers are plotted individually using the '+' symbol.

The second specimen resulted in a median positional error 10.3 mm with an IQR of 21.7 mm, while the median orientation error was 34.9° with an IQR of 67.1°.

The third specimen resulted in a median positional error 2.0 mm with an IQR of 4.4 mm, while the median orientation error was 4.3° with an IQR of 9.6°.

IV. DISCUSSION

In this study, the influence of migration and tissue deformation was assessed for multiple *ex vivo* specimen and relative rotations and translations were quantified. Our preliminary work on three tissue specimen suggests relative stability of transponders when implanted in tumor tissue even in dynamic experiments. However, large orientation errors are observed when transponders are implanted in the rectal or sigmoid wall. Therefore, accuracy of our proposed wireless navigation setup may improve with implantation of transponders inside of the tumor compared to the rectal wall.

Intertransponder distance evaluation showed higher errors for both rectosigmoid specimen of up to 10.8 mm using EMTS data, while the maximum error seen in the tumor specimen was 0.3 mm. These results are backed up by the CT data and indicate a better positional stability of the transponders inside of the tumor tissue. Similarly, during ${}^{Tf}T_{T3}$ evaluation higher errors are seen for both rectosigmoid specimen, when compared to the tumor specimen. Here, *T3* is expressed in the virtual coordinate system (*Tf*), therefore these errors indicate a combination of orientational and positional stability of all three transponders in the specimen. For accurate visualization and RM assessment during surgical navigation, both errors play an important role.

Positional errors for transponders placed in the rectosigmoid wall between static measurements in this study ranged between 1.5 mm – 23.7 mm, while dynamic measurements showed errors up to 150 mm. These errors could be caused by migration and deformation properties of the multi-layered rectal wall. However, all results are derived from evaluation of ${}^{Tf}T_{T3}$ data, when *T3* is expressed in this virtual coordinate system, position errors can be caused by translations of *T3* as well as rotations and translations of both tumor tracker transponders. A larger distance between sensors can increase influence of tissue deformation, scale rotation errors and therefore affect navigation accuracy, which could be a cause of the higher position errors seen in the second specimen. Therefore, it is recommended to minimize intertransponder distance in future experiments.

Previous studies have shown transponders to be positionally stable in prostate tissue with a root mean square error of inter-transponder distances of 1.5 mm (std: ≤1.2 mm) for up to 1 month [11]. Migration of 0.9 mm (std: 1.0 mm) was observed in breast tissue when comparable fiducials were in-situ for 60 days [12]. These studies evaluated *in vivo* stability over a longer time period, whereas our study was limited to assessment of stability between three manipulation cycles. It is recommended to repeat these measurements over a clinically relevant time period, for example between preclinical scanning and a post-operative acquisition during a navigation study.

Clinically, positioning of the transponders near the distal border of the tumor in the rectal wall would be preferred since potential spillage caused by implantation could have a negative effect on tumor recurrence rates. However, as this study indicates the orientation stability of the transponders in healthy rectal or sigmoid wall is not high enough for accurate surgical navigation, as can be seen by the high position and orientation errors for ${}^{Tf}_{EMTS}T_{T3}$ in static and dynamic measurements. Compared to the rectal wall, a rectal tumor is a more rigid anatomical structure. Therefore, when implanting the transponders in tumor tissue, tissue deformation will influence navigation accuracy less, as well as constraining movement of transponders, which is reflected in the error values of the static measurements being below 0.2 mm and 1°. Fibrous tissue, caused by neo-adjuvant radiotherapy, could have similar rigid properties as the tumor while still allowing placement of transponders near the distal border of the tumor in the rectal wall. Furthermore, positioning of transponders inside of tumorous tissue will not be a viable option for all patients. For example when tumor size is very small in primary resection of local regrowth after a clinical complete response on neoadjuvant (radio)therapy and a watchful waiting approach. Therefore, it is recommended to assess relative stability of transponders in fibrous tissue as it could prevent spillage, broaden applicability of surgical navigation applications, while maintaining a rigid relation with the tumor as needed for surgical navigation.

Alternatively, methods could be developed to secure a set of two transponders on the surface of the rectal wall, thereby eliminating the need for implantation. For example, a clip could be developed in which two sensors are embedded at an optimal angle. Therefore eliminating rotation and translation between the two tumor tracker transponders. Kok et al. secured a tumor sensor against rectal tumors during their navigation study using a round silicone surgical wound drain (3.3 mm). However, their workflow might be optimized for positioning the proposed clip.

This study was conducted in a controlled setting, with optimal TA positioning. Where Chapter 3 showed precision errors increase drastically near the top the field up to 2.72 mm and 1.63° – i.e. furthest away from the TA -. Therefore alignment of the more precise lower levels of eFOV with the target area, as performed in this study, would be ideal. However, during laparoscopic surgery, the operating area is occluded by surgical instruments – e.g. trocars, laparoscopic instruments –, the surgeon, surgical assistant, and equipment – e.g. anesthesiology setup or surgical supply carts -. Therefore, positioning of the Calypso system and aligning the TA and eFOV with the target area, could prove a challenging task. Mitigating the decreased precision by adding constraints to positioning of the TA - i.e. aligning the more precise lower levels of the eFOV with the target - is therefore not feasible. Furthermore, as can be seen in dynamic measurements of specimen 3, individual measurements can deviate significantly when the specimen is being manipulated. This can be caused by several factors, including jitter, tissue deformation, migration and transponder velocity combined with update rate of 8 Hz per transponder. It is therefore recommended to assess navigation data based on multiple data samples instead of single values while static measurements are preferred to dynamic assessment. Alternatively, filtering of using a Savitzky-Golay or Kalman filter is proposed.

For clinical application, the maximum of three tracked transponders may prove challenging. In laparoscopic rectal cancer surgery, navigation will be used primarily for tumor localization and subsequent resection margin assessment. When more transponders would be available, tracking of the tumor could be performed using three transponders, eliminating the need for accurate orientation information and ZDR corrections. Since the Calypso system is limited in tracking a maximum of three transponders, where two are needed for tumor tracking and one for a tracked tool, hybrid tracking possibilities – e.g. addition of a OTS to the navigation setup - could be a suitable alternative. The absolute accuracy values in Chapter 3 show the accuracy with which these systems can be calibrated, and the secondary structures can be shown, being approximately 1 mm an 0.4°.

For surgical navigation purposes, based on this study, it not recommended to position transponders in the rectal wall, but rather inside the tumor for positional and orientational stability due to the more rigid anatomical structure. However, more data should be gathered to support this hypothesis, while positioning transponders in fibrous tissue around the tumor should be investigated. Finally, *in vivo* assessment of these errors in a clinically relevant period between implantation of the transponders and after excision of the tumor during a navigation study is recommended.

V. REFERENCES

[1] F. Bray, J. Ferlay, I. Soerjomataram, R. L. Siegel, L. A. Torre, and A. Jemal, "Global cancer statistics 2018: GLOBOCAN estimates of incidence and mortality worldwide for 36 cancers in 185 countries," *CA. Cancer J. Clin.*, vol. 68, no. 6, pp. 394–424, Nov. 2018.

[2] P. Rawla, T. Sunkara, and A. Barsouk, "Epidemiology of colorectal cancer: Incidence, mortality, survival, and risk factors," *Prz. Gastroenterol.*, vol. 14, no. 2, pp. 89–103, 2019.

[3] Intergraal Kankercentrum Nederland (IKNL), "Behandeling darmkanker." [Online]. Available: https://iknl.nl/kankersoorten/darmkanker/registratie/behandeling. [Accessed: 10-Apr-2021].

[4] R. Veldkamp *et al.*, "Laparoscopic surgery versus open surgery for colon cancer: Short-term outcomes of a randomised trial," *Lancet Oncol.*, vol. 6, no. 7, pp. 477–484, Jul. 2005.

[5] H. J. Bonjer *et al.*, "A Randomized Trial of Laparoscopic versus Open Surgery for Rectal Cancer," *N. Engl. J. Med.*, vol. 372, no. 14, pp. 1324–1332, 2015.

[6] A. S. Rickles *et al.*, "Rickles (2015) - High rate of positive circumferential resection margins following rectal cancer surgery.pdf," *Ann. Surg.*, vol. 262, no. 6, pp. 891–898, 2015.

[7] C. G. C. Pales, S. An, J. P. Cruz, K. Kim, and Y. Kim, "Postoperative bowel function after anal sphincter-preserving rectal cancer surgery: Risks factors,

diagnostic modalities, and management," *Annals of Coloproctology*, vol. 35, no. 4. Korean Society of Coloproctology, pp. 160–166, 2019.

[8] W. S. Lee *et al.*, "Risk factors and clinical outcome for anastomotic leakage after total mesorectal excision for rectal cancer," *World J. Surg.*, vol. 32, no. 6, pp. 1124–1129, Jun. 2008.

[9] R. Eppenga, K. Kuhlmann, T. Ruers, and J. Nijkamp, "Accuracy assessment of target tracking using two 5-degrees-of-freedom wireless transponders," *Int. J. Comput. Assist. Radiol. Surg.*, vol. 15, no. 2, pp. 369–377, 2019.

[10] R. Eppenga, K. Kuhlmann, T. Ruers, and J. Nijkamp, "Accuracy assessment of wireless transponder tracking in the operating room environment," *Int. J. Comput. Assist. Radiol. Surg.*, vol. 13, no. 12, pp. 1937–1948, 2018.

[11] D. W. Litzenberg *et al.*, "Positional Stability of Electromagnetic Transponders Used for Prostate Localization and Continuous, Real-Time Tracking," *Int. J. Radiat. Oncol. Biol. Phys.*, vol. 68, no. 4, pp. 1199–1206, Jul. 2007.

[12] T. Alderliesten, C. E. Loo, K. E. Pengel, E. J. T. Rutgers, K. G. A. Gilhuijs, and M. J. T. F. D. Vrancken Peeters, "Radioactive seed localization of breast lesions: An adequate localization method without seed migration," *Breast J.*, vol. 17, no. 6, pp. 594–601, Nov. 2011.

Chapter 7: Electromagnetic Tracking and Robotic-Assisted Surgery

Electromagnetic Tracking and Robotic-Assisted Surgery

Influence of distortion by a da Vinci surgical system on the tracking accuracy of electromagnetic tracking systems for surgical navigation

I. INTRODUCTION

Rectal cancer is the eight most common cancer worldwide with an annual incidence of 704,000, constituting 3.9 percent of all diagnosed cancers [1]. Worldwide, surgery is the primary curative option in non-metastasized rectal cancer, which accounts for 75% of all diagnoses [2]. In the Netherlands, as much as 95% of patients with stadium I-III rectal cancer get surgical treatment [3]. Minimally invasive procedures, robotic assisted- and laparoscopic surgery, have progressively replaced open rectal surgery due to favorable short-term outcomes, such as less pain, reduced blood loss, and improved recovery time [4], [5]. Where, despite a steep learning curve, longer operating times and high costs, robotic assisted surgery has grown particularly for use in more complex operations where the high quality and stable camera platform, the free-moving multijoint tools and better ergonomics are appreciated [6], [7]. However, minimally invasive rectal cancer surgery is associated with positive resection margin rates of 10-15% [5]–[8], while larger margins are shown to negatively impact functional outcome [9], [10]. Therefore, indicating a need for accurate tumor localization and margin assessment during minimally invasive rectal cancer surgery. To this end, surgical navigation is proposed, where preoperative imaging, showing relevant anatomy and the surgical target, is used intraoperatively to guide a surgeon using tracked surgical instruments.

During robotic assisted rectal cancer surgery, the surgical navigation setup can be utilized to actively track the tumor location and correlate the preoperative imaging to the intraoperative setting. To this end, an electromagnetic tracking system (EMTS) can be used, which can track sensors inside of a specified field of view (FOV) with high accuracy while overcoming the direct line of sight limitation of optical tracking systems (OTS) [11]–[13]. Therefore, the 6 degree of freedom (DOF) position and orientation of the tumor can be determined by placing a sensor close to the tumor [14]–[16]. For successful implementation of a navigation setup an intraoperative accuracy below 1 cm should be achieved. To attain this sub- centimeter threshold for tumor tracking, the 6DOF position and orientation -i.e. pose - of the tumor must be determined accurately.

Basically, the intraoperative accuracy is affected by the trueness and precision with which the used tracking system can track the pose of the EM sensors. In turn, this tracking accuracy can be affected by distortions of the magnetic field, which is utilized by the EMTS for tracking of the sensors. There are three major sources of distortions in a magnetic field, being: 'Ferromagnetic materials'; 'Eddy currents in conductive materials, induced by the magnetic field itself'; and 'External currents inside the magnetic field, e.g. electronic devices' [11]. Minimally invasive robotic systems, such as the da Vinci® (DV) surgical system (Intuitive Surgical, Sunnyvale, CA), may cause all three of these types of distortion in the magnetic field and can consequently impact tracking accuracy of the navigation setup. Therefore, it is important to quantify the influence of these systems on the tracking accuracy to assess feasibility of EMTS based surgical navigation during robotic assisted rectal cancer surgery.

As part of a standardized EMTS assessment protocol, Hummel et al. and Franz et al. showed distortion effects of metallic cylinders with positional errors up to 3.2 mm for the Calypso system (Varian Medical Systems Inc., USA), up to 4.2 mm for the NDI Aurora system (Northern Digital Inc, Waterloo, Canada) and up to 80 mm for the Ascension microBIRD (Ascension Technology Corp., USA) [12], [13]. Kenngott et al. assessed the influence of distortion of a da Vinci system on dynamic instrument tracking using the NDI Aurora EMTS, resulting in maximum errors in the FOV of 37.9 mm which did not differ between the DV in standby or in-motion settings [17]. However, their setup might have influenced the tracking accuracy by measuring on an operating table with ferromagnetic characteristics, was limited to 3DOF position evaluation and distinction between trueness and precision could not be made. Furthermore, influence of the DV could differ between dynamic instrument tracking and proposed tumor tracking applications. For the latter application, EM sensors will remain relatively stationary in the FOV while configuration of the robotic arms will change intraoperatively as well as the distance of the robotic instruments to the EM sensors.

In this study, we evaluate the influence of two da Vinci systems – i.e. Si and Xi systems - on the tracking accuracy of the Calypso GPS for the body system and the NDI Aurora Tabletop field generator (TTFG) with an OTS reference. These systems are used since they enable positioning of the flat field generators (FG) on the operating table under the reclining patient during rectal cancer surgery. It is assumed that the FGs can be positioned on the operating table in such a way that the x- y plane of the EMTS is parallel to the patient and starts at the top of the operating table matrass, as implemented by Kok et al. for use of the NDI Aurora during surgical navigation in laparoscopic rectal cancer surgery [16]. During this study, the tumor sensor was located approximately 10 cm along the z-axis from the start of the FOV, therefore grid accuracy was assessed at this level (+- 2.5 cm) in the FOV of both EMTS. Furthermore, influence of robotic arm configurations was assessed as well as influence of converging robotic instruments on the sensor location.

II. METHODS AND MATERIALS

A. Tracking systems

The Calypso GPS for the body system consists of an EM Tracking Array (TA), a readout system and three 5DOF implantable wireless Beacon transponders with different excitation frequencies – i.e. 300, 400, 500 kHz -, a diameter of 1.85 mm and 8 mm long. The electromagnetic tracking system (EMTS) has a cubic FOV of 27.5 x 27.5 x 22.5 cm (in x-, y-, z-direction), starting at 5.5 cm offset from the TA, in which the transponders can be tracked. The x- and y- axes define a parallel plane with regard to the TA while the z-axis is perpendicular, pointing away from the TA. Transponder position trueness has been reported at 0.2 mm, while precision has been reported at 1.3 mm standard deviation in Chapter 3. The z-axis direction reversal detection and correction algorithm, described in Appendix A is applied on the orientation data. Furthermore, the TTV sensor fusion method by Eppenga et al. is implemented to fuse 5DOF pose of two transponders into a single 6DOF virtual sensor – Appendix B .

The NDI Aurora system consists of a tabletop field generator (TTFG), a readout system, sensor interface units, a system control unit and a 6DOF disk sensor with a diameter of 25 mm and 5 mm high. This EMTS has an oval FOV of 42 x 60 x 60 cm (in x-, y-, z-direction), starting at 12 cm offset from the FG. Single transponder position trueness ranges from 0.3 to 0.9 mm (average Euclidian distance), while precision of 0.05 mm standard deviation has been reported [18].

For absolute accuracy measurements of the EMTS the NDI Polaris Spectra (Northern Digital Inc, Waterloo, Canada), an optical tracking system (OTS), is used. The OTS utilizes passive reflective markers, commonly in a 4-marker configuration, which can be tracked with a Root Mean Square Error (RMSE) of <0.17 mm [19]. To avoid any influence on the accuracy by camera movement, an optical tracker was rigidly attached to the TA as reference.

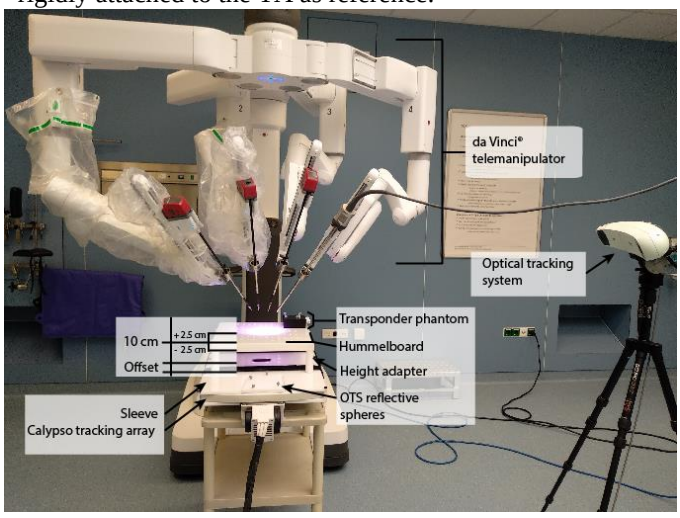

Figure 1 Image of the measurement setup inside the operating room of the NKI.

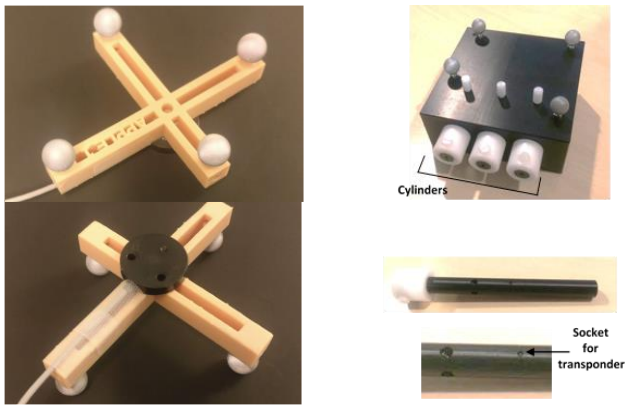

Figure 2 Front view (left) and rear view (right) of the combined sensor, which consists of a 6DOF EM disk sensor and an 6DOF optical sensor.

B. Measurement Setup

The accuracy assessments were performed in the operating room of the Netherlands Cancer Institute (NKI), being the proposed operational environment of the EMTS. Here, measurements were performed using custom made sleeves, incasing the TA and TTFG, stackable height adapter boxes and a Hummel board -depicted in Figure 1-, for accurate, stable and reproducible positioning of sensors in the FOV [15], [20]. To enable sensor fusion for the Calypso system, two 5DOF wireless transponders were positioned in an approximate 90-degree angle to each other, embedded in a transponder phantom size 10 x 10 x 4 cm. Four OTS passive reflective markers were rigidly attached to the transponder phantom. The NDI disk sensor was rigidly attached to a 3D printed four-marker OTS sensor, see Figure 2.

Three measurement settings were evaluated:

- Grid measurements
- Robotic arm configuration measurements
- Instrument convergence measurements

All measurements were assessed for both the da Vinci Xi and da Vinci Si systems, where the systems were positioned in a typical operation setup used for rectal cancer surgery [21]. Grid measurements were performed at three levels in z-direction – i.e. 7.5 cm, 10 cm and 12.5 cm from start of the FOV -. Where, EMTS and OTS measurements were taken at five positions, at the corners – where x = ±15 cm and y = ±15 cm - and middle of the FOV, per level for a total of 15 measurement locations in the FOV. For grid measurements the robotic arms and instruments were positioned using a positioning phantom and kept static. Contrastingly, during robotic arm configuration as well as instrument convergence measurements the robotic arms and instruments were moved between measurements while the sensors were positioned at a static central location in the FOV (z=10 cm). Here, robotic arm configuration measurements assessed the influence of five robotic arm configurations, positioned randomly in a clinically relevant area, while instrument convergence assessed influence of increasing distance of instruments to the EM

sensors – i.e. 1, 3 and 5 cm instrument-sensor distances -, see Figure 3.

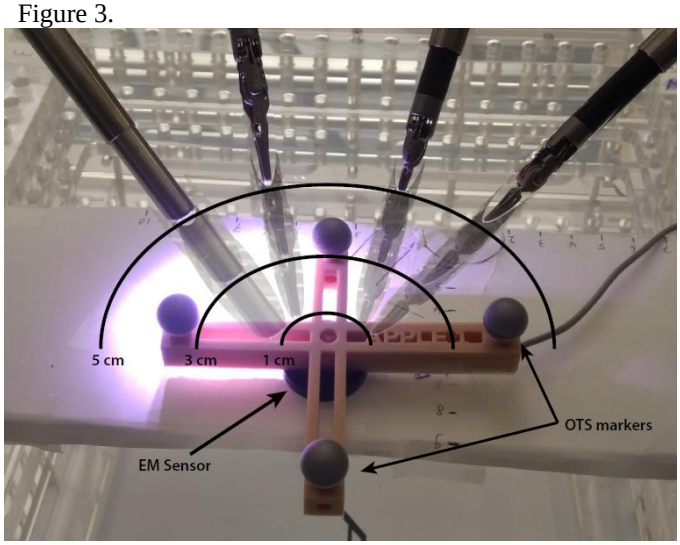

Figure 3 Measurement setup in the center of the FOV for instrument convergence measurements. All three instrument positions with a distance of 1, 3 and 5 cm to the EM sensor are depicted.

For each measurement, 150 samples were recorded at an average sample rate of 50 Hz for EMTS and OTS. Each sample consisted of the following pose information:

- The 6DOF pose of the EM sensor – i.e. virtual transponder or disk sensor - expressed in the EMT coordinate system ${}^{EMT}T_{EMsensor}$
- The 6DOF pose of the optical reference sensor rigidly attached to the TA or TTFG expressed in the optical coordinate system ${}^{OT}T_{FG}$
- The 6DOF pose of the optical sensor attached to the OTS-EMTS combined target expressed in the optical coordinate system ${}^{OT}T_{OTsensor}$

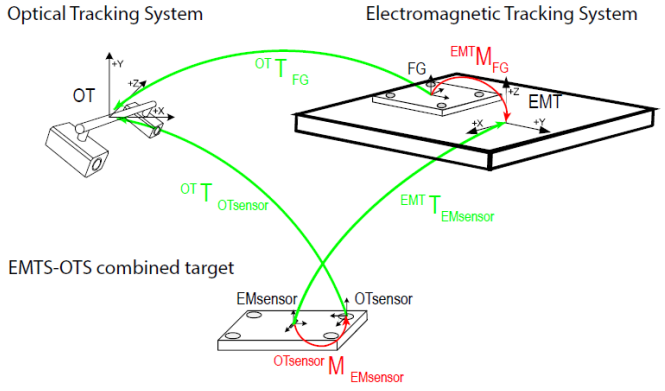

Figure 4 The basic EMTS-OTS setup containing measured and calculated transformations. The transformations from the optical sensor attached to the combined target to the EM sensor and from the FG to EM Tracker (both red) are initially unknown and can be computed by the hand-eye calibration procedure. The other mappings can change dynamically in real-time and are reported by the tracking systems.

All poses were represented by a 4 x 4 transformation matrix T, communicated through OpenIGTLink TRANSFORM messages and analyzed using MATLAB (MATLAB, version R2019a, Natick, Massachusetts: The MathWorks Inc.). The superscript OT or EMT implies the coordinate system in which the specific pose is given, e.g., Optical Tracker or EM Tracker. The subscript specifies the tool or transponder of which the pose is expressed in this coordinate system. Therefore, ${}^{EMT}T_{EMsensor}$ is the pose of the 6DOF EM sensor expressed in the EMT coordinate system. The pose of the EMTS-OTS combined target was calculated with respect to the TA reference sensor using:

$$\begin{aligned} {}^{FG}_{OTS}T_{OTsensor} &= {}^{FG}T_{OT}\ {}^{OT}T_{OTsensor} \\ &= {}^{OT}T_{TG}^{-1}\ {}^{OT}T_{Phantom} \end{aligned} \quad (7.1)$$

The additional subscript, OTS, highlights the fact that this measurement originates from the optical tracking system.

For readout of the Calypso system, specialized readout software, provided by the manufacturer, was used. The readout of the NDI system and OTS hardware was performed using PlusServer from the Plus Toolkit (https://plustoolkit.github.io/) [22].

C. EMTS-OTS Calibration

The calibration between the EMTS and OTS was described by the transformation matrix ${}^{EMT}M_{FG}$, transforming the optical FG marker to the EMT coordinate system – Figure 2 -. A second static transformation was estimated ${}^{OTsensor}M_{EMsensor}$, transforming the EM sensor to the optical marker on the combined EMTS-OTS target. Calibration was performed in two steps. First, hand-eye calibration – Appendix C - was used for initial estimation of these transformation matrices [23], [24]. To this end, a combined EMTS-OTS dataset was collected at three levels (z = 7.5, 10 and 12.5 cm) with 5 sampled poses per level, for a total of 15 measurement poses. For increased robustness and precision of the calibration, the position and orientation of the combined sensor was varied as much as possible, resulting in measurement locations in the center and corners of each level. For each pose, 20 values were acquired and subsequently averaged.

Second, an optimization algorithm - Levenberg-Marquardt, Appendix D - was applied using the calibration dataset, resulting in a final transformation estimation [25]. The final static calibration is used to estimate an absolute reference dataset of the fused transponder pose in EMT coordinates, based on optical measurements, using:

$${}^{EMT}_{OTS}T_{EMsensor} = {}^{EMT}M_{FG}\ {}^{FG}_{OTS}T_{OTsensor}\ {}^{OTsensor}M_{EMsensor} \quad (7.2)$$

Accuracy of the calibration is assessed using the Fiducial Registration Error (FRE) of the calibration dataset – i.e. grid matching error between ${}^{EMT}_{OTS}T_{EMsensor}$ and ${}^{EMT}T_{EMsensor}$, see Chapter 3 -.

D. Data evaluation

All three measurement settings were evaluated on absolute trueness, as compared to the OTS reference, and precision, defined as jitter error.

Absolute trueness

For absolute error calculations, the optical reference ${}^{EMT}_{OTS}T_{EMsensor} = \begin{bmatrix} {}^{EMT}R_{EMsensor} & {}^{EMT}t_{EMsensor} \\ 0 & 1 \end{bmatrix}$, as calculated by (7.1), and ${}^{EMT}T_{EMsensor}$ were compared. Before evaluation, ${}^{EMT}_{OTS}R_{EMsensor}$ and ${}^{EMT}R_{EMsensor}$ were transformed to a quaternion representation $({}^{EMT}_{OTS}q_{EMsensor}, {}^{EMT}_{OTS}q_{EMsensor})$.

For absolute position trueness, the mean position of both systems, ${}^{EMT}_{OTS}\bar{t}_{EMsensor}(i)$ and ${}^{EMT}\bar{t}_{EMsensor}(i)$, over the 150 ($j$=1..150) samples was calculated per measurement (i). Subsequently, the absolute Euclidean position error was computed:

$$Err_{pos}(i) = \left\| {}^{EMT}\bar{t}_{EMsensor}(i) - {}^{EMT}_{OTS}\bar{t}_{EMsensor}(i) \right\|_2 \quad (7.3)$$

Where $|\ldots|_2$ denotes the Euclidian norm.

Similarly, for absolute orientation trueness, the mean orientation of both systems, ${}^{EMT}_{OTS}\bar{q}_{EMsensor}(i)$ and ${}^{EMT}\bar{q}_{EMsensor}(i)$, was calculated, using the quaternion averaging method proposed by Markley et al. [26]. Subsequently, the error was defined as:

$$Err_{or}(i) = \frac{180}{\pi} \cdot 2 \cdot arcsin\left(\left\| vec\left({}^{EMT}\bar{q}_{EMsensor}(i) * {}^{EMT}_{OTS}\bar{q}_{EMsensor}(i)^{-1} \right) \right\| \right) \quad (7.4)$$

Here, $vec\left({}^{EMT}\bar{q}_{EMsensor} * {}^{EMT}\bar{q}_{EMsensor}{}^{-1} \right)$ implies the vector part of the quaternion product[27].

Additionally, for robotic arm configuration measurements the absolute position and orientation error was summarized by calculating the Root Mean Square Error (RMSE) over all five error values, using:

$$\text{RMSE} = \sqrt{\frac{1}{N}\sum_i^N Err_{(pos\,|\,or)}(i)^2} \quad (7.5)$$

Precision

The jitter error – defined as the standard deviation - was calculated for both position and orientation as a measure of precision:

$$Jitter_{pos}(i) = \sqrt{\frac{1}{N}\sum_{j=1}^{N} \left\| {}^{EMT}t_{EMsensor}(i,j) - {}^{EMT}\bar{t}_{EMsensor}(i) \right\|_2^2} \quad (7.6)$$

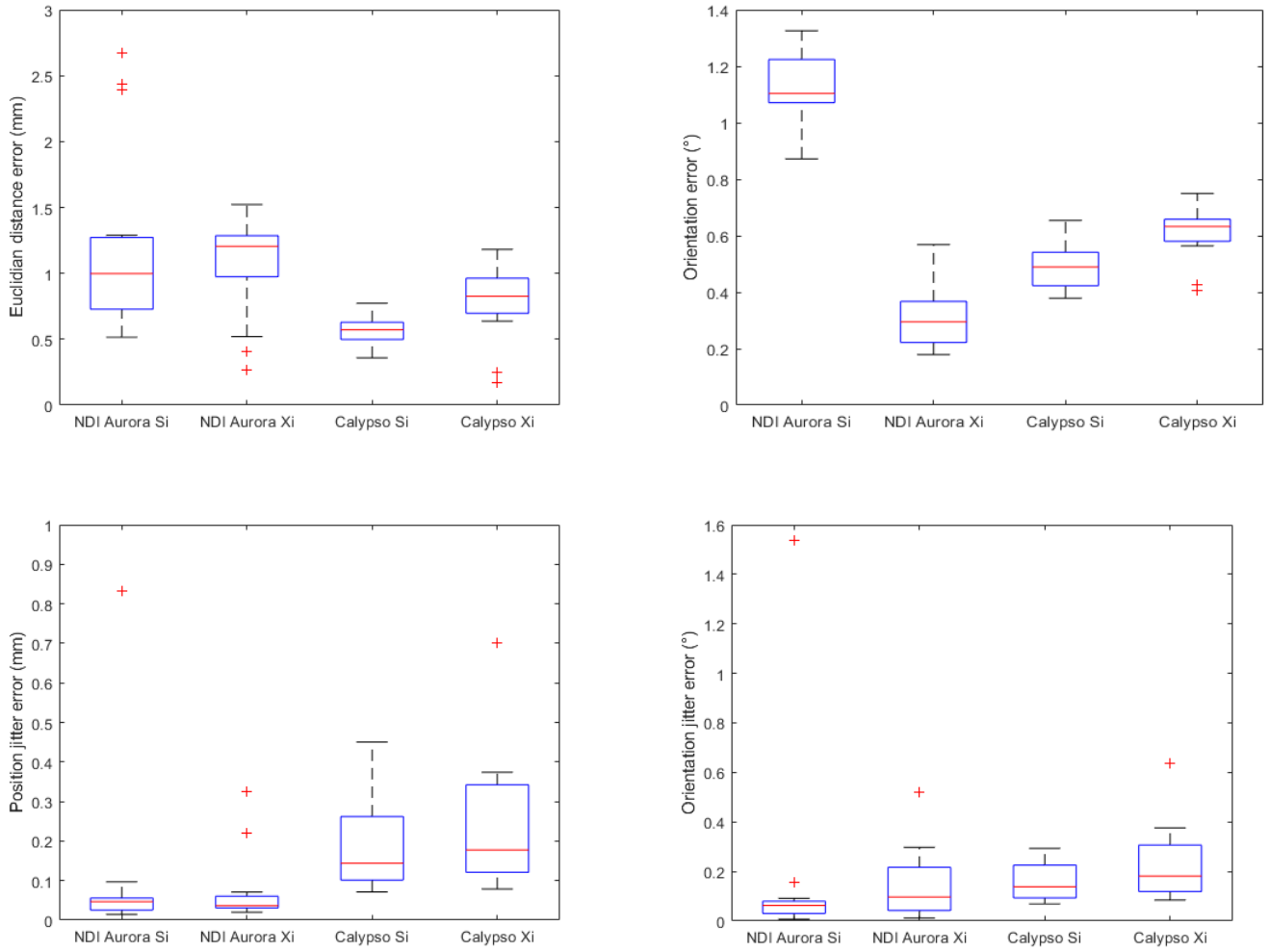

Figure 5 Boxplots of grid measurements, Absolute position and orientation trueness over 15 grid locations with OTS reference (above); Jitter over 15 grid locations (below). On each box, the central mark indicates the median, and the bottom and top edges of the box indicate the 25th and 75th percentiles, respectively. The whiskers extend to the most extreme data points not considered outliers (1.5 times the interquartile range from the box), and the outliers are plotted individually using the '+' symbol.

$$Diff_{or}(i,j) = \frac{180}{\pi} \cdot 2 \cdot arcsin\left(\left\| vec\left({}^{EMT}q_{Tf}(i,j) * {}^{EMT}\bar{q}_{Tf}(i)^{-1}\right)\right\|\right) \quad (7.7)$$

$$Jitter_{or}(i) = \sqrt{\frac{1}{N}\sum_{j=1}^{N}\|Diff_{or}(i,j)\|_2^2} \quad (7.8)$$

Additionally, for robotic arm configuration measurements the jitter error was summarized by calculating the RMSE.

III. RESULTS

Calibration between the NDI Aurora and OTS systems resulted in a FRE of 0.48 mm and 0.28°, while the Calypso to OTS calibration resulted in a FRE of 0.39 mm and 0.24°.

Grid measurements

Results of grid measurements are shown as boxplots over all 15 measurement locations per DV-EMTS combination in Figure 5. Concerning the position trueness error, median Euclidian distance error of 15 measured positions per DV-EMTS combination ranged from 0.57 mm to 1.20 mm. Outlier are seen in all measurements, exempt the Calypso-Si combination. Median error values are lower for the Calypso system compared to the Aurora system for both DV systems. Considering position precision, median jitter error values ranging from 0.04 to 0.18 mm are observed. Comparable to position trueness, outliers are seen for all EMTS-DV combinations but the Calypso-Si combination. Median jitter error values are lower for the NDI Aurora system compared to the Calypso system for both DV systems.

Concerning orientation trueness, median error values ranged from 0.30° to 1.10°. Outliers are seen for the Calypso-Xi combination. Median error values for the Si system are lower for the Calypso system, whereas opposite is true for the Xi system. Considering orientation precision, median jitter error values ranged from 0.06° to 0.18°. Comparable to position precision, jitter error values are lower for the NDI Aurora system compared to the Calypso system for both DV systems.

Robotic arm configuration measurements

All errors per DV and EMTS combination are given in Figure 6 as RMSE over 5 robotic arm configurations. Exempt the NDI-Xi combination, the Calypso system shows a higher trueness and lower precision for both orientation and position compared to the NDI system for all EMTS-DV combinations. Position RMSE values range from 0.51 mm to 1.27 mm for trueness while precision values range from 0.02 mm to 0.31 mm. Considering orientation, trueness RMSE values range from 0.23° to 1.05° and precision values range from 0.02° to 0.31°.

Instrument convergence measurements

Considering trueness of the Calypso system, position errors to OTS reference ranged from 0.52 mm to 0.77 mm and orientation errors ranged from 0.42° to 0.79°. Orientation trueness of the Aurora system increased with an increasing distance of the instruments to the sensor from 5.30° to 0.54° for the Xi system and from 1.65° to 0.97° for the Si system. Similarly, position trueness increased with an increasing distance for the NDI-Si combination from 1.41 mm to 0.93 mm. However, the NDI-Xi combination showed a decrease in position trueness with an increase in distance between sensor and instruments from 0.41 mm to 1.04 mm.

Considering position precision, jitter errors for all three instrument positions and two DV combinations range from 0.01 mm to 0.02 mm for the NDI system and from 0.16 mm to 0.25 mm for the Calypso system. Orientation jitter error for all three instrument positions and two DV combination was 0.01° for the NDI system while ranging from 0.15° to 0.17° for the Calypso system.

IV. DISCUSSION

This study shows that both the Calypso and NDI Aurora EMTS can be reliably used for tumor tracking in a clinically relevant FOV in combination with da Vinci surgical systems. In the clinically relevant FOV, as estimated from tumor position data of a previous *in vivo* study [16], median trueness errors for grid accuracy were below 1.20 mm and 1.10° for all EMTS-DV combinations. These errors are not directly comparable to literature, since they were taken in a non-standardized way, with a limited FOV and errors are calculated with respect to an OTS reference and therefore impacted by calibration errors. However, our results suggest that the DV have hardly any effect on the accuracy of both EMTS, since absolute accuracy assessment over 30 positions at this level for the Calypso system in a distortion free setup, as assessed in Chapter 3, resulted in a RMSE of 0.84 mm and 0.35°. Absolute RMSE values ranging from 1.8 mm to 2.3 mm and from 0.02° to 0.34° were reported for whole FOV of the NDI system in a distortion free environment[20]. In contrast, relative distortion errors were reported of up to 3.2 mm for the Calypso system and 4.2 mm for the NDI Aurora system for metallic cylinders positioned between the sensor and FG[12], [13]. Furthermore, precision errors for all EMTS-DV combinations between of 0.0 - 0.2 mm and 0.1° - 0.2°, are directly comparable to errors found in literature for distortion free environments.

Kenngott et al. assessed the influence of DV on the maximum deviation from centerline in a dynamic setup for the

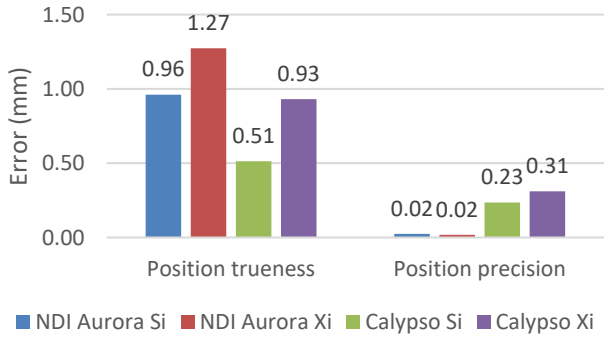

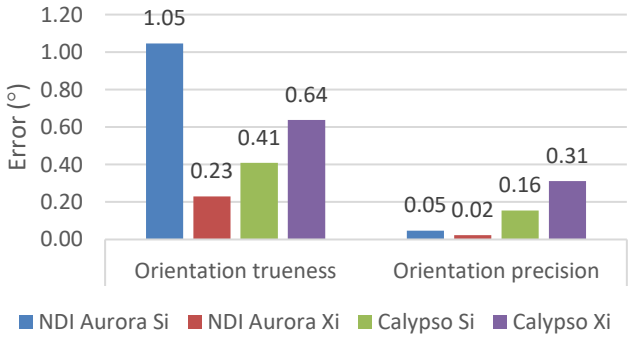

Figure 6 Outcome of robotic arm configuration measurements as RMSE over 5 configurations per da Vinci and EMTS combination.

NDI system with a planar FG using a custom-made measuring facility. With a limited FOV, errors were observed of 8.5 mm with a passive DV and 8.9 mm with an active DV, while without DV the recorded maximum error was 8.3 mm. They argued that their setup might have influenced the tracking accuracy by measuring on an operating table with ferromagnetic characteristics. Furthermore, it was limited to 3DOF position evaluation and distinction between trueness and precision could not be made. Finally, effect of dynamic sensor errors was not taken into account, where it has been reported to result in increasing position errors of up to 2.3 mm for increasing velocities up to 1.2 m/s [11], [28]. Murphy et al. assessed sensor motion errors to the Calypso system but found no effects [29]. Here, we show results for influence of DV on position and orientation accuracy of two EMTS for tumor tracking using grid measurement, different robotic arm configurations and robotic instruments converging on the EM sensors in a clinically relevant FOV.

Robotic arm configuration measurements showed higher position and orientation trueness of the Calypso system compared to the NDI Aurora, exempt for the higher orientation trueness when the NDI Aurora was combined with the da Vinci Xi system. Similarly, this lower orientation error for the combination shows both in the grid measurements and with 5 cm distance between the sensor and instruments during instrument convergence measurements. Generally, instruments convergence measurements showed an increase of accuracy with an increasing distance between the instruments and sensor, which was expected. This effect was more prominent with the NDI system, where it was more pronounced in trueness values compared to precision, compared to the Calypso, where it only showed in jitter errors. One clear exception can be seen in the position trueness for the NDI-Xi combination, in sharp contrast with the orientation trueness errors of 5.30° for the same combination. However, accuracy values at 5 cm distance were all comparable to the median values observed in the grid measurements. All in all indicating close proximity of the robotic instruments may influence the tracking accuracy of the EMTS, which could be an important consideration for development of tracked robotic tools.

A surgical navigation setup for real time tumor tracking and margin assessment was recently assessed by Kok et al. by placement of an additional EM sensor on the tumor using a proctoscope, resulting in a feasible, safe and accurate workflow [16]. Given positioning of the sensor at the center of the tumor and a mean rectal tumor diameter of 4.5 cm, as reported by Kornprat et al., an orientation trueness error of for example 1° would result in a positional error at the tumor border of 0.39 mm [22]. At the distal resection margin – i.e. 1 cm from distal tumor border and therefore 3.25 cm from the transponder – this position error would be 0.57 mm, whereas at the proximal resection margin – i.e. 5 cm from proximal

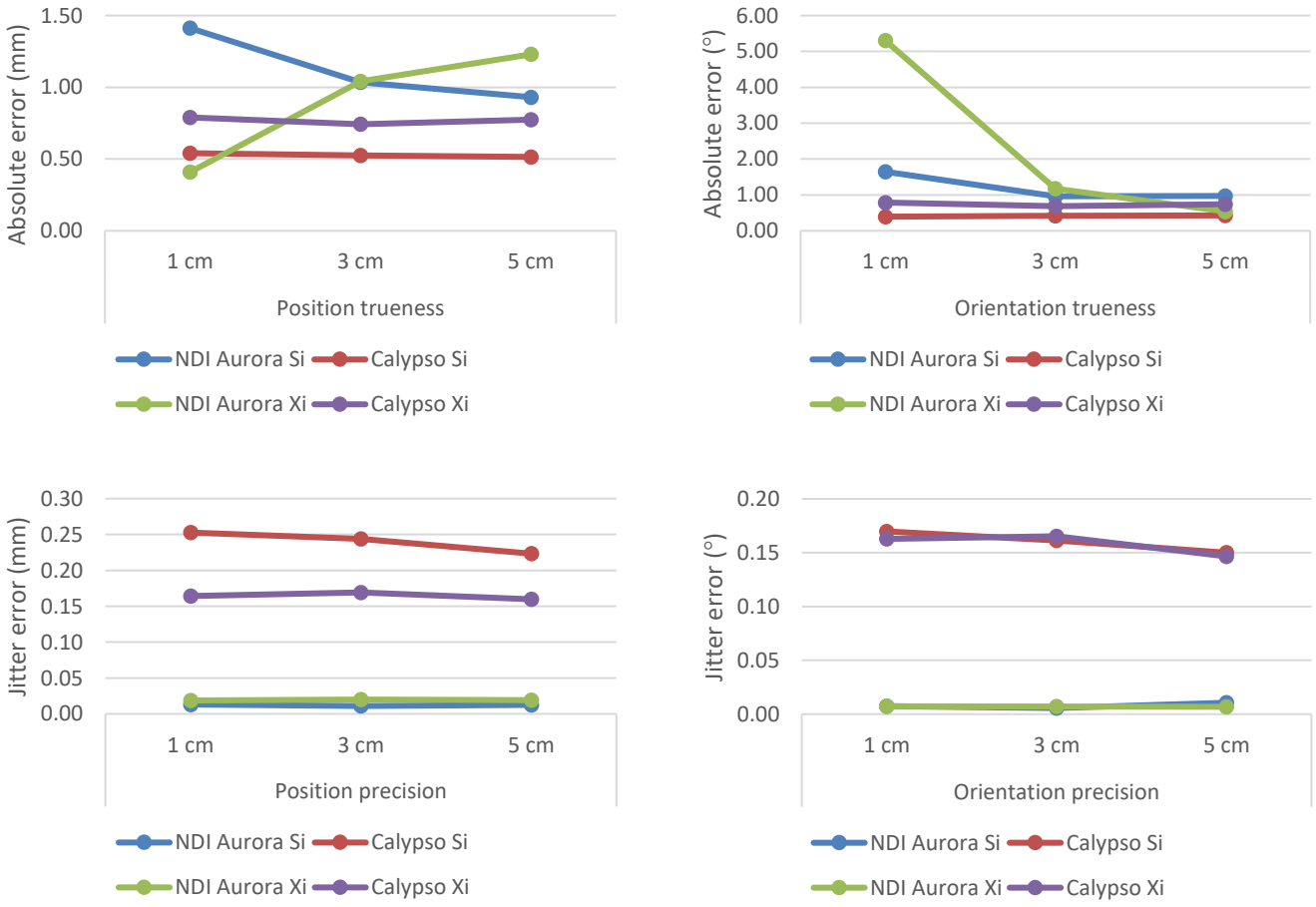

Figure 7 Results Instrument Convergence per EMTS-DV combination; errors plotted over the measured instrument to sensor distances.

tumor border and therefore 7.25 cm from the transponder – the orientation error would translate to a deviation of 1.27 mm. This error range is comparable to position trueness errors, therefore indicating the importance of orientation accuracy for rectal tumor tracking.

Concerning workflow, both EMTS have different limitations. For the NDI Aurora, CBCT registration is needed due to intraoperative placement of wired EM sensors. This CBCT is acquired to correlate the tumor- and patient sensors to the patient's anatomy. During acquisition, the patient receives additional radiation dose and surgical workflow is interrupted, since all surgical staff is required to leave the OR. Furthermore, a hybrid OR is needed hindering broader implementation of surgical navigation techniques. Using the wireless Calypso system, transponders can be implanted preoperatively, enabling preoperative registration and eliminating the need for intraoperative CBCT imaging. Therefore, overcoming the limitations of the earlier wired EM tracking approaches for accurate navigation in rectal surgery [16]. The main constraint of the wireless navigation setup is that the Calypso system is limited to tracking of three transponders. In a surgical setting, one transponder is needed for use in a tracked surgical tool, e.g. Pointer or Stapler, and two sensors are available for 6DOF tumor tracking. Therefore, the setup, in contrast to the wired approach, is not able to track any surrounding structures, limiting the spatial orientation in the 3D model and correlation to the intraoperative setting by the surgeon.

In summary, the NDI Aurora system and Calypso system can be used for reliable tumor tracking in combination with DV surgical systems in a clinically relevant FOV.

V. REFERENCES

[1] F. Bray, J. Ferlay, I. Soerjomataram, R. L. Siegel, L. A. Torre, and A. Jemal, "Global cancer statistics 2018: GLOBOCAN estimates of incidence and mortality worldwide for 36 cancers in 185 countries," *CA. Cancer J. Clin.*, vol. 68, no. 6, pp. 394–424, Nov. 2018.

[2] P. Rawla, T. Sunkara, and A. Barsouk, "Epidemiology of colorectal cancer: Incidence, mortality, survival, and risk factors," *Prz. Gastroenterol.*, vol. 14, no. 2, pp. 89–103, 2019.

[3] Intergraal Kankercentrum Nederland (IKNL), "Behandeling darmkanker." [Online]. Available: https://iknl.nl/kankersoorten/darmkanker/registratie/behandeling. [Accessed: 10-Apr-2021].

[4] R. Veldkamp *et al.*, "Laparoscopic surgery versus open surgery for colon cancer: Short-term outcomes of a randomised trial," *Lancet Oncol.*, vol. 6, no. 7, pp. 477–484, Jul. 2005.

[5] H. J. Bonjer *et al.*, "A Randomized Trial of Laparoscopic versus Open Surgery for Rectal Cancer," *N. Engl. J. Med.*, vol. 372, no. 14, pp. 1324–1332, 2015.

[6] M. J. Kim *et al.*, "Robot-assisted Versus Laparoscopic Surgery for Rectal Cancer: A Phase II Open Label Prospective Randomized Controlled Trial," in *Annals of Surgery*, 2018, vol. 267, no. 2, pp. 243–251.

[7] X. Li *et al.*, "The safety and effectiveness of robot-assisted versus laparoscopic TME in patients with rectal cancer," *Medicine (United States)*, vol. 96, no. 29. Lippincott Williams and Wilkins, p. 29, 01-Jul-2017.

[8] A. S. Rickles *et al.*, "Rickles (2015) - High rate of positive circumferential resection margins following rectal cancer surgery.pdf," *Ann. Surg.*, vol. 262, no. 6, pp. 891–898, 2015.

[9] C. G. C. Pales, S. An, J. P. Cruz, K. Kim, and Y. Kim, "Postoperative bowel function after anal sphincter-preserving rectal cancer surgery: Risks factors, diagnostic modalities, and management," *Annals of Coloproctology*, vol. 35, no. 4. Korean Society of Coloproctology, pp. 160–166, 2019.

[10] W. S. Lee *et al.*, "Risk factors and clinical outcome for anastomotic leakage after total mesorectal excision for rectal cancer," *World J. Surg.*, vol. 32, no. 6, pp. 1124–1129, Jun. 2008.

[11] A. M. Franz, T. Haidegger, W. Birkfellner, K. Cleary, T. M. Peters, and L. Maier-Hein, "Electromagnetic tracking in medicine -A review of technology, validation, and applications," *IEEE Trans. Med. Imaging*, vol. 33, no. 8, pp. 1702–1725, 2014.

[12] A. M. Franz *et al.*, "Standardized accuracy assessment of the calypso wireless transponder tracking system," *Phys. Med. Biol.*, vol. 59, no. 22, pp. 6797–6810, 2014.

[13] J. B. Hummel *et al.*, "Design and application of an assessment protocol for electromagnetic tracking systems," *Med. Phys.*, vol. 32, no. 7, pp. 2371–2379, 2005.

[14] R. Eppenga, K. Kuhlmann, T. Ruers, and J. Nijkamp, "Accuracy assessment of target tracking using two 5-degrees-of-freedom wireless transponders," *Int. J. Comput. Assist. Radiol. Surg.*, vol. 15, no. 2, pp. 369–377, 2019.

[15] R. Eppenga, K. Kuhlmann, T. Ruers, and J. Nijkamp, "Accuracy assessment of wireless transponder tracking in the operating room environment," *Int. J. Comput. Assist. Radiol. Surg.*, vol. 13, no. 12, pp. 1937–1948, 2018.

[16] E. N. D. Kok *et al.*, "Accurate surgical navigation with real-time tumor tracking in cancer surgery," *npj Precis. Oncol.*, vol. 4, no. 8, pp. 1–7, 2020.

[17] H. G. Kenngott *et al.*, "Magnetic tracking in the operation room using the da Vinci® telemanipulator is feasible," *J. Robot. Surg.*, vol. 7, no. 1, pp. 59–64, 2013.

[18] L. Maier-Hein and A. M. Franz, "Standerdized assesment of new electromagnetic field generators in an interventional radiology setting," *Med. Phys.*, vol. 39, no. 6, pp. 3424–3434, 2012.

[19] R. Elfring, M. de la Fuente, and K. Radermacher, "Assessment of optical localizer accuracy for computer aided surgery systems," *Comput. Aided Surg.*, vol. 15, no. 1–3, pp. 1–12, Feb. 2010.

[20] J. Nijkamp *et al.*, "Comparing position and orientation accuracy of different electromagnetic sensors for

tracking during interventions," *Int. J. Comput. Assist. Radiol. Surg.*, vol. 11, no. 8, pp. 1487–1498, Aug. 2016.

[21] J. L. Lee, H. A. Alsaleem, and J. C. Kim, "Robotic surgery for colorectal disease: Review of current port placement and future perspectives," *Ann. Surg. Treat. Res.*, vol. 98, no. 1, pp. 31–43, 2020.

[22] T. Ungi, A. Lasso, C. Pinter, A. Rankin, T. Heffter, and G. Fichtinger, "PLUS: Open-Source Toolkit for Ultrasound-Guided Intervention Systems," *IEEE Trans. Biomed. Eng.*, 2014.

[23] F. C. Park and B. J. Martin, "Robot sensor calibration: solving AX=XB on the Euclidean group," *IEEE Trans. Robot. Autom.*, vol. 10, no. 5, pp. 717–721, 1994.

[24] M. Shah, R. D. Eastman, and T. Hong, "An overview of robot-sensor calibration methods for evaluation of perception systems," in *Performance Metrics for Intelligent Systems (PerMIS) Workshop*, 2012, pp. 15–20.

[25] M. Feuerstein, T. Reichl, J. Vogel, J. Traub, and N. NAVAB, "New approaches to online estimation of electromagnetic tracking errors for laparoscopic ultrasonography," *Comput. Aided Surg.*, vol. 13, no. 5, pp. 311–323, Jan. 2008.

[26] F. L. Markley, Y. Cheng, J. L. Crassidis, and Y. Oshman, "Averaging Quaternions," *J. Guid. Control. Dyn.*, vol. 30, no. 4, pp. 1193–1197, Jul. 2007.

[27] F. L. Markley, "How do I calculate the smallest angle between two quaternions?" [Online]. Available: / www . researchgate . net / post / How _ do _ I _ calculate _ the _ smallest _ angle _ between _ two _ quaternions. [Accessed: 10-Sep-2020].

[28] J. Hummel, M. Figl, M. Bax, R. Shahidi, H. Bergmann, and W. Birkfellner, "Evaluation of dynamic electromagnetic tracking deviation," *Proc. SPIE*, vol. 7261, pp. 72612U–1:7, 2009.

[29] M. J. Murphy, R. Eidens, E. Vertatschitsch, and J. N. Wright, "The Effect of Transponder Motion on the Accuracy of the Calypso Electromagnetic Localization System," *Int. J. Radiat. Oncol. Biol. Phys.*, vol. 72, no. 1, pp. 295–299, 2008.

Chapter 8: General Discussion

General Discussion

In this study, a novel wireless navigation setup is presented for real-time tumor tracking during laparoscopic rectal cancer surgery. Our preliminary work suggests improvement in accurate tumor localization and RM assessment. The setup presented here, has the major advantage of being wireless, eliminating the need for intraoperative sensor placement and CBCT acquisition needed for comparable wired navigation systems, which results in additional radiation dose for the patient and surgical workflow interruptions,. Therefore, the presented wireless navigation setup shows potential for use during rectal cancer surgery, aiming to reduce positive RM while sparing healthy tissue.

Promising results are shown for transponder accuracy, with relative position and orientation accuracy below 1mm and 1° (Chapter 3). However, precision errors increase drastically near the top the field up to 2.72 mm and 1.63° – i.e. furthest away from the TA -. Therefore alignment of the more precise lower levels of eFOV with the target area would be ideal. However, during laparoscopic surgery, the operating area is occluded by surgical instruments – e.g. trocars, laparoscopic instruments –, the surgeon, surgical assistant and equipment – e.g. anesthesiology setup or surgical supply carts -. Therefore, positioning of the Calypso system and aligning the TA and eFOV with the target area, could prove a challenging task. Mitigating the decreased precision by adding constraints to positioning of the TA - i.e. aligning the more precise lower levels of the eFOV with the target - is therefore not feasible. It is therefore recommended to assess navigation data based on multiple data samples instead of single values. Alternatively, filtering of these errors using a Savitzky-Golay or Kalman filter is proposed.

No signs of EMI were found for our proposed navigation setup for laparoscopic rectal cancer surgery, however monitoring of signs of EMI during clinical implementation is recommended (Chapter 4). Also, care should be taken with equipment prone to eddy currents, e.g. carbon fibers, when close to the TA. In future studies, it could be beneficial to position the TA in close proximity to the Maquet CF plate, e.g. incorporate the TA in the operating table system. For example, for optimizing positioning with regard to workflow and compatibility during laparoscopic and robot assisted surgery or for additional intraoperative CBCT imaging. In that case, shorter active tracking periods, electromagnetic shielding, cooling solutions or different material composition of the operating table plates could be considered to minimize heating due to active tracking.

Our novel wireless navigation setup is presented for real-time tumor tracking during laparoscopic rectal cancer surgery and intraoperative workflow and visualization has shown good usability and accuracy (Chapter 5). Participating surgeons were enthusiastic about usability and indicate potential for more decisive action based on the navigation setup. During surgery, the aim of using a surgical navigation setup is to give the surgeon accurate real-time information on tumor location and consequently determine the RM. Therefore, the surgeon needs to correlate the navigation information to the intraoperative setting. Here we used application specific camera views, which could complemented with display of CT and MRI images based on the location of the pointer tip. Additionally a partial model of the rectal wall, where it is assumed to be rigid to the transponders, was added in this study as a tracked anatomical reference. However, when starting with the eventual resection of the rectum, using a surgical stapler, the rectum is significantly deformed and display of the rigid model is therefore invalid. Subsequently, visualization should be restricted to transponder and tool poses. Since the transponders are placed distal to the tumor and RM has been determined before resection, this visualization still yields most important information.

The influence of migration and tissue deformation was assessed for multiple ex vivo specimen and relative rotations and translations were quantified (Chapter 6). Our preliminary work on three tissue specimen suggests relative stability of transponders when implanted in tumor tissue even in dynamic experiments. However, large orientation errors are observed when transponders are implanted in the rectal or sigmoid wall. For surgical navigation purposes, based on this study, it not recommended to position transponders in the rectal wall, but rather inside the tumor for positional and orientational stability due to the more rigid anatomical structure. However, more data should be gathered to support this hypothesis, while positioning transponders in fibrous tissue around the tumor should be investigated. Furthermore, in vivo assessment of intertransponder distance errors between implantation of the transponders and after excision of the tumor during a navigation study is recommended.

This study shows that both the Calypso and NDI Aurora EMTS can be reliably used for tumor tracking in a clinically relevant FOV in combination with da Vinci surgical systems (Chapter 7). In the clinically relevant FOV, as estimated from tumor position data of a previous *in vivo* study, median trueness errors for grid accuracy were below 1.20 mm and 1.10° for all EMTS-Da Vinci combinations compared to an OTS reference. However, close proximity of the robotic instruments may influence the tracking accuracy of an EMTS, which could be an important consideration for development of tracked robotic tools.

Chapter 9: Appendix

APPENDIX A

Z-AXIS DIRECTION REVERSAL

The 5DOF orientation data of a single transponder, as determined by the Calypso system, is accurate as shown in Chapter 3 and by Eppenga et al. [1]. However, a direction reverse of the z-axis is observed at specific positions and orientations in the eFOV. The cause of this "flip" is unknown and cannot be pinpointed since the specialized readout software, provided by the manufacturer, does not give insight into the used pose estimation algorithms or lookup tables.

This does not hinder the clinical application of the Calypso system in radiotherapy setting, since only position information of the transponders is used to define a Volume of Interest (VOI). When only using position information to define the required 6DOF tumor pose, three transponders would be needed to define a plane and consequently an 6DOF coordinate system – Figure A. 1 -. However, in a surgical setting, one transponder is needed for use in a tracked surgical tool, e.g. Pointer or Stapler. Therefore, two sensors are available for 6DOF tumor tracking , as described in Appendix B. In any case, accurate and stable 5DOF information of at least one transponder is needed. Consequently, a detection and correction method is needed in order to cope with the z-axis direction reversal (ZDR).

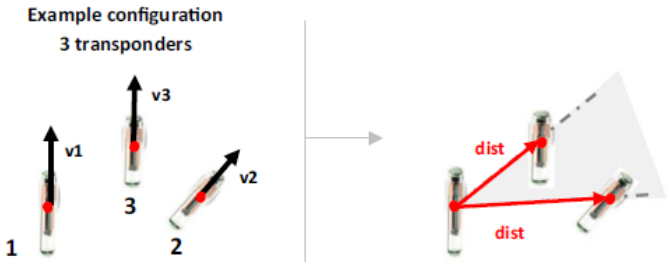

Figure A. 1 Illustration of how a plane (indicated with a light gray area) is defined out of three transponders. The black arrows v1, v2 and v3 represent the three z-axis vectors of the transponders. The red arrows, dist, represent the 3D distance vectors between two transponder origins. Adapted and reprinted with permission, from Eppenga et al [1].

Each pose can be represented using a transformation matrix, using a translation (t) and rotation matrix (R) with respect to a reference coordinate system. A measured transponder in the EM Tracker coordinate system, ${}^{EMT}T_{Tx}$, can therefore be represented using:

$$ {}^{EMT}T_{Tx} = \begin{bmatrix} {}^{EMT}R_{Tx} & {}^{EMT}t_{Tx} \\ 0 & 1 \end{bmatrix} \quad (A.1) $$

In case of a transponder with respect to the EMTracker, the orientation can be extracted from the transformation matrix and represented as a rotation matrix:

$$ {}^{EMT}R_{Tx} = \begin{bmatrix} {}^{EMT}x_{Tx} & {}^{EMT}y_{Tx} & {}^{EMT}z_{Tx} \end{bmatrix} \quad (A.2) $$

With each column representing the basis vectors of the Tx coordinate system with respect to EMT. These basis vectors follow the orthogonality- and unit length constraints. The Calypso system is able to track 5DOF position (*x, y, z*) and orientation (*pitch, yaw*) of Beacon transponders. As a consequence of a single coil design, a *roll* angle of the transponder cannot be estimated. Therefore, the 2DOF orientation information can be represented in one column of the rotation matrix, ${}^{EMT}z_{Tx}$ in this specific case.

Since ${}^{EMT}z_{Tx}$ specifies a single basis vector we can view the 5DOF information given by the Calypso system as a point and single vector – Figure A. 1 -. As specified, 180° direction reversal of this vector need to be detected and corrected. Therefore, a reference vector (v_{ref}) is needed. This could be the previously (t-1) acquired pose. By extracting ${}^{EMT}z_{Tx}$ from the current (v(t)) and previous pose (v(t-1)), the angle (φ) between these vectors can be calculated using the inner product:

$$ (p, q) = \|p\|\|q\|\cos(\varphi) \quad (A.3) $$

As such, when this angle exceeds a predefined threshold of 90°, a z-axis direction reversal is detected and could be corrected by rotation of 180° around y-axis using:

$$ {}^{EMT}R_{Tx\_corrected} = {}^{EMT}R_{Tx} \begin{bmatrix} \cos(180^\circ) & 0 & \sin(180^\circ) \\ 0 & 1 & 0 \\ -\sin(180^\circ) & 0 & \cos(180^\circ) \end{bmatrix} \quad (A.4) $$

This method assumes the true angle between two consecutive vectors to be below 90°. Based on the given update frequency (approximately 8 Hz per transponder) of the system and expected intraoperative angular velocities of transponders, the true angle should not exceed this 90-degree threshold. Therefore, this threshold is assumed to be sufficiently robust. Potential improvement of this method could be achieved by use of a 1-step ahead prediction as v_{ref} based on n-previous vectors. Either way, the described method requires storing a previous vector, which could prove problematic when reentering the EM FOV from an opposing angle with tracked surgical tools, or when no such vector exists at initial entry of the FOV. Therefore, other reference vectors can be used, e.g. a vector between the laparoscope port and tumor for correction of surgical pointer data.

The implementation of a ZDR algorithm in MATLAB is specified in Appendix G, while an implementation in python is specified in Appendix F.

Appendix B

SENSOR FUSION: 6DOF TUMOR TRACKING USING TWO 5DOF TRANSPONDERS

The Calypso system can track three transponders with 5DOF in a 3D space. In order to track an object with 6DOF - assuming a rigid relation between all transponders and the object - the data of multiple transponders has to be fused. A default sensor fusion method is proposed by Eppenga et al. where only position data is used and based on the distance vectors between the transponders [1]. This method needs a minimum of 3 positions, defining a plane and subsequently a coordinate system – Figure B. 1 -. However, during surgical navigation at least one tool, e.g. pointer or stapler, has to be tracked in addition to a tracked tumor. Therefore, Eppenga et al. defined two alternative methods for use with the Calypso system and determined the accuracy of both methods compared to this default method [1]. As can be seen in Figure B. 1, the first method uses the orientation information of both transponders and is therefore called the 'two transponder vectors' (TTV) method. The second method uses the orientation information of one transponder and the distance vector between the two transponders, it is therefore called the 'one transponder vector' (OTV) method. Here, the TTV and OTV methods are described mathematically, and implementation of both methods is shown in MATLAB (Appendix G) and Slicer (Appendix F).

The 5DOF transponders data can be described with a unit vector, positioned at the transponder origin and oriented along its length axis – Figure B. 1 -. The pose information of each transponder is given by the rotation matrix and origin position $\{^{EMT}R_{Tx}, {}^{EMT}t_{Tx}\}$ with respect to the EMTracker (EMT) coordinate system. The 2DOF orientation vector of a single transponder is depicted in the z-column, $^{EMT}z_{Tx}$, of this rotation matrix. Therefore, the complete 5DOF pose of a single transponder can be given by $\{^{EMT}z_{Tx}, {}^{EMT}t_{Tx}\}$.

The assumption is that the transponders have rigid relation with each other and the tumor. In order to define a complete 3DOF rotation matrix, $^{EMT}R_{Tf}$, three basis vectors need to be defined, denoted in the columns of the rotation matrix:

$$^{EMT}R_{Tf} = [^{EMT}x_{Tf} \quad ^{EMT}y_{Tf} \quad ^{EMT}z_{Tf}] \tag{B.1}$$

These basis vectors follow the orthogonality- and unit length constraints.

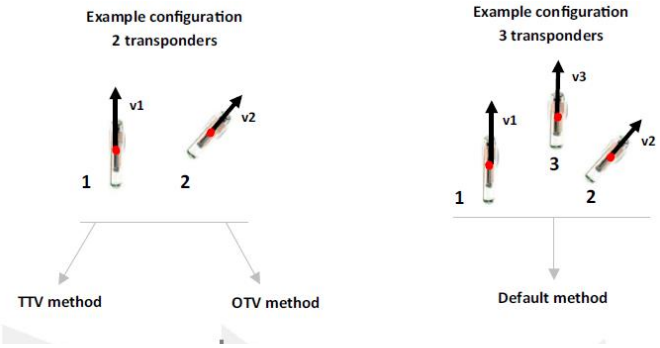

Figure B. 1 Illustration of how a 2D plane (indicated with a lightgray area) is defined out of two 5-degrees-of-freedom transponders, using the TTV and OTV methods (left) and out of three transponders using the Default method (right). The black arrows v1, v2 and v3 represent the three transponder vectors of transponders 1, 2 and 3, respectively. The red arrows, dist, represent the 3D distance vectors between two transponder origins[1]..

First, considering the z column of the fused sensor, in both TTV and OTV methods, this vector is set equal to the orientation vector of the first transponder $^{EMT}z_{T1}$:

$$^{EMT}z_{Tf} = [R_{xx} \quad R_{xy} \quad R_{xz}]^T = {}^{EMT}z_{T1} \tag{B.2}$$

This vector will be normalized to adhere to the unit length constraint:

$$^{EMT}z_{Tf-n} = \frac{^{EMT}z_{Tf}}{\|^{EMT}z_{Tf}\|} \tag{B.3}$$

Second, the vectors spanning the plane, i.e. two transponder vectors for TTV and one transponder vector and a distance vector for OTV, are used to calculate the surface normal at $^{EMT}t_{T1}$. Calculating this orthogonal vector is done using the cross product:

$$^{EMT}x_{Tf} = {}^{EMT}z_{T2} \times {}^{EMT}z_{T1} \quad \text{(For TTV)} \tag{B.4}$$

$$^{EMT}x_{Tf} = (^{EMT}t_{T2} - {}^{EMT}t_{T1}) \times {}^{EMT}z_{T1} \quad \text{(For OTV)} \tag{B.5}$$

Where the angle (φ) between these vectors is not 0° or 180°, e.g. parallel or anti-parallel. The resulting vector will, after normalization, define the x vector of the fused sensor:

$$^{EMT}x_{Tf-n} = \frac{^{EMT}x_{Tf}}{\|^{EMT}x_{Tf}\|} \tag{B.6}$$

Third, the y vector of the fused sensor follows directly from the orthogonality constraint. Therefore, it will be defined by the cross product of $^{EMT}x_{Tf-n}$ and $^{EMT}z_{Tf-n}$;

$$^{EMT}y_{Tf} = {}^{EMT}z_{Tf-n} \times {}^{EMT}x_{Tf-n} \tag{B.7}$$

$$^{EMT}y_{Tf-n} = \frac{^{EMT}y_{Tf}}{\|^{EMT}y_{Tf}\|} \tag{B.8}$$

Finally, the calculated basis vectors of the fused coordinate system are set in the rotation matrix:

$$^{EMT}R_{Tx} = [^{EMT}x_{Tf-n} \quad ^{EMT}y_{Tf-n} \quad ^{EMT}z_{Tf-n}] \tag{B.9}$$

Position of the fused coordinate system, $^{EMT}t_{Tf}$, could be set either at $^{EMT}t_{T1}$, $^{EMT}t_{T2}$ or the mean of both positions. Therefore, the 6DOF tumor pose can be given by $\{^{EMT}R_{Tf}, {}^{EMT}t_{Tf}\}$ and is usually represented in a transformation matrix:

$$^{EMT}T_{Tf} = \begin{bmatrix} ^{EMT}R_{Tf} & ^{EMT}t_{Tf} \\ 0 & 1 \end{bmatrix} \tag{B.10}$$

APPENDIX C

HAND-EYE EMTS-OTS CALIBRATION

Calibration of the Calypso system with a second tracking system can have multiple advantages. For example, the second system can be used as an absolute reference to assess accuracy of the Calypso system – Chapter 3 -. Furthermore, an absolute reference could indicate how accurate the Calypso system can be calibrated with another tracking system, opening up intraoperative hybrid tracking possibilities. Also, a calibrated setup could provide an absolute reference for future measurements where a Hummel board-based assessment is not feasible, e.g., intraoperative or distortion measurements were obtaining a relative reference is not possible. Here, we use the hand-eye calibration as proposed by Tsai et al. to calibrate the Calypso system with the NDI Polaris Spectra optical tracking system (Northern Digital Inc, Waterloo, Canada) [2].

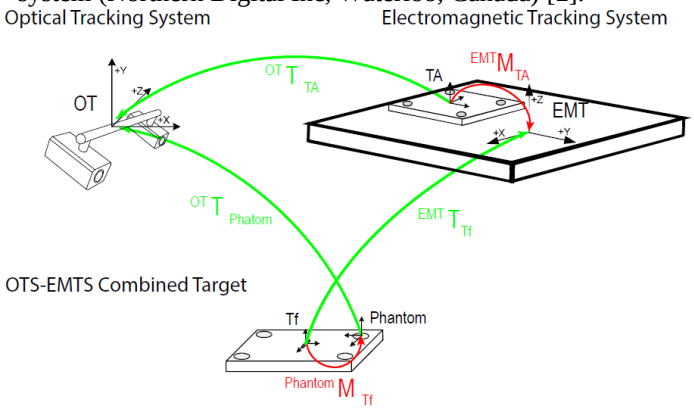

Figure C. 1 The basic EMTS-OTS setup containing measured and calculated transformations. The transformations from the Transponder Phantom to the EMTS transponder and from the Tracking Array to EM Tracker (both red) are initially unknown and can be computed by the hand-eye calibration procedure. The other mappings can change dynamically in real-time and are reported by the tracking systems.

The basic setup for hand-eye calibration is illustrated in Figure C. 1. Three dynamic transforms are acquired:

- The 6DOF pose of the fused EM transponders (Tf) expressed in the EM coordinate system ${}^{EMT}T_{Tf}$
- The 6DOF pose of the optical reference sensor rigidly attached to the TA expressed in the optical coordinate system ${}^{OT}T_{TA}$
- The 6DOF pose of the transponder phantom expressed in the optical coordinate system ${}^{OT}T_{Phantom}$

Two calibration steps are needed in order to use the OTS system as a reference, determining two static transformations: ${}^{EMT}M_{TA}$ and ${}^{Phantom}M_{Tf}$. Wherein, ${}^{EMT}M_{TA}$ is defined as the transformation matrix between the optical coordinate system, as defined with respect to the TA, and the EMT coordinate system. ${}^{Phantom}M_{Tf}$ is defined as the transformation between the fused EM transponder and the coordinate system defined by the transponder phantom. First, the transformation of the optical marker on the transponder phantom to the fused EM transponder is estimated (${}^{Phantom}M_{Tf}$) using hand-eye calibration. The fundamental hand-eye equation is given by:

$$A \cdot X = X \cdot B \tag{C.1}$$

The, to be estimated, transformation between both coordinate systems is given by X. A gives the transformation between two poses for the optically measured transponder phantom (i.e. the motion of the transponder phantom). B represents a transformation of the fused electromagnetic transponder between same two poses. The resulting equation is given by:

$$T_{Phantom_{k_i \to k_j}} \cdot {}^{Phantom}M_{Tf} = {}^{Phantom}M_{Tf} \cdot T_{Tf_{k_i \to k_j}} \tag{C.2}$$

A minimum of three poses (i.e. two different motions) of the combined target are required to determine this relation. Each measured pose, allows calculation of a motion to all previously measured poses. Therefore, the total of calculatable motions per number of poses (n) is given by $\sum_{k=1}^{n}(k-1) = \frac{n(n-1)}{2}$. Consequently, adding additional equations to an overdetermined equation system from which the 6DOF transformation ${}^{Phantom}M_{Tf}$ can be computed.

Here, five different poses at three levels in the EMTS FOV are used for calibration, resulting in a total of 15 poses and 105 motions. For each pose, the three dynamic transformations were measured 150 times each, in order to account for jitter. Subsequently, the mean position was computed and the orientations were averaged using the quaternion averaging method proposed by Markley et al. [3]. The resulting averaged transformations were used to determine the motion from $k_i \to k_j$:

$$T_{Phantom_{k_i \to k_j}} = \left({}^{OT}P_{Phantom}(k_j)\right)^{-1} {}^{OT}P_{Phantom}(k_i) \tag{C.3}$$

$$T_{Tf_{k_i \to k_j}} = \left({}^{EMT}T_{Tf}(k_j)\right)^{-1} {}^{EMT}T_{Tf}(k_i) \tag{C.4}$$

The measured poses can be reused to determine ${}^{EMT}M_{TA}$, by redefined the motions using:

$$T_{EMT_{k_i \to k_j}} = {}^{EMT}T_{Tf}(k_j)\left({}^{EMT}T_{Tf}(k_i)\right)^{-1} \tag{C.5}$$

$$T_{TA_{k_i \to k_j}} = \left(\left({}^{OT}T_{Phantom}(k_j)\right)^{-1} {}^{OT}T_{TA}(k_j)\right)^{-1} \cdot \left(\left({}^{OT}T_{Phantom}(k_i)\right)^{-1} {}^{OT}T_{TA}(k_i)\right) \tag{C.6}$$

The hand-eye equation is then defined by:

$$T_{EMT_{k_i \to k_j}} \cdot {}^{EMT}M_{TA} = {}^{EMT}M_{TA} \cdot T_{TA_{k_i \to k_j}} \tag{C.7}$$

Appendix G shows implementation of this algorithm in MATLAB using an open-source package[4].

APPENDIX D

LEVENBERG-MARQUARDT OPTIMIZATION ALGORITHM

Calibration accuracy using a deterministic methods, such as hand-eye calibration, highly depends on the tracking accuracy of both tracking systems. If acquired poses are imprecise in any way, this will negatively affect the calibration results. Therefore, the Levenberg-Marquardt algorithm can be used to optimize the estimated transforms ${}^{EMT}M_{TA}$ and ${}^{Phantom}M_{Tf}$. The optimization transformation is described in the following way:

$$T_\delta = \begin{bmatrix} R_\delta & t_\delta \\ 0 & 1 \end{bmatrix} = {}^{Tf}M_{Phantom} \cdot {}^{Phantom}T_{OT} \cdot {}^{OT}T_{TA} \cdot {}^{TA}M_{EMT} \cdot {}^{EMT}T_{Tf} \quad \text{(D.1)}$$

When OTS and EMTS acquisitions are accurate and undistorted, the optimization transform would be an identity matrix. However, this cannot be assumed due to the reported sub millimeter positional errors and sub degree orientation errors. Therefore, Feuerstein et al. proposed the use of a cost function for optimization of calibration results using T_δ [5]:

$$\delta = \delta_{pos} + 5 \cdot \tan(\delta_{or}) \quad \text{(D.2)}$$

$$\delta_{pos} = \|t_\delta\| \quad \text{(D.3)}$$

$$\delta_{or} = arccos\left(\frac{trace(R_\delta)-1}{2}\right) \quad \text{(D.4)}$$

Wherein, the Euclidian norm of the translation is taken as positional error (D.3). The angle of rotation is calculated with (D.4), where $trace(R_\delta)$ is the trace of the matrix (i.e. the sum of the diagonal elements). Subsequently, this angle is weight along an arm with length 5 (mm; i.e. equal to unit of positional error) transforming the orientation error to a positional error using (D.2). Using the set of equations, the cost function can be minimized iteratively resulting in the optimized transformations: ${}^{EMT}M_{TA}$ and ${}^{Phantom}M_{Tf}$.

APPENDIX E

ANGULAR DEVIATION OF SIGNAL ELEMENT FROM CENTERLINE OF TRANSPONDER CAPSULE

The main constraint of the wireless navigation setup is that the Calypso system is limited to tracking of three transponders. In a surgical setting, at least two transponders are needed for 6DOF tumor tracking, leaving one transponder for use in a tracked surgical tool, e.g. Pointer or Stapler. Because of a single coil design, a roll angle of the transponder cannot be estimated. Consequently, the surgical navigation setup is able to track 5DOF position (x, y, z) and orientation (pitch, yaw) of these tools, as can be described with a vector, positioned at the transponder origin and oriented along its length axis.

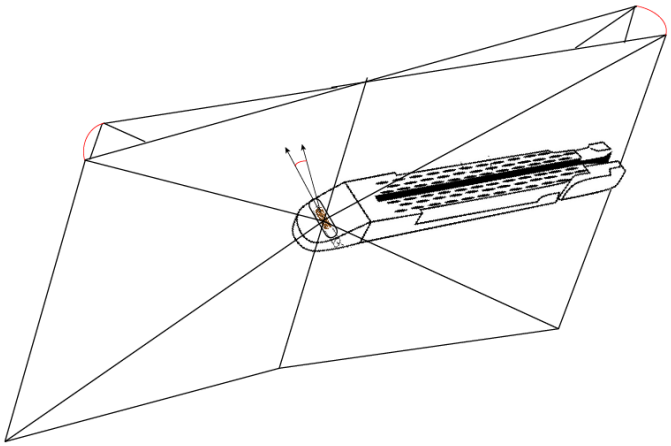

Figure E. 1 Schematic representation of cutting plane deviation due to angular deviation of the signal element from centerline of the transponder capsule.

Beacon transponders of the Calypso tracking system contain a ferromagnetic core, an insulated wire coil around this core, and a capacitator [6]. Together they form a signal element with a specific magnetic resonance frequency. When energized, the signal element generates a magnetic field with a magnetic center point located along the central axis of the transponder. Furthermore, the signal element is encapsulated in an inert material, defining the geometric shape of the transponder. In development of surgical tools, this geometric shape is used for exact placement of the transponders with respect to the tool -i.e. length axis of transponder orthogonal to cutting plane of laparoscopic stapler, or concentric within the laparoscopic pointer -.

However, the signal element, located by the EMTS, and the geometric shape, used for positioning of the transponders in tracked tools, are not concentric resulting in potential orientation errors. For example, for an anvil length of 60 mm of the laparoscopic stapler, a deviation of 2° results in a positional error of 2.10 mm at the end of the anvil which could translate to errors in resection margin assessment, see Figure E.1. Therefore, the aim of this study is to quantify the angular deviation of the signal element from centerline of the transponder capsule.

Methods

Measurements were performed in a laboratory setting, where the tracking array (TA) was positioned on a distortion free table. For high tracking accuracy, a polyoxymethylene plate was positioned parallel to the TA, in the x- and y- plane, at distance of 5.5 cm [7]. For readout of the EMTS system, specialized readout software, provided by the manufacturer, was used. All poses were represented by a 4 x 4 transformation matrix T and communicated through OpenIGTLink TRANSFORM messages. Subsequently, all data was received and analyzed using 3D Slicer [8].

During measurements, 25 transponders were tested separately in the center of the x- y- plane of the EMTS FOV, by rolling them between two flat high friction surfaces to avoid slipping of transponders. Subsequently, the recorded orientation vector is projected on a 2D plane, at distance d from sensor position, orthogonal to the average vector. If there is no deviation, the projection results in a straight line, however when signal element deviates from the geometric centerline of the transponder capsule this generates a sinusoid, see Figure E.2. Based on peak-to-peak amplitude (A_{p-p}) of the sinusoid data, the angular deviation (α) was calculated using:

$$\tan(\alpha) = \frac{A_{p-p}}{2 * d}$$

Results

Results for all 25 measured transponders are summarized as a boxplot in Figure E.3. The minimum deviation between the signal element and transponder capsule was 0.38°, maximum deviation was 3.43° while the average angular deviation is 1.96°.

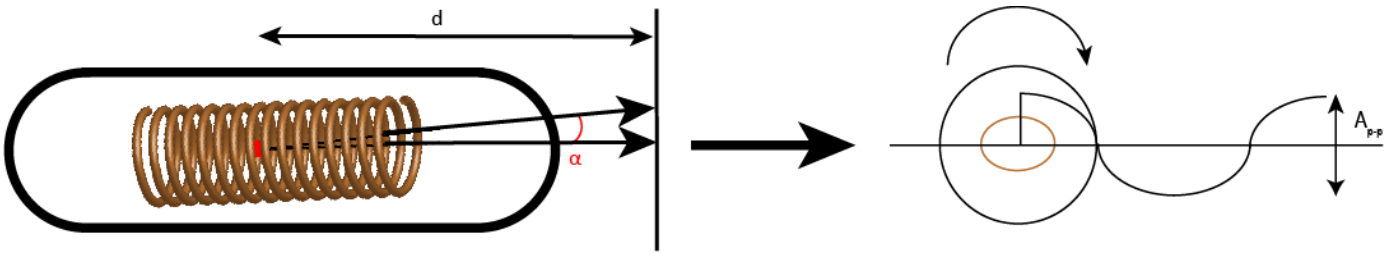

Figure E. 2 Schematic representation of Angular deviation (α) projection plane at distance d; and sinusoid and peak-to-peak amplitude (A_{p-p}) resulting from signal element deviating from the geometric centerline of the transponder capsule.

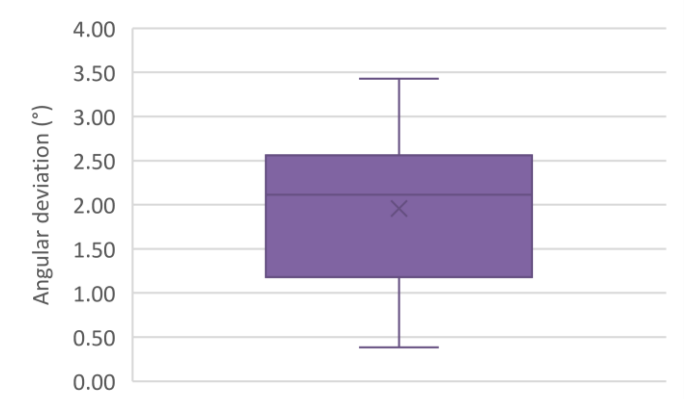

Figure E. 3 Results of angular deviation of the signal element from centerline of the transponder capsule evaluation for 25 measured transponders.

Discussion

Significant deviations between the signal element and transponder capsule of up to 3.43° are observed. Given the 400 mm long pointer an error of up to 23.97 mm could be observed, which is a visualization error and due to the design only translates to positional error at the tip of 0.06 mm – i.e. over 1 cm transponder-tip distance -. However, for an anvil length of 60 mm, this results in positional errors of up to 3.60 mm at the end of the anvil which could translate to errors in RM assessment. Furthermore, such errors can affect the perceived usability and reliability of a setup. Since calibration of these errors is not possible because of the 5DOF pose, it recommended to use the transponders with the smallest deviations in tracked tools.

The described method for determining the deviation is cumbersome and might be subject to errors related to the rolling motion of the transponders. Therefore, for future assessment of this error, a tool is proposed, see Figure E.4. This tool can be positioned in a static orientation in the accurate lower levels of the EMTS FOV while multiple transforms are averaged to eliminate jitter error. Subsequently, the angle between the transponder vector (${}^{EMT}z_{T1}$) and the distance vector between the assessed transponder position (${}^{EMT}t_{T1}$) and a reference transponder (${}^{EMT}t_{T2}$), used as geometric centerline, can be determined using the inner product. For accuracy of the distance vector the tool will have to be precisely machined, or 3D printed from a rigid material. Furthermore, since the distance vector is affected by position trueness error, the orientation accuracy will increase with an increased distance between the two transponders.

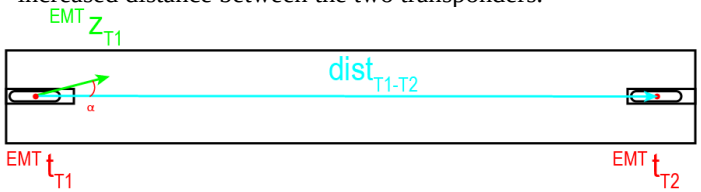

Figure E. 4 Proposed tool for determination of angular deviation of signal element from centerline of transponder capsule

Appendix References

[1] R. Eppenga, K. Kuhlmann, T. Ruers, and J. Nijkamp, "Accuracy assessment of target tracking using two 5-degrees-of-freedom wireless transponders," *Int. J. Comput. Assist. Radiol. Surg.*, vol. 15, no. 2, pp. 369–377, 2019.

[2] R. Tsai and R. Lenz, "Real Time Versatile Robotics Hand/Eye Calibration using 3D Machine vision," *Proc. IEEE Int. Conf. Robot. Autom.*, vol. 1, pp. 554–561, 1988.

[3] F. L. Markley, Y. Cheng, J. L. Crassidis, and Y. Oshman, "Averaging Quaternions," *J. Guid. Control. Dyn.*, vol. 30, no. 4, pp. 1193–1197, Jul. 2007.

[4] Q. Ma and K. M. Ackerman, "AXXB calibration Matlab package." .

[5] M. Feuerstein, T. Reichl, J. Vogel, J. Traub, and N. NAVAB, "New approaches to online estimation of electromagnetic tracking errors for laparoscopic ultrasonography," *Comput. Aided Surg.*, vol. 13, no. 5, pp. 311–323, Jan. 2008.

[6] M. Gisselberg, E. Hadford, S. C. Dimmer, J. Goldberg, J. Pelton, and K. Zublin, "MINATURE RESONATING MARKER ASSEMBLY," US 7,535,363 B2, 2009.

[7] R. Eppenga, K. Kuhlmann, T. Ruers, and J. Nijkamp, "Accuracy assessment of wireless transponder tracking in the operating room environment," *Int. J. Comput. Assist. Radiol. Surg.*, vol. 13, no. 12, pp. 1937–1948, 2018.

[8] A. Fedorov *et al.*, "3D Slicer as an Image Computing Platform for the Quantitative Imaging Network," *Magn Reson Imaging*, vol. 30, no. 9, pp. 1323–1341, 2012.

APPENDIX F

LIST OF SURGICAL EQUIPMENT AS SCORED FOR EMI EVALUATION

		If all previous criter	If all previous criter	If all previous criteria are met:	
	Used during surgical navigation	Plausible Electromagnetic Interference	Critical for patient safety	No viable substitute readily available	Totaal
Operating Table System (Magnus, Maquet)		1	1	1	1	4
Surgical lighting (Devon, Covidien)		1	1	0		2
Medical display systems (multiple systems, Barco)		1	1	0		2
Control unit warming element (Hot Dog, Emergo)		1	1	0		2
Ventilation system (Primus, Dräger)		1	1	1	1	4
ECG Measurement System (Intellivue, Philips)		1	1	1	1	4
(Electro-) cautery energy platform (Force Triad, Covidien)		1	1	1	0	3
Smoke evacuation system (Safe Air (SFR) Compact, Stryker; IES 300, Erbe)		1	1	0		2
High Flow Insuflation Unit (UHI-4 & UHI-3, Olympus)		1	1	0		2
Video System centre (EVIS EXERA III, Olympus)		1	1	0		2
Xenon Light source (EVIS EXERA III, Olympus)		1	1	0		2
Harmonic, Ultrasonic Shear energy platform (Endo-Surgery, Ethicon)		1	1	1	0	3
3D visualization unit (3DV-190, Olympus)		1	1	0		2
Convective Warming system (Cocoon, Care Essentials)		1	1	0		2
Fluid warmer (Hotline 2, Smiths)		1	1	0		2
Syringe pumps (Alaris plus, Carefusion)		1	1	1	1	4
Reusable sets						
Basisnet		1	0			1
Laparotomie net		1	0			1
Plastisch net		1	0			1
Laparoscopie net (advanced, groot)		1	0			1
Optiek Exera HD		1	1	1	1	4
APR set		1	0			1
Curettage & Conisatieset		1	0			1

Harmonicnet	1	1	0		2
Laparoscopische hechtset	1	0			1
Knotsen & Satinskyklem	1	0			1
Omnitract bladen (klein)	1	0			1
Omnitract stangen (klein)	1	0			1
Lone star spreider	1	0			1
Lone star haakjes	1	0			1
Other Reusables					
Beenbladen (lang)	1	0			1
Warming element (Hot Dog, Emergo)	1	1	1	0	3
Vacuum mattrass	1	0			1
Surgical supply cart	1	0			1
Surgical suction mobile bottle	1	0			1
Trash container	1	0			1
Pillow	1	0			1
ECG leads	1	1	1	1	4
Medical head lamp (BTP15, Xenosys)	1	1	0		2
Laryngoscope	1	1	0		2
Patient positioning straps	1	0			1
Gelpads	1	0			1
Metalic and/or powered disposables					
Linear Cutter NTLC55	1	0			1
Linear cutter TLC55	1	0			1
Curved cutter CS40G	1	0			1
Ligasure impact instrument X6 LF4418	1	1	0		2
Ligaclip MCA 20 Medium clips MCM20	1	0			1
Harmonic ace + 7 lap'sc shears HARH36	1	1	0		2
Echelon circular powered stapler (CDH31P, CDH29P)	1	1	0		2
Powered Echelon (PSE45A, PSE60A)	1	1	0		2
Vulling echelon (ECR45B, ECR60B)	1	0			1
Monopolar electrosurgical pencil (ERBE)	1	1	0		2

Suters	1	0			1
IV needles	1	0			1
Other disposables					
Gelpoint path transanal acces platform 4x5.5cm	1	0			1
Surgicel 5x35cm M1901B	1	0			1
Hem-o-Lok clips paars 544240	1	0			1
Medical Mouthmask	1	0			1
Sugical cap	1	0			1
Sterile covers	1	0			1
Sterile gown	1	0			1
Sterile gloves	1	0			1
ECG elektrodes	1	1	1	1	4
IV tubing	1	0			1
Syringe	1	0			1
(hypoallerfig) Adhesive tape	1	0			1
Endotracheal tubes	1	0			1
Catheter	1	0			1
Lamp covers	1	0			1
Non Medical products/ Miscellaneous					
Mobile phone	0				0
Workphone	1	1	0		2
Surgical glasses	1	0			1
Scrubs	1	0			1
Operating room clogs	1	0			1
Pasjes, pashouders, sleutels, pennen, papier, etc.	1	0			1

LIST OF SURGICAL EQUIPMENT AS SCORED FOR DISTORTION EVALUATION

	Within tracking volume of surgical navigation setup	Used during laparoscopic surgical navigation	Possibly distorting	Totaal
Operating Table System (Magnus, Maquet)	1	1	1	3
Surgical lighting (Devon, Covidien)	0	1	1	2
Medical display systems (multiple systems, Barco)	0	1	1	2
Control unit warming element (Hot Dog, Emergo)	0	1	1	2
Ventilation system (Primus, Dräger)	0	1	1	2
ECG Measurement System (Intellivue, Philips)	0	1	1	2
(Electro-) cautery energy platform (Force Triad, Covidien)	0	1	1	2
Smoke evacuation system (Safe Air (SFR) Compact, Stryker; IES 300, Erbe)	0	1	1	2
High Flow Insuflation Unit (UHI-4 & UHI-3, Olympus)	0	1	1	2
Video System centre (EVIS EXERA III, Olympus)	0	1	1	2
Xenon Light source (EVIS EXERA III, Olympus)	0	1	1	2
Harmonic, Ultrasonic Shear energy platform (Endo-Surgery, Ethicon)	0	1	1	2
3D visualization unit (3DV-190, Olympus)*	0	1	1	2
Convective Warming system (Cocoon, Care Essentials)	0	1	1	2
Fluid warmer (Hotline 2, Smiths)	0	1	1	2
Syringe pumps (Alaris plus, Carefusion)	0	1	1	2
Reusable sets				
Basisnet	1	1	1	3
Laparotomie net	0	0	1	1
Plastisch net	0	0	1	1
Laparoscopie net (advanced, groot)	1	1	1	3
Optiek Exera HD	1	1	1	3

APR set	0	1	1	2
Curettage & Conisatieset	0	0	1	1
Harmonicnet	1	1	1	3
Laparoscopische hechtset	0	1	1	2
Knotsen & Satinskyklem	0	1	1	2
Omnitract bladen (klein)	0	0	1	1
Omnitract stangen (klein)	0	0	1	1
Lone star spreider	0	0	1	1
Lone star haakjes 3311-1G	0	0	1	1
Other Reusables				
Beenbladen (lang)	0	1	1	2
Warming element (Hot Dog, Emergo)	1	1	1	3
Vacuum mattrass	1	1	0	2
Surgical supply cart	0	1	1	2
Surgical suction mobile bottle	0	1	1	2
Trash container	0	1	1	2
Pillow	0	1	0	1
ECG leads	0	1	1	2
Medical head lamp (BTP15, Xenosys)	0	1	1	2
Laryngoscope	0	1	1	2
Patient positioning straps	0	1	1	2
Gelpads	0	1	0	1
Metalic and/or powered disposables				
Linear Cutter NTLC55	0	0	1	1
Linear cutter TLC55	0	0	1	1
Curved cutter CS40G	0	1	1	2
Ligasure impact instrument X6 LF4418	1	1	1	3
Ligaclip MCA 20 Medium clips MCM20	0	0	1	1
Harmonic ace + 7 lap'sc shears HARH36	1	1	1	3
Echelon circular powered stapler (CDH31P, CDH29P)	0	1	1	2
Powered Echelon (PSE45A, PSE60A)	1	1	1	3

Vulling echelon (ECR45B, ECR60B)	1	1	1	3
Monopolar electrosurgical pencil (ERBE)	0	1	1	2
Suters	0	1	0	1
IV needles	0	1	0	1
Other disposables				
Gelpoint path transanal acces platform 4x5.5cm	0	0	0	0
Surgicel 5x35cm M1901B	0	1	0	1
Hem-o-Lok clips paars 544240	1	1	0	2
Medical Mouthmask	0	1	0	1
Sugical cap	0	1	0	1
Sterile covers	1	1	0	2
Sterile gown	0	1	0	1
Sterile gloves	0	1	0	1
ECG elektrodes	0	1	1	2
IV tubing	0	1	0	1
Syringe	0	1	0	1
(hypoallergic) Adhesive tape	0	1	0	1
Endotracheal tubes	0	1	0	1
Catheter	0	1	0	1
Lamp covers	0	0	0	0
Non Medical products/ Miscellaneous				
Mobile phone	0	1	1	2
Workphone	0	1	1	2
Surgical glasses	0	1	0	1
Scrubs	0	1	0	1
Operating room clogs	0	1	0	1
Pasjes, pashouders, sleutels, pennen, papier, etc.	0	1	1	2

APPENDIX G

MATLAB SCRIPT: ZDR OF 5DOF POSE INFORMATION

```
function [Tout] = FlipCorrectRotmZ(Tin,ThresDegree,CompareTo)
%FLIPDETECT Detects and corrects for flips of the z-axis (z-axis
%diection reversal). This is an issue of the Calypso Electromagnetic
%Tracking System (Varian Medical).

% Author: Wouter ten Bolscher

%   Z-axis rotations of 180 degrees can be seen in the 5DOF
orientation
%   data from the Calypso Electromagnetic Tracking System (Varian
Medical).
%   This function detects these flips by comparing the z-axis
information
%   of the 4x4xN(xM) transform matrix Tin and rotating 180
%   degree around the y-axis to correct.

% Input:
%     Tin: 4x4xN(xM) transform matrix. The flipcorrection is
%     performed between Transfoms along dimension N. Therefore, Tin
should
%     consist of N measured poses of a certain sensor in a 4x4xN
%     transform matrix. The function is able to handle Tin over multiple
%     measurement locations stored in the 4th dimension of T(M)
%     CompareTo: the index of N indicating the reference pose. All
other
%     poses stored in Tin will be compared to the pose specified by
%     4x4x'CompareTo'(xM).
%     ThresDegree: The threshold, in degree, for flip detection and
%     correction. If the angle, as calculated by the inverse cosine of the
%     dot product of the z vector of each pose with the z vector of the
%     reference pose, is larger than this threshold, the z orientation is
%     flipped 180 degrees around the y-axis.

% Output:
%     Tout: The flip corrected version of Tin. Size of Tout is equal to Tin

% Code is written for compatibility with the IGT-link dataformat and the
% Calypso Electromagnetic tracking system(Varian Medical).

% Set Tout
Tout=Tin;

%Set rotation matrix for 180 degree rotation around y axis in order to
%correct flipedp z-axis.
Ry=[cosd(180) 0 sind(180);0 1 0; -sind(180) 0 cosd(180)];

% Calculate the angle between the poses using the inverse cosine of
the dot
% product of the z vector of each pose with the z vector of the
reference
% pose. If this angle is larger than the set threshold, the z orientation
% is flipped 180 degrees around the y-axis. The flip corrected rotation
% matices are stored in the transform matrix Tout.
for i=1:size(Tin,4)
    Rotm= Tin(1:3,1:3,:,i);
    for ii=1:size(Rotm,3)
        Dot=acosd(dot(Rotm(:,3,CompareTo),Rotm(:,3,ii)));
        if Dot>ThresDegree
            Rotm(:,:,ii)=Rotm(:,:,ii)*Ry;
        end
    end
    Tout(1:3,1:3,:,i)=Rotm;
end
end
```

MATLAB SCRIPT: SENSOR FUSION TTV

```
function [CombinedSensor] = Comb2SensTTV(Sensor1,Sensor2)
%Combination of two 5 Degree of Freedom (DOF)sensors into one
6DOF sensor,
%using the z orientation information of both sensors.

% Author: Wouter ten Bolscher

% Both input, Sensor 1 and 2, and output,CombinedSensor, are 4x4xN
% Transform matrices. Important note: z-axis orientation of both
% sensors should not be similar (minimal angular difference between
the
% z-axes is 2 degrees). Furthermore the sensors should have a
static/rigid
% relationship to each other.

% Code is written for compatibility with the IGT-link dataformat and the
% Calypso Electromagnetic tracking system(Varian Medical).

% OTV and TTV definition as described by Eppenga et al.
% https://doi.org/10.1007/s11548-019-02088-9

%Get Posistions of sensor 1, which will be the position of the
combined
%sensor
PComb= permute(Sensor1(1:3,4,:),[1 3 2]);
Size2=size(PComb,2);

%set size of combined sensor (4x4xN Transform matrix with N being
the same
%size as the input sensors
CombinedSensor=zeros(4,4,Size2);
CombinedSensor(4,4,:)=1;

%Define 1ste vector as the Z vector of Sensor 1, this is the axis of
%which information is accurate from the Calypso System
Vector1= permute(Sensor1(1:3,3,:),[1 3 2]);

%Normalize this vector before handling
for i=1:Size2
    Vector1(:,i)=Vector1(:,i)/norm(Vector1(:,i));
end
%The 2nd vector, which is the z vector of the second sensor, is used
to
%estimate the third vector, which will in turn be used to estimate the
%final 2nd vector. This because it is not guaranteed that the first and
%second vector are perpendicular. In the end, all vectors will be based
on
%measured data giving true 6DOF information.
ApproxVector2= permute(Sensor2(1:3,3,:),[1 3 2]);

%Normalize this vector before handling
for i=1:Size2
    ApproxVector2(:,i)=ApproxVector2(:,i)/norm(ApproxVector2(:,i));
end

% Calculate 3rd vector by cross product of the 1st and aproximation of
the
% second vector, making the 3rd a perpendicular vector through the
plane
% described by the previous two
Vector3 = cross(ApproxVector2,Vector1);

%Normalize this vector before handling
for i=1:Size2
    Vector3(:,i)=Vector3(:,i)/norm(Vector3(:,i));
end

%Now estimate 2nd vector by taking the cros product of the 1st and
3rd,
%agian giving a perpendicular vector on the plane defined by these
vectors
Vector2 = cross(Vector1,Vector3);
```

```
%Normalize this vector before handling
for i=1:Size2
   Vector2(:,i)=Vector2(:,i)/norm(Vector2(:,i));
end

% Insert vectors in Transform matrix defining an accrate 6DOF
% coordinate system based on the information of the two sensors
CombinedSensor(1:3,1,:)=Vector3;
CombinedSensor(1:3,2,:)=Vector2;
CombinedSensor(1:3,3,:)=Vector1;
CombinedSensor(1:3,4,:)=PComb;
end
```

MATLAB SCRIPT: SENSOR FUSION OTV

```
function [CombinedSensor] = Comb2SensOTV(Sensor1,Sensor2)
%Combination of two 5 Degree of Freedom (DOF) into one 6DOF
sensor, using
%the z orientation vector of sensor 1 and the distance vector between
%sensor 1 and 2.

% Author: Wouter ten Bolscher

% Both input, Sensor 1 and 2, and output,CombinedSensor, are 4x4xN
% Transform matrices. Important note: Sensor 2 should not be
% positioned on the z-axis of sensor 1. Furthermore the sensors
should have
% a static/rigid relationship to each other.

% Code is written for compatibility with the IGT-link dataformat and the
% Calypso Electromagnetic tracking system(Varian Medical).

% OTV and TTV definition as described by Eppenga et al.
% https://doi.org/10.1007/s11548-019-02088-9

%Get Posistions of sensor 1, which will be the position of the
combined
%sensor
PComb= permute(Sensor1(1:3,4,:),[1 3 2]);
Size2=size(PComb,2);

%set size of combined sensor (4x4xN Transform matrix with N being
the same
%size as the input sensors
CombinedSensor=zeros(4,4,Size2);
CombinedSensor(4,4,:,:)=1;

%Define 1ste vector as the Z vector of Sensor 1, this is the axis of
%which information is accurate form the Calypso System
Vector1= permute(Sensor1(1:3,3,:),[1 3 2]);

%Normalize this vector before handling
for i=1:Size2
   Vector1(:,i)=Vector1(:,i)/norm(Vector1(:,i));
end
%The 2nd vector, which is the distance vector between the two
sensors is
%used to estimate the the third vector, which will in turn be used to
%estimate the final 2nd vector. This because it is not guaranteed that
the
%first and second are perpendicular, however because of this, in the
end
%all vectors will be based on measured date. Giving true 6DOF
information.
ApproxVector2= permute((Sensor2(1:3,4,:) - Sensor1(1:3,4,:)), [1 3 2]);

%Normalize this vector before handling
for i=1:Size2
   ApproxVector2(:,i)=ApproxVector2(:,i)/norm(ApproxVector2(:,i));
end

% Calculate 3rd vector by cross product of the 1st and aproximation of
the
% second vector, making the 3rd a perpendicular vector through the
plane
% described by the previous two
Vector3 = cross(ApproxVector2,Vector1);

%Normalize this vector before handling
for i=1:Size2
   Vector3(:,i)=Vector3(:,i)/norm(Vector3(:,i));
end

%Now estimate 2nd vector by taking the cros product of the 1st and
3rd,
%agian giving a perpendicular vector on the plane defined by these
vectors
Vector2 = cross(Vector1,Vector3);

%Normalize this vector before handling
for i=1:Size2
   Vector2(:,i)=Vector2(:,i)/norm(Vector2(:,i));
end
% Insert vectors in Transform matrix defining an accrate 6DOF
% coordinate system based on the information of the two sensors
CombinedSensor(1:3,1,:)=Vector3;
CombinedSensor(1:3,2,:)=Vector2;
CombinedSensor(1:3,3,:)=Vector1;
CombinedSensor(1:3,4,:)=PComb;
end
```

MATLAB SCRIPT: QUATERNION DIFFERENCE ANGLE

```
function [Theta] = QuatDifference(Q1,Q2)
%QuatDifference
%   Calculates the difference angle Theta between quaternion1 and
%   quaternion2 using the following formula:
%   Theta = 2*asin(norm of the vector part of the quaternion product
q1*q2^(-1))
%   Source:
https://www.researchgate.net/post/How_do_I_calculate_the_smallest_
angle_between_two_quaternions
%
%   Q1 = 4xM quaternion with notation [w x y z], w = scalar, x y z =
%   vector
%   Q2 = 4xM quaternion with notation [w x y z], w = scalar, x y z =
%   vector.
%   Q1 and Q2 are of the same size, Exeption: if Q2 is a single
reference
%   quaternion, this can be a single 4x1 matrix while Q1 is a 4xM
matrix;
%   For example when calculating the orientation difference between a
%   sample set (stored in Q1) and its average (stored in Q2)
%   Theta = angle difference in degrees in 1x1(or M)

Theta=zeros(1,size(Q1,2));

if size(Q2,2)>1
   for i=1:size(Q1,2)
   Q12 = quatmultiply(Q1(:,i)',quatconj(Q2(:,i)')); % Quaternion product
   VectorPart = Q12(2:4); % Vector part of the quaternion product
   Theta(:,i) = rad2deg(2*asin(norm(VectorPart))); % Difference angle
in degrees
   end
else
    for i=1:size(Q1,2)
   Q12 = quatmultiply(Q1(:,i)',quatconj(Q2')); % Quaternion product
   VectorPart = Q12(2:4); % Vector part of the quaternion product
   Theta(:,i) = rad2deg(2*asin(norm(VectorPart))); % Difference angle
in degrees
   end
end
```

MATLAB SCRIPT: TRANSFORMATION MATRIX AVERAGING

```
function [Tavg] = TAverage(T)
%TAVERAGE Averaging over N of a 4x4xN(xM) transform matrix T,
%using euclidian positional averaging and quartanion orientation
averaging.

% Author: Wouter ten Bolscher

% Positional averaging is performed using a standard euclidian mean.
% However, an average orientation cannot just be obtained by taking a
% Euclidean mean. Therefore, a function based on the work done by
F. Landis
% Merkley is used to calculate the average quaternion.  Markley, F.
Landis,
% Yang Cheng, John Lucas Crassidis, and Yaakov Oshman.
"Averaging
% quaternions." Journal of Guidance, Control, and Dynamics 30, no. 4
% (2007): 1193-
1197.http://www.acsu.buffalo.edu/~johnc/ave_quat07.pdf

% Input:
%     T: 4x4xN(xM) transform matrix. Averaged over 3rd
%     dimension. Therefore T should consist of several, to be
%     averaged, measured poses of a certain sensor in a 4x4
%     transform matrix. The function is able to handle T being averaged
over
%     multiple measurement locations stored in the 4th dimension of
T(M)
% Output:
%     Tavg: 4x4(xM) transform matrix, expressing the averaged
%     pose over N of input variable T.

% Code is written for compatibility with the IGT-link dataformat and the
% Calypso Electromagnetic tracking system(Varian Medical).

%Set Size of Tavg to match 4x4(xM)
Tavg=zeros(4,4,size(T,4));
Tavg(4,4,:)=1;

% positional averaging and quartanion averaging performed for each
% measurement location M
for i=1:size(T,4)
    PosT=T(1:3,4,:,i);
    Pos_avg_T=mean(PosT,3);

    QuatT=rotm2quat(T(1:3,1:3,:,i))';
    Q_avg_T = avg_quaternion_markley(QuatT')';
    Q_avg_T = quatnormalize(Q_avg_T);

    Tavg(1:3,4,i)= Pos_avg_T;
    Tavg(1:3,1:3,i)= quat2rotm(Q_avg_T);
end
end
```

MATLAB SCRIPT: JITTER CALCULATION

```
function [PJitter,QJitter] = JitterTM(TM)
%JitterHM; Position and orientation Jitter of 4x4xN Transform Matrix
%matrix over N samples stored in 3rd dimension of TM input matrix

% Author: Wouter ten Bolscher

% Jitter is defined as the root mean square (RMS) error between the N
% amount of samples and their mean (equal to the standard deviation):
% Jitter = sqrt( 1/N sum( (difference to mean per N)^2 ))
% for orientation: difference to mean per N = 2*asin(norm of the vector
% part of the quaternion product Q(N)*Qavg^(-1));
% for position:  difference to mean per N =norm( P(N) - Pavg )

% Input:
%     TM: 4x4xN Transformation matrix, with N the number of samples
% Output:
%     PJitter: 1x1 double; expressing the positional jitter
%     QJitter: 1x1 double; expressing the (quartanion based) orientation
jitter

%%  Compatibility and used functions
% Code is written for compatibility with the IGT-link dataformat and
% requires use of QuatDifference2 and avg_quaternion_markley.
% Positional averaging is performed using a euclidian mean.
% However, an orientation difference or average orientation cannot
just be
% obtained by subtraction or taking a Euclidean mean. Therefore, the
% orientation difference if calculated using the QuatDifference2 by
Wouter
% ten Bolscher. Which is based on the following formula: Theta =
% 2*asin(norm of the vector part of the quaternion product q1*q2^(-1))
% Source:
%
https://www.researchgate.net/post/How_do_I_calculate_the_smallest_
angle_between_two_quaternions
% Furthermore, the function avg_quaternion_markley by Tolga Birdal
is
% used for calculation of an average orientation, which is based on the
% work done by F. Landis Merkley. Markley, F. Landis, Yang Cheng,
John
% Lucas Crassidis, and Yaakov Oshman. "Averaging quaternions."
Journal of
% Guidance, Control, and Dynamics 30, no. 4 (2007):
% 1193-1197.http://www.acsu.buffalo.edu/~johnc/ave_quat07.pdf
%%
% TM:4x4xN (samples)
% split TM in positional an orientation data
P=permute(TM(1:3,4,:),[1 3 2]); %3xN
Q=rotm2quat(TM(1:3,1:3,:)); %Nx4

% Positional and Orientation Averages
Pavg=mean(P,2); %3x1
Qavg=avg_quaternion_markley(Q); %4x1

% Positional and Orientation Differences
Pdiff = P-Pavg;%3xN
Qdiff = QuatDifference2(Q',Qavg); %1xN

% Euclidian norm of the positional error
    for ii=1:size(Pdiff,2)
        Pdiff_eucl(:,ii)=sqrt((Pdiff(1,ii).^2)+(Pdiff(2,ii).^2)+(Pdiff(3,ii).^2));
%1xN
    end

% RMS of the Positional and Orientation error
PJitter=rms(Pdiff_eucl,2);
QJitter=rms(Qdiff,2);

end
```

MATLAB SCRIPT: TRUENESS CALCULATION

```
function [P_RMSE, P_EuclidError,Q_AngDiff, Euclid_dist, Q_Diff] =
AccuracyTMavg(SensorInput,ReferenceSensorInput)
%AccuracyTMavg; Position and orientation error of 4x4(xM)
Transformation Matrix
%matrices with M measurement locations stored in 3rd dimension of
TM input matrix

% Author: Wouter ten Bolscher

% Positional accuracy is calculated as a mean absolute euclidian error
and
% RMSE over M measurement locations between the Sensor(Input)
and a
% Reference(SensorInput).
% Orientation error is calculated as the RMS of the angular differences
% over M measurement locations between the Sensor(Input) and a
```

```
% Reference(SensorInput).

% Input:
%     SensorInput: 4x4xM transform matrix, with M the number of
%     measurement locations.
%     ReferenceSensorInput: 4x4xM transform matrix, with M the
%     number of measurement locations.
% Output:
%     P_RMSE: 1x1 double; expressing the positional RMSError.
%     P_EuclidError: 1x1 double; expressing the positional mean
absolute
%     euclidian error.
%     Q_AngDiff: expressing the Orientation error as (quartanion
based) RMS
%     of the angular differences.

% note: SensorInput needs to be a static measurement at a specific
% measurement location and its (absolute or relative) reference stored
in
% ReferenceSensorInput. If multiple samples are acquired per
measurement
% location, SensorInput should be averaged before calling this
function.

% note: if M=1, no RMSE will be calculated as the RMS with M=1
equals the
% mean absolute euclidian error

% Extract Positional information from TM input
P_Sens=SensorInput(1:3,4,:);
P_Ref=ReferenceSensorInput(1:3,4,:);

%Calculate Positional error between sensor and reference as euclidian
distance
PDiff=P_Sens-P_Ref;
Euclid_dist=sqrt(PDiff(1,:).^2+ PDiff(2,:).^2+ PDiff(3,:).^2);
P_EuclidError=mean(Euclid_dist);

% Extract Orientation information from TM input
Q_Sens=rotm2quat(SensorInput(1:3,1:3,:));
Q_Ref=rotm2quat(ReferenceSensorInput(1:3,1:3,:));

% Calculate angular deviation between the Quaternion representation
of the
% sensor orientation and its reference
Q_Diff=QuatDifference2(Q_Sens',Q_Ref');

% check size of input, if M=1 RMSE will not be calculated
if size(SensorInput,3)>1
    P_RMSE=rms(Euclid_dist);
    Q_AngDiff=rms(Q_Diff);

else
    P_RMSE=['Positional RMSE will not be calculcated since only one
measurement location was given'];
    Q_AngDiff=Q_Diff;

end

end
```

MATLAB SCRIPT: HAND-EYE CALIBRATION

```
function [EmSensToOptSens,OptFGObjectToEmTracker, Diff,
EM_validation] = ExtHandEyeCal(EM,Opt,FGobj)
% Solution to the Hand-Eye Calibration problem AX=YB using the
Kronecker
% method

% Author: Wouter ten Bolscher

%   Hand-Eye Calibration solution for calibration of Electromagnetic
%   tracking system (EMTS) and Optical Tracking system(OTS).
Wherin the optical
%   tracking system uses a stationary Field Generator object (FGobj)
%   attached to the EM field generator, as to make the optical
measurements
%   independent of camera position.
%   For solving of this problem, a complementary EMTS-OTS dataset
is
%   required, wherein a combined EMTS-OTS target is positioned in
%   multiple different poses (N>=3).
%   Input:
%     EM: a 4x4xN transform matrix expressing measured pose
%     (position and orientation) of EM sensor on combined target in the
EM
%     coordinate system
%     Opt: a 4x4xN transform matrix expressing measured pose of
%     Optical sensor on combined target in the Optical coordinate
system
%     FGobj:a 4x4xN transform matrix expressing measured pose
%     of Optical sensor attached to the EM field generator in the Optical
%     coordinate system
%   Output:
%     EmSensToOptSens: a 4x4 transform matrix expressing the
%     estimated Transformation from the optical sensor on the
combined
%     target to the EM sensor on the combined target
%     OptFGObjectToEmTracker: a 4x4 transform matrix expressing
%     the estimated Transformation from the EMtracker coordinate
system
%     (=EM field coordinate system) to Optical FG object  coordinate
system
%     (= used optical coordinate system, since it makes optical
%     measurements independent of camera position)
%     EM_validation: a 4x4xN transform matrix expressing
%     orginal optical sensor pose, on the combined target, in EMtracker
%     coordinate system using the estimated Transformation matrices
%     (EmSensToOptSens, OptFGObjectToEmTracker)

%set size of matrices for calculation transformations between poses of
%different measurement positions
Combinations=nchoosek(1:size(Opt,3),2);
Possibilities=size(Combinations,1);

A=zeros(4,4,Possibilities);
A2=zeros(4,4,Possibilities);
B=zeros(4,4,Possibilities);
B2=zeros(4,4,Possibilities);

%Calculating the transformations between the poses of the different
%measurement positions. Accuracy of the solution is increased when
%differences between poses are larger.

for i=1:Possibilities
A(:,:,i)=inv(Opt(:,:,Combinations(i,1)))*Opt(:,:,Combinations(i,2));
B(:,:,i) = inv(EM(:,:,Combinations(i,1)))*EM(:,:,Combinations(i,2));
A2(:,:,i) = EM(:,:,Combinations(i,1))*inv(EM(:,:,Combinations(i,2))); %
Calculate transformation from position i to i+1
B2(:,:,i) =
inv(inv(Opt(:,:,Combinations(i,1)))*FGobj(:,:,Combinations(i,1)))*(inv(O
pt(:,:,Combinations(i,2)))*FGobj(:,:,Combinations(i,2)));
end

% Finding the solution to the Hand-Eye Calibration problem AX=YB
using the
% Kronecker method
EmSensToOptSens = kronecker(A,B);
OptFGObjectToEmTracker = kronecker(A2,B2);

% Calculation of the 4x4xN transform matrix expressing orginal
% optical sensor pose, on the combined target, in EMtracker
coordinate
```

```
% system using the estimated Transformation matrices
(EmSensToOptSens,
% OptFGObjectToEmTracker)
for i=1:size(EM,3)
    EM_validation(:,:,i) =
OptFGObjectToEmTracker*inv(FGobj(:,:,i))*Opt(:,:,i)*EmSensToOptSe
ns;
end

Diff = EM-EM_validation;
% accurate representation of positional difference between original EM
% sensor pose and estimated pose based on optical sensor data and
the
% Transformation matrices. Orientation gives a good indication of the
% error, but not really accurate. For accurate Orientation error
% information it is recommended to using quartanions culculations.
End
```

MATLAB SCRIPT: LEVENBERG-MARQUARDT OPTIMIZATION

```
function
[OptFGObjectToEmTracker_optimized,EmSensToOptSens_optimized,
EM_validation_optimized] =
LMOptimization(EmSensToEmTracker,OptFGObjectToEmTracker,
OptFGObjectToOptTracker, OptSensToOptTracker,
EmSensToOptSens)
%
Ainv = EmSensToEmTracker; % EM sensor to EM tracker (will be
inverted in next step)
A = zeros(4,4,size(Ainv,3)); % EM tracker to EM sensor
B = OptFGObjectToEmTracker; % Optical object to EM tracker
Cinv = OptFGObjectToOptTracker; % Optical object to optical tracker
C = zeros(4,4,size(Cinv,3)); % Optical tracker to optical object
D = OptSensToOptTracker; % Optical sensor to optical tracker
E = EmSensToOptSens; % EM sensor to optical sensor

% Settings for costfunction and Levenberg-Marquardt algorithm
for i=1:size(Ainv,3) % Invert every transform
    A(:,:,i) = inv(Ainv(:,:,i));
    C(:,:,i) = inv(Cinv(:,:,i));
end

% Reshape arrays, needed for Levenberg algorithm
A2 = reshape(A,1,16*size(A,3));
A2 = permute(reshape(A2,16,size(A,3)),[2,1]);
C2 = reshape(C,1,16*size(C,3));
C2 = permute(reshape(C2,16,size(C,3)),[2,1]);
D2 = reshape(D,1,16*size(D,3));
D2 = permute(reshape(D2,16,size(D,3)),[2,1]);

% Set inputparameters for Levenberg algorithm
x0 = [B(1:3,:);E(1:3,:)]; % Initial transforms, will be optimized by
algorithm (no scaling)
xdata = [A2,C2,D2]; % Measured transform data of the EM and optical
trackers
ydata = zeros(1,size(xdata,1)); % Output delta of costfunction should
be zero

% Create function and set options
fun = @(x0,xdata)costfunction(x0,xdata);
options = optimoptions('lsqcurvefit','Algorithm','levenberg-
marquardt','Display','iter');
options.StepTolerance = [1.00000000000000e-14]; % e-6 is default
options.FunctionTolerance = [1.00000000000000e-6]; % e-6 is default
options.MaxFunctionEvaluations = [4.8e5]; % 4.8e3 is default
lb = [];
ub = [];

% Run Levenberg-Marquardt algorithm
[x,resnorm,residual,exitflag,output] =
lsqcurvefit(fun,x0,xdata,ydata,lb,ub,options);
[x1,resnorm1,residual1,exitflag1,output1] =
lsqcurvefit(fun,x,xdata,ydata,lb,ub,options);

% Create optimized transforms B and E
B_optimized = [x1(1:3,:);0,0,0,1];
E_optimized = [x1(4:6,:);0,0,0,1];

% Evaluation, delta should be close to zero
delta = costfunction(x0,xdata);
delta = costfunction(x,xdata);
delta = costfunction(x1,xdata);

OptFGObjectToEmTracker_optimized = B_optimized;
EmSensToOptSens_optimized = E_optimized;

for i=1:size(A,3)
    EM_validation_optimized(:,:,i) =
OptFGObjectToEmTracker_optimized*inv(OptFGObjectToOptTracker(:
,:,i))*OptSensToOptTracker(:,:,i)*EmSensToOptSens_optimized;
end
end
```

APPENDIX G

PYTHON SCRIPT: REAL-TIME ZDR OF TWO 5DOF TRANSPONDERS AND SENSOR FUSION USING TTV METHOD

```
def BSensorFusionTTV(caller, event):
    CurrentTransform1 = TNode_B1ToEM.GetTransformToParent()                    #Get current Transform, Matrix and Z vector of first transponder
    PreviousTransform1 = TNode_B1ToEMPre.GetTransformToParent()
    CurrentMatrix1 = vtk.vtkMatrix4x4()
    CurrentMatrix1=CurrentTransform1.GetMatrix()
    CurrentZVector1 = CurrentTransform1.TransformVector([0, 0, 1])
    PreviousZVector1 = PreviousTransform1.TransformVector([0, 0, 1])
    AngleZ1 = vtk.vtkMath.AngleBetweenVectors(CurrentZVector1, PreviousZVector1)#Calculate angle between Current and Previous Z vectors
    TNode_B1ToEMPre.SetMatrixTransformToParent(CurrentMatrix1)
    if AngleZ1>1.4:
        print("Flip detected for B1!")
        print("Angle change is:")
        print(AngleZ1)
        vtk.vtkMatrix4x4.Multiply4x4(Flipper1, FlipMatrix, Flipper1)           #Correct if ZDR
        TNode_FlipCorrectorB1.SetMatrixTransformToParent(Flipper1)             #not used in visualisation, main use is debugging
    CurrentTransform2 = TNode_B2ToEM.GetTransformToParent()                    #Get current Transform, Matrix and Z vector of Seconnd transponder
    PreviousTransform2 = TNode_B2ToEMPre.GetTransformToParent()
    CurrentMatrix2 = vtk.vtkMatrix4x4()
    CurrentMatrix2=CurrentTransform2.GetMatrix()
    CurrentZVector2 = CurrentTransform2.TransformVector([0, 0, 1])
    PreviousZVector2 = PreviousTransform2.TransformVector([0, 0, 1])
    AngleZ2 = vtk.vtkMath.AngleBetweenVectors(CurrentZVector2, PreviousZVector2)
    TNode_B2ToEMPre.SetMatrixTransformToParent(CurrentMatrix2)
    if AngleZ2>1.4:
        print("Flip detected for B2!")
        print("Angle change is:")
        print(AngleZ2)
        vtk.vtkMatrix4x4.Multiply4x4(Flipper2, FlipMatrix, Flipper2)           #Correct if ZDR
        TNode_FlipCorrectorB2.SetMatrixTransformToParent(Flipper2)             #not used in visualisation, main use is debugging
#Get Posistions of sensors and take mean location, which  is used to set the position of the combined sensor
    B1 = CurrentTransform1.GetPosition()
    B2 = CurrentTransform2.GetPosition()
    B_mean = np.mean([B1,B2],axis=0)
# z-axis information of both
    TransformMatrix1 = vtk.vtkMatrix4x4()
    TransformMatrix2 = vtk.vtkMatrix4x4()
    vtk.vtkMatrix4x4.Multiply4x4(CurrentMatrix1,Flipper1,TransformMatrix1)
    vtk.vtkMatrix4x4.Multiply4x4(CurrentMatrix2,Flipper2,TransformMatrix2)
    B1ZVector = TransformMatrix1.MultiplyPoint([0, 0, 1, 0])
    B2ZVector = TransformMatrix2.MultiplyPoint([0, 0, 1, 0])
# Tumor z-axis is normalized B1ZVector (which should already be the case)
    TZVectorUnit = np.divide(B1ZVector[0:3],np.sqrt(np.sum(np.square(B1ZVector[0:3]))))
# normalized B2ZVector is used to determine x vector
    ApproxYVector = np.divide(B2ZVector[0:3],np.sqrt(np.sum(np.square(B2ZVector[0:3]))))
#cross product of B1ZVector and B2ZVector, defining the X axis of tumor
    TXVector = np.cross(ApproxYVector,TZVectorUnit)
# normalized TXVector defines X axis of tumor
    TXVectorUnit = np.divide(TXVector,np.sqrt(np.sum(np.square(TXVector))))
#cross product of TZVectorUnit and TXVector, defining the Y axis of tumor
    TYVector = np.cross(TZVectorUnit,TXVectorUnit)
# normalized TYVector defines Y axis of tumor
    TYVectorUnit = np.divide(TYVector,np.sqrt(np.sum(np.square(TYVector))))
# set x-, y-, z-axes in temporary matrix
    TumorArray = np.array([
    [TXVectorUnit[0],TYVectorUnit[0],TZVectorUnit[0], B_mean[0]],
    [TXVectorUnit[1],TYVectorUnit[1],TZVectorUnit[1], B_mean[1]],
    [TXVectorUnit[2],TYVectorUnit[2],TZVectorUnit[2], B_mean[2]],
    [0, 0, 0, 1]]
    )
#set temporary matrix to replace tumor pose
    TumorToTtemp = vtk.vtkMatrix4x4()
    slicer.util.updateVTKMatrixFromArray(TumorToTtemp, TumorArray)
    TNode_TToEM.SetMatrixTransformToParent(TumorToTtemp)

TNObsT=TNode_B1ToEM.AddObserver(slicer.vtkMRMLTransformNode.TransformModifiedEvent, BSensorFusionTTV)
```

PYTHON SCRIPT: REAL-TIME DISTANCE CALCULATION BETWEEN POINTER/STAPLER AND CLOSEST POINT ON TUMOR SURFACE

```
def DistancePointerTumor(caller, event):
    SMatrix = slicer.util.arrayFromTransformMatrix(TNode_CorrectionP, toWorld=True)   #Get Pointer matrix
    PPosition = SMatrix[0:3,3]                                                        #Get Position of the pointer
    TCTArray=slicer.util.arrayFromTransformMatrix(TNode_CTToEM, toWorld=True)         #Get all concatenated transform from CT to Tumor
    n_point_em=np.dot(TCTArray,numpy_nodes_t)                                         #Transform all points of tumor model to current Tumor
position
    v_Points=np.transpose(n_point_em[0:3,:])-PPosition                                #Calculcate the difference vector between the tumor
points and pointer
    v_dist1=np.linalg.norm(v_Points, axis=1)                                          #Calculate the euclidian norm for all vectors
    k = v_dist1.argmin()                                                              #Get the argument of the minimum euclidian norm -i.e.
shortest distance-
    RNode_PointerToTumor.SetPosition1(n_point_em[0,k],n_point_em[1,k],n_point_em[2,k])      #Set rulerpoints for visualisation of shortest
distance
    RNode_PointerToTumor.SetPosition2(PPosition)

TNObsPointerRuler=TNode_PToEM.AddObserver(slicer.vtkMRMLTransformNode.TransformModifiedEvent, DistancePointerTumor)

def DistanceStaplerTumor(caller, event):
    SMatrix = slicer.util.arrayFromTransformMatrix(TNode_PToEM, toWorld=True)         #Get Stapler matrix
    SMatrix_inv = np.linalg.inv(SMatrix)                                              #Calculate inverse of Stapler matrix for projection
calculations
    TCTArray=slicer.util.arrayFromTransformMatrix(TNode_CTToEM, toWorld=True)         #Get all concatenated transform from CT to Tumor
    n_point_em=np.dot(TCTArray,numpy_nodes_t)                                         #Transform all points of tumor model to current Tumor
position
    n_ProjectedPoint=np.dot(SMatrix_inv,n_point_em)                                   #Calculate the projection of all tumor points on the stapler
plane
    n_ProjectedPoint[2,:] = 0
    n_ProjectedPoint = np.dot(SMatrix,n_ProjectedPoint)
    v_ProjectedPoint = np.subtract(n_ProjectedPoint[0:3,:],n_point_em[0:3,:])         #Calculcate the difference vector between the tumor
points their projected points on the stapler plane
    v_dist2=np.linalg.norm(v_ProjectedPoint, axis=0)                                  #Calculate the euclidian norm for all vectors
    k = v_dist2.argmin()                                                              #Get the argument of the minimum euclidian norm -i.e.
shortest distance-
    RNode_StaplerToTumor.SetPosition1(n_point_em[0,k],n_point_em[1,k],n_point_em[2,k])  #Set rulerpoints for visualisation of shortest distance
    RNode_StaplerToTumor.SetPosition2(n_ProjectedPoint[0,k],n_ProjectedPoint[1,k],n_ProjectedPoint[2,k])

TNObsStaplerRuler=TNode_PToEM.AddObserver(slicer.vtkMRMLTransformNode.TransformModifiedEvent,
DistanceStaplerTumor)#TNode_PToEM.RemoveObserver(TNObsStaplerRuler)
```

PYTHON SCRIPT: DYNAMIC CUTTING PLANE VIEW

```
def CameraUpdaterStaplerView(caller, event, ViewUp1=ViewUp):
    CurrentPTransform= TNode_PToEM.GetTransformToParent()                             # Get current Transforms, Matrices and z vectors
    CurrentPMatrix = vtk.vtkMatrix4x4()
    CurrentPMatrixc = vtk.vtkMatrix4x4()
    CurrentPMatrix= CurrentPTransform.GetMatrix()
    CurrentPVectorZ = CurrentPTransform.TransformVector([0, 0, 1])
    iniPoint1=[0,0,0,0]
    iniPoint2=[0,0,0,0]
    markupsNode_IniVectorStapler.GetNthFiducialWorldCoordinates(0, iniPoint1)
    markupsNode_IniVectorStapler.GetNthFiducialWorldCoordinates(1, iniPoint2)
    IniVectorStapler= np.subtract(iniPoint2[0:3],iniPoint1[0:3])
    AngleZ = vtk.vtkMath.AngleBetweenVectors(CurrentPVectorZ, IniVectorStapler)       #Flipcorrect Current P vector
    if AngleZ>1.4:
        vtk.vtkMatrix4x4.Multiply4x4(CurrentPMatrix, FlipMatrix, CurrentPMatrixc)
    else:
        CurrentPMatrixc=CurrentPMatrix
    CurrentPVectorZc= CurrentPMatrixc.MultiplyPoint([0, 0, 1, 0])
    ProposedFocalpoint1=CurrentPTransform.GetPosition()                               #Set proposed focalpoint
    ViewUpUnit=np.divide(ViewUp1,np.sqrt(np.sum(np.square(ViewUp1))))                 #Calculate unitvector of the Viewup (based on tiltdata of
IMU)
    TYVector = np.cross(CurrentPVectorZc[0:3],ViewUpUnit)                             #For setting a camera coordinate system; Calculate the Y
vector using corrected zvector and viewup
    TYVectorUnit = np.divide(TYVector,np.sqrt(np.sum(np.square(TYVector))))           #Calculate unitvector
    TXVector = np.cross(TYVectorUnit,CurrentPVectorZc[0:3])                           #Calculate Xvector using the corrected zvector and
calculated Yvector; therefore projecting the Viewup (based on IMU) on the staplerplane
    TXVectorUnit = np.divide(TXVector,np.sqrt(np.sum(np.square(TXVector))))           #Calculate unitvector
    TZVector=CurrentPVectorZc[0:3]
    TZVectorUnit = np.divide(TZVector,np.sqrt(np.sum(np.square(TZVector))))           #Calculate unitvector
    # set x-, y-, z-axes in temporary matrix
    Rpup = np.array([
    [TXVectorUnit[0],TYVectorUnit[0],TZVectorUnit[0]],
```

```
    [TXVectorUnit[1],TYVectorUnit[1],TZVectorUnit[1]],
    [TXVectorUnit[2],TYVectorUnit[2],TZVectorUnit[2]]
    ])
    Rrotatedx=np.dot(Rpup,Rzx)                                  #Calculate rotated matrix x degrees around zvector axis,
therefore rotating through the staplerplane
    VproposedviewUnit=Rrotatedx[:,0]                            #Extracting viewvector
    ProposedCameraPosition1= np.add(ProposedFocalpoint1,np.multiply(Zoom,VproposedviewUnit))
    threedView1 = slicer.app.layoutManager().threeDWidget(1).threeDView()      #Setting Camera settings
    renderWindow1 = threedView1.renderWindow()
    renderer1 = renderWindow1.GetRenderers().GetFirstRenderer()
    camera1 = renderer1.GetActiveCamera()
    camera1.SetFocalPoint(ProposedFocalpoint1[0],ProposedFocalpoint1[1],ProposedFocalpoint1[2])
    camera1.SetPosition(ProposedCameraPosition1[0],ProposedCameraPosition1[1],ProposedCameraPosition1[2])
    camera1.SetViewUp(ViewUp1[0],ViewUp1[1],ViewUp1[2])
    markupsNode_Camera.SetNthFiducialPosition(0, ProposedFocalpoint1[0], ProposedFocalpoint1[1], ProposedFocalpoint1[2])
    markupsNode_Camera.SetNthFiducialPosition(1, ProposedCameraPosition1[0], ProposedCameraPosition1[1], ProposedCameraPosition1[2])

TNObsView=TNode_PToEM.AddObserver(slicer.vtkMRMLTransformNode.TransformModifiedEvent, CameraUpdaterStaplerView)
```

PYTHON SCRIPT: REAL-TIME CUTTING PLANE VISUALISATION ON RECTUM MODEL

```
def planeCutter(caller, eventId):
    # Update cutting plane position
    M4x4S2 = TNode_PToEM.GetMatrixTransformToParent()           # get 4x4Matrix transform of stapler sensor transform
    plane.SetOrigin(M4x4S2.GetElement(0,3),M4x4S2.GetElement(1,3),M4x4S2.GetElement(2,3)) # Transform origin
    M4x4S2.SetElement(0,3,0)                                    # Set translational part of matrix to zero
    M4x4S2.SetElement(1,3,0)
    M4x4S2.SetElement(2,3,0)
    planeNormal = M4x4S2.MultiplyPoint([0,0,1,1])               # Transform normal of plane with rotational part
    plane.SetNormal(planeNormal[0],planeNormal[1],planeNormal[2])

    # Update TransformPolyDataFilter
    PDFilterCTEM.Update()

    # Update cutter
    cutter.Update()

ModifiedTag = TNode_PToEM.AddObserver(slicer.vtkMRMLLinearTransformNode.TransformModifiedEvent, planeCutter)
```